METHOD FOR REAL-TIME SIGNAL SELECTION FOR PASSIVE COHERENT LOCATION SYSTEMS

by

NICHOLAS T. JOHNSON
B.S. Electrical Engineering, University of West Florida, 2006
M.S. Electrical Engineering, University of Central Florida, 2010

A dissertation submitted in partial fulfillment of the requirements
for the degree of Doctor of Philosophy
in the Department of Electrical Engineering and Computer Science
in the College of Engineering and Computer Science
at the University of Central Florida
Orlando, Florida

Summer Term
2017

Major Professor: W. Linwood Jones

ABSTRACT

Passive coherent location (PCL) systems use signals of opportunity to perform traditional radar detection, targeting, and tracking functions. Traditionally these signals include FM radio, digital TV, GSM, and GPS because of their availability in most urban environments. A benefit of having an abundance of signals is the ability to choose which of those best meet the desired system intentions. For example, one may want to choose a digital TV signal over an FM radio signal due to its range resolution characteristics. This work presents a novel algorithm for characterizing commercial signals for use in a PCL system. By analyzing each signal's ambiguity function in terms of amplitude, transmitter geometry, range and Doppler resolution, and sidelobe levels, a comparative evaluation can be made to decide which signals are best suited for an intended radar function. In addition, this research shows that multiple signals can be combined in the detection process to increase the probability of detection over that of a single signal. Finally, this research investigates the geometric considerations for PCL systems in terms of bistatic radar geometry. The results show zones of linear and non-linear relationships between time delay, range, and Doppler frequency.

ACKNOWLEDGMENTS

I would like to express my sincerest gratitude to my advisor, Dr. W. Linwood Jones, for his patience, support and guidance during this research. I would also like to thank my committee members at the University of Central Florida Dr. Mikhael Wasfy and Dr. Xun Gong for their support and critique that strengthened my research.

I am also greatly indebted to my committee members at SPAWAR Systems Center, Pacific, Dr. Christopher Lichtenberg and Dr. John Rockway. Their guidance and support have kept me focused and provided the framework for this research.

TABLE OF CONTENTS

LIST OF FIGURES

LIST OF TABLES

CHAPTER 1: INTRODUCTION

Passive Bistatic Radar (PBR) and Passive Coherent Location (PCL) refer to a type of radar system that exploits radio frequency (RF) signals of opportunity emitted from a geographically separated non-cooperative transmission site [1], [2]. The signals used by PCL have traditionally included commercially broadcast FM and digital TV. These signals are broadcast over a large area to cover a specific area [1], [2]. Once the signal is received, it can be used to extract information about a potential target located near the passive receiving sensor and transmitter of opportunity [3]. A PCL system is ultimately a bistatic radar, and as such is subjected to the same challenges and more. The main challenges for implementing a high-performing PCL system are related to signal to noise ratio (SNR). Commercial broadcast FM radio and digital TV transmitters typically have effective radiated power (ERP) values from 10 kW up through 100 kW, far less than a traditional radar system. The antennas for these transmitters are also configured to radiate below a horizontal elevation to reach their intended subscribers. This creates a less than ideal situation for detecting air targets with these emissions. In an effort to overcome these challenges, this research presents several methods to ensure optimal performance of a PCL system.

1.1 Dissertation Objectives

The specific research objectives of this research are as follows:

- Develop a process for independent characterization and ranking of commercial broadcast signal features derived from the ambiguity function such as amplitude, range/Doppler resolution, peak-to-sidelobe ratio, integrated sidelobe ratio, and distance function measurements.

- Create a technique for improving probability of detection by using multiple signals during the detection process

- Derive geometric constraints for PCL systems in terms of bistatic angle, time delay, range, and Doppler frequency

1.2 Dissertation Overview

This dissertation is organized as follows. Chapter one has provided a brief introduction to this work, including specific research objectives. Chapter two presents an overview of PCL concepts and a brief history of the subject. Chapter three describes development of a prototype

PCL system and presents several data collection examples. Chapter four describes a proposed method for characterizing, evaluating, and ranking commercial signals of opportunity for PCL systems. Chapter five describes a new method for employing multiple commercial signals in a PCL system, for reducing the signal-to-noise-ratio (SNR) required per channel. Chapter six discusses geometric considerations for PCL systems and how the bistatic angle can affect the observed range delay and Doppler frequency. Chapter seven is a review of previous discussions with conclusions and recommended future work.

CHAPTER 2: OVERVIEW OF PASSIVE COHERENT LOCATION

Passive Radar and Passive Coherent Location, or PCL, denote a method of detecting and tracking targets using non-cooperative signals of opportunity [1]. These signals traditionally include broadcast FM radio and digital TV [4], but research has also been performed using GPS [5] and cell phone signals [6]. PCL systems have become more popular because of their low cost and immunity to electronic jamming [4]. In addition, the rapid proliferation of signals of opportunity have created broad areas of coverage for passive radar systems. This chapter presents an overview of PCL concepts and technology, and includes a brief history of how legacy PCL systems have evolved into modern radar systems.

2.1 Passive Coherent Location History

Passive radar has a storied history dating back to 1935 when the UK conducted the Daventry experiment [7]. Sir Watson Watt developed a bistatic radar experiment using a 6 MHz BBC transmitter to detect a bomber aircraft at a range of 8km. The aircraft was slow and large, with a wingspan of 75m. It flew a profile of several altitudes, giving Watt and his assistant an opportunity to measure fluctuations in the received signal with an oscilloscope [8].

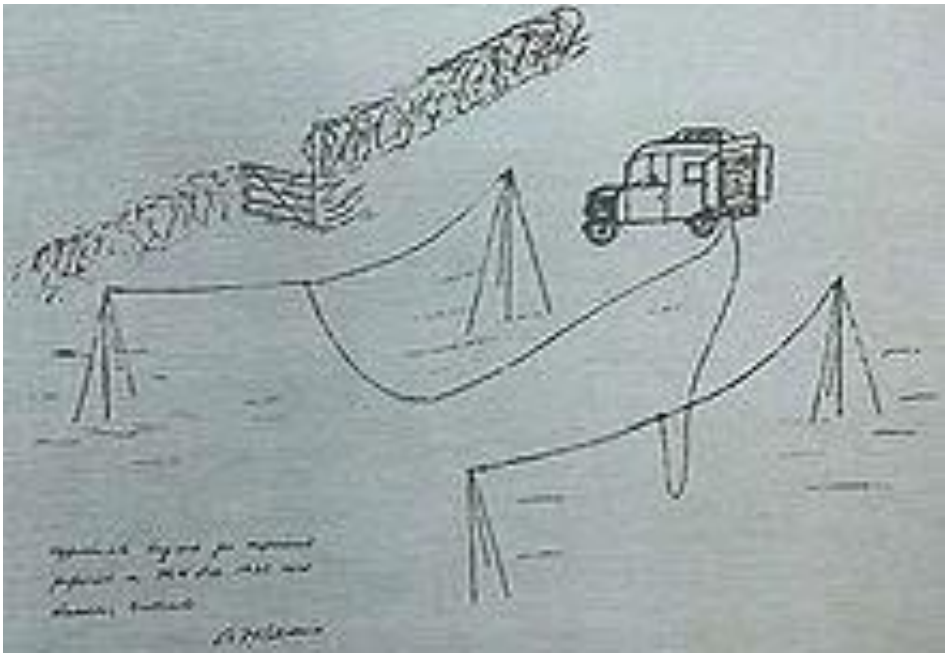

Figure 2.1: Sketch of the Daventry Experiment. This figure was obtained from [8].

Watt's research on passive bistatic radar led him to become the Superintendent of the Bawdsey Research Station as part of England's Air Ministry. His work later founded the development of the Chain Home Radar System installed along the east and south costs of England. The Chain Home was an installation of several radars designed as bistatic radar systems for strategic deployment of Royal Air Force (RAF) fighter aircraft [9]. The radars were transmitting a frequency of 20-30 MHz with 350 kW transmitter power, 20 μs pulse width, and pulse repetition frequency (PRF) of 12.5 or 25 Hz [9]. The PRF was synchronized with the frequency of the local power grid to minimize interference. The transmit antennas were designed to radiate a broad beamwidth pattern to illuminate a large area. The receive antenna arrays included orthogonal half-

wave dipoles to measure both azimuth and elevation [10]. The transmit and receive antennas can be seen in figure 2.2.

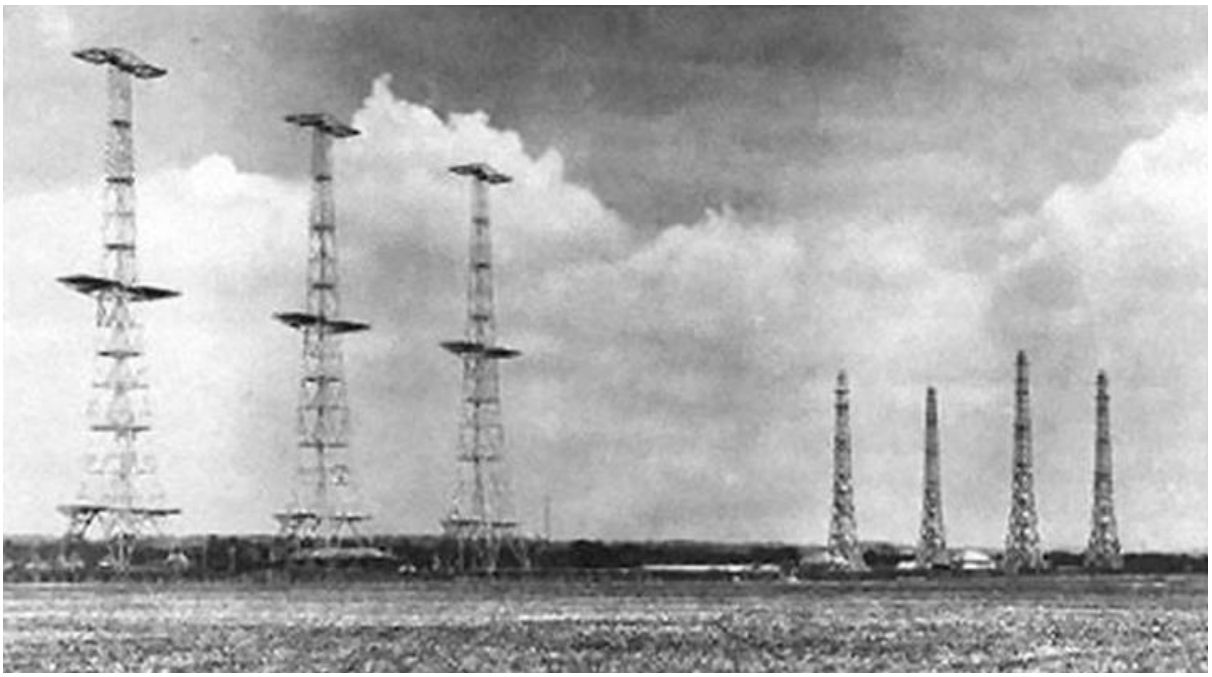

Figure 2.2: The British Chain Home Radar. This figure was obtained from [8] .

In response to the British's early warning radar system, the German's developed and deployed the Klein Heidelberg passive radar system. Prior to the beginning of World War II, the Germans had collected signals from the Chain Home radar system, but initially determined it to be a navigation aid [9]. Once they realized it was a surveillance radar system, they began unsuccessful attempts to bomb or electronically jam the sites. The Germans recognized they needed an early warning radar system of their own that was not susceptible to jamming and mostly undetectable by British radar intercept receivers [9]. They began development of the world's first passive radar system. Through much experimentation, the final design consisted of six receive-

only sites along the west coast of France, The Netherlands, and Belgium [9]. The geographic configuration of Chain Home and one of the Klein Heidelberg systems can be seen in figure 2.3. Figure 2.4 shows the antenna of the Klein Heidelberg at Oostvoorne.

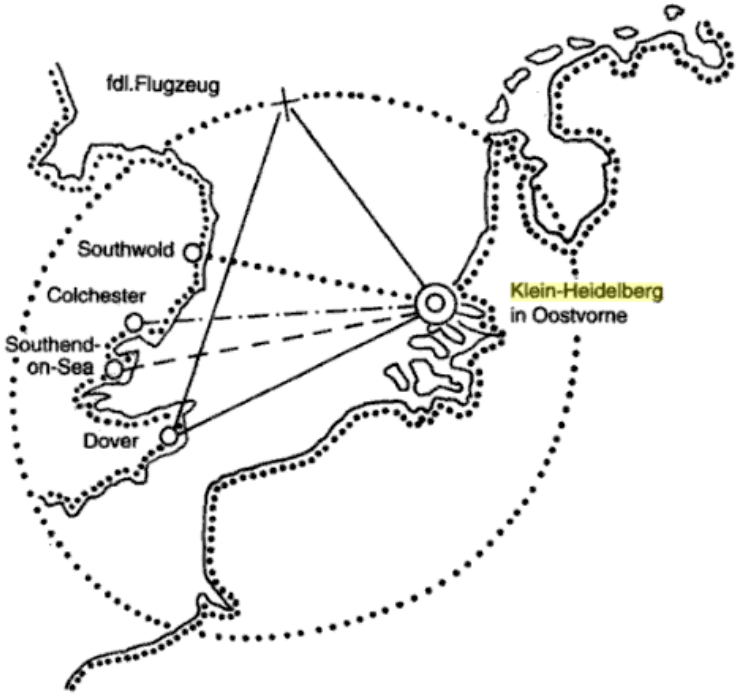

Figure 2.3: Locations of the Chain Home radar system Along the South and East Coast of the UK and the Klein-Heidelberg passive radar system. This figure was obtained from [10].

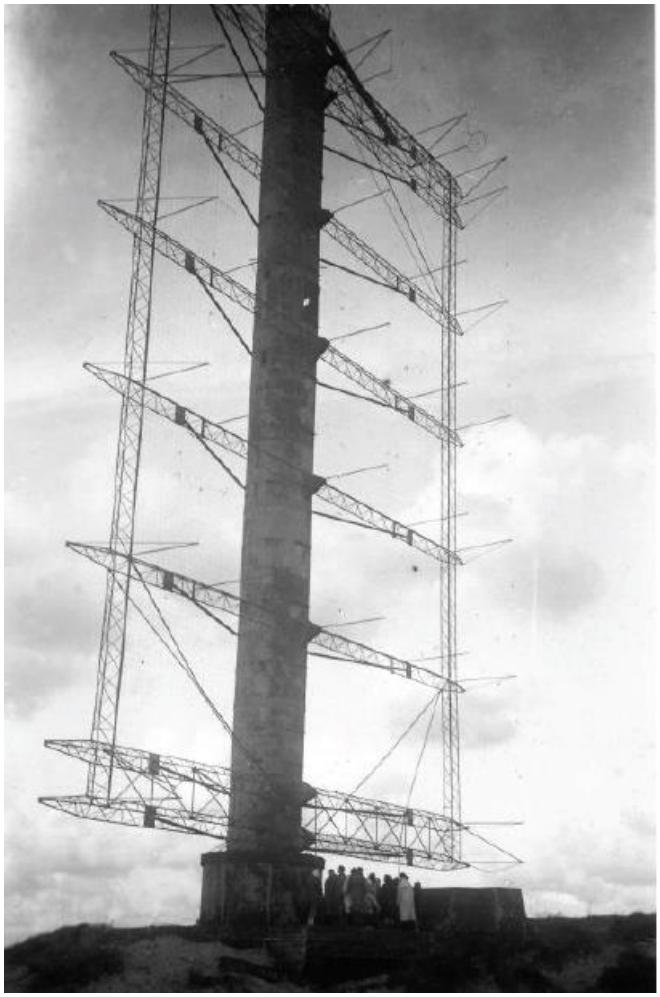

Figure 2.4: Klein Heidelberg antenna at the Oostvoorne site. This figure was obtained from [10].

The Klein Heidelberg took advantage of the signal data collected from the Chain Home radar system. It used radar signal processing theory developed by Dipl.–Ing Wachter that exploited the bistatic nature of a passive radar system. The principle of operation as shown in figure 2.5 is based on the geometric relationship between transmitter, receiver, and target. Because locations of the Chain Home and Klein Heidelberg were known a priori, forty

different range sum measurements were made to produce individual ellipses. The radar operator would plot a radial line from the measured angle of arrival and measurements from the A-scope. The target location was determined to be at the intersecting point of the target bearing and corresponding ellipse.

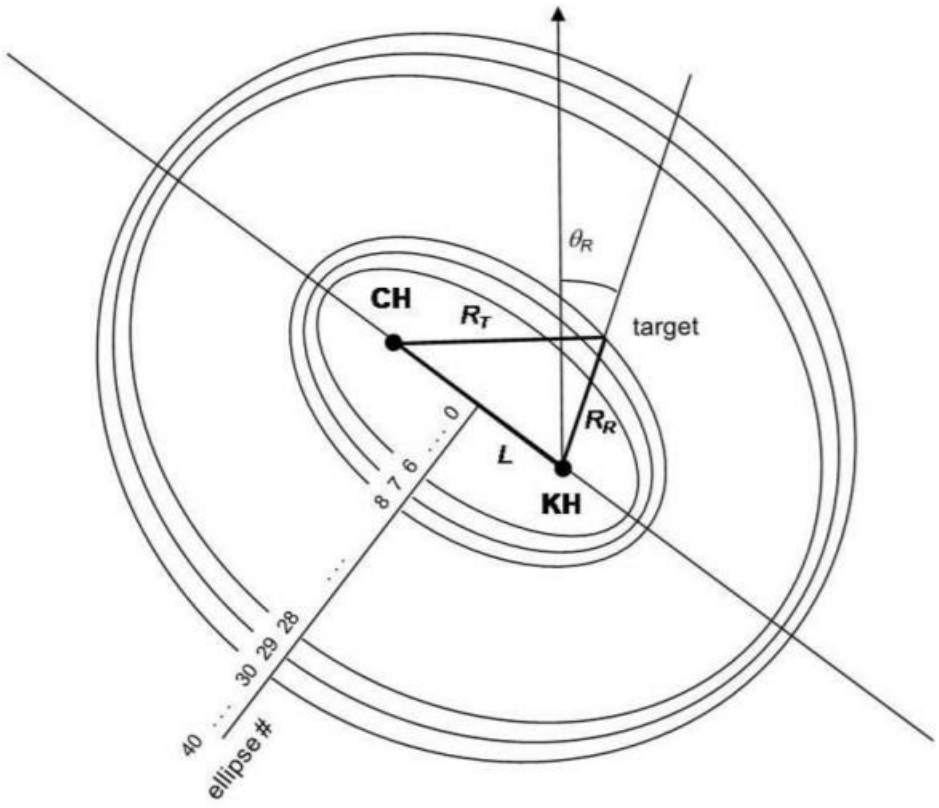

Figure 2.5: Klein Heidelberg theory of operation developed by Wachter. This figure was obtained from [11].

Moving forward 60 years to the 1990s, the NATO defense research group (DRG) began a study on passive and noise radar [8]. This study included using both commercial FM/TV signals

and non-cooperative pulsed signals as illuminators of opportunity. This seemed to create a resurgence in the development of PCL systems. Companies such as Thales, Selex, and Lockheed Martin developed and marketed commercial PCL systems which exploited FM and TV signals.

Figure 2.6: Thales HA100 PCL System Antenna. This figure was obtained from [8].

Figure 2.7: Selex Aulos PCL System. This figure was obtained from [8].

Figure 2.8: Lockheed Martin Silent Sentry PCL System. This figure was obtained from [8].

Modern PCL systems such as those shown in figures 2.6, 2.7, and 2.8 have been further developed to exploit digital broadcast signals. They provide an inexpensive, covert means of maintaining locations of aerial targets. These systems have been marketed as defense solutions, but have also been used in civilian applications. As passive radar sensor development continue to modernize, PCL systems may become an affordable, reliable alternative to traditional radar systems.

2.2 Passive Coherent Location Concepts

Passive Coherent Location (PCL) systems can be described as bistatic radar systems that exploit non-cooperative signals of opportunity to detect and track targets [12]. Research has been published describing PCL systems that exploit FM radio, digital television, cell phone, and HF

CODAR signals. Similar to traditional monostatic radar systems, PCL systems use a matched filter based on a signal's ambiguity function for range and Doppler processing [13]. A typical PCL system relies on the use of two antennas, one to receive the direct-path signal of interest, the other as a surveillance channel. In processing, the direct-path signal is subtracted from the surveillance channel, leaving only potential target responses [14]. A threshold is then applied to the remaining signals in preparation for target detection.

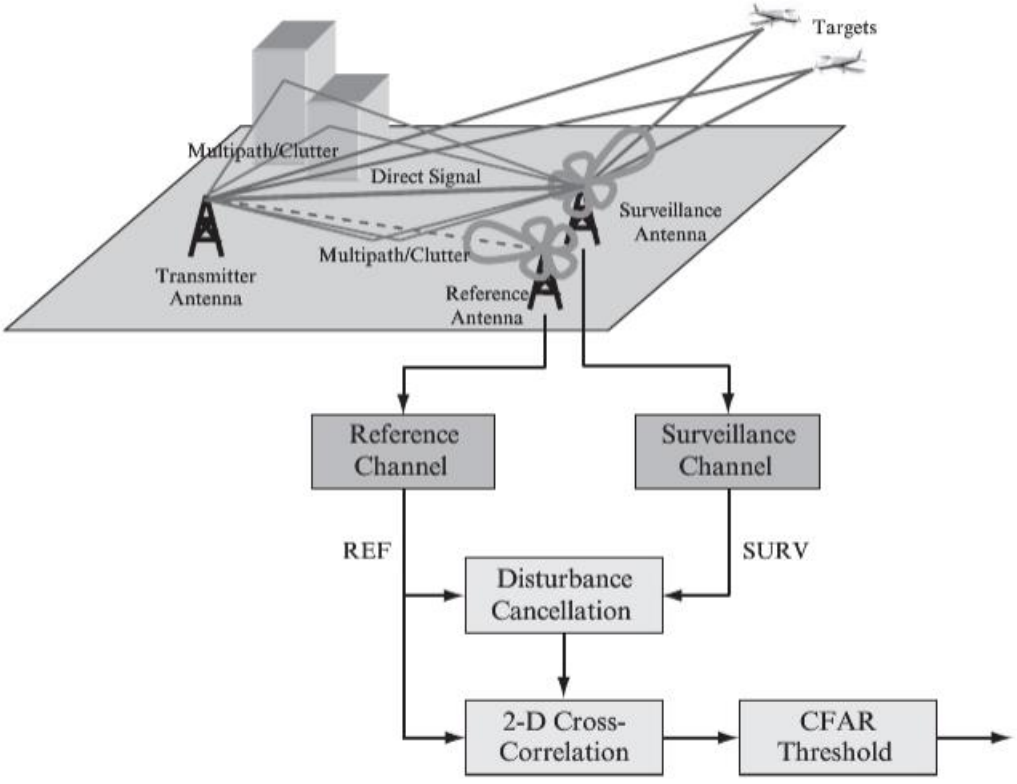

Figure 2.9: Passive Coherent Location Diagram of Operation. This figure was obtained from [15].

The following sections provide details on how PCL systems cooperate under several of the same constraints as bistatic radar. We will first discuss the bistatic radar equation, which lays the foundation for PCL principles of operation. We next discuss bistatic radar cross section and how it has advantages and disadvantages over monostatic radar. The discussion then focuses on PCL signal processing methods, signals of opportunity, and the ambiguity function. This chapter ends with a brief discussion on potential implementations of a PCL system in regards to selection of antennas and hardware.

2.2.1 Bistatic Radar Equations

The fact that PCL systems rely on transmitters of opportunity geographically separated from the receiver makes them bistatic radar systems. A diagram of two-dimensional bistatic geometry can be seen in the figure below. The diagram illustrates one of the main differences between monostatic and bistatic radar, which is the presence of two range paths and an incidence angle at the target.

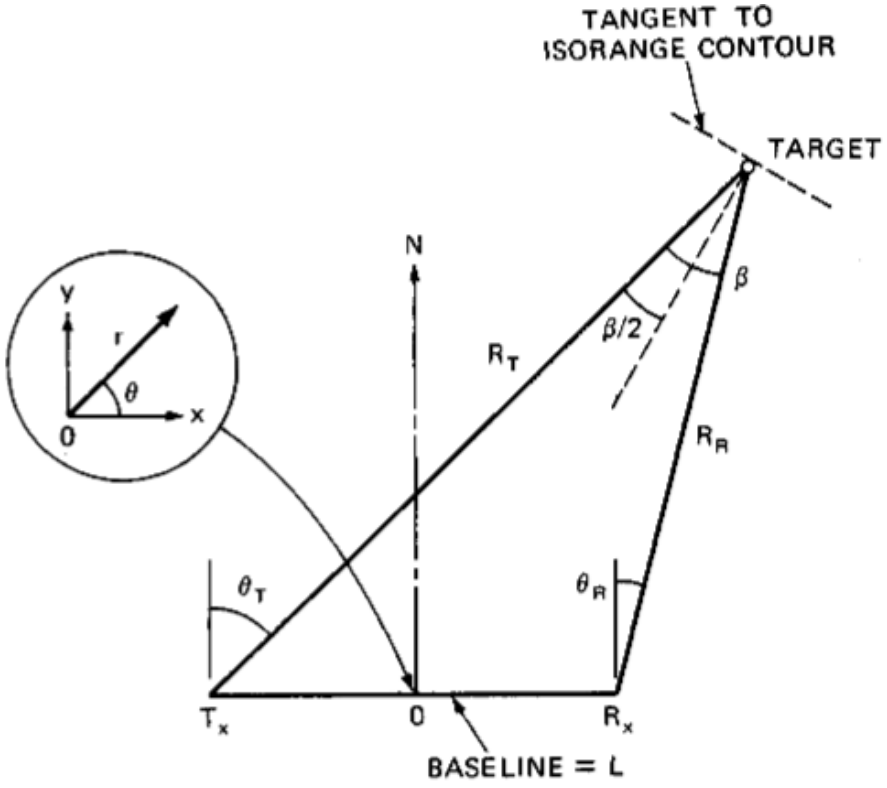

Figure 2.10: Two Dimensional Bistatic Radar geometry. This figure was obtained from [3].

From [16], the bistatic radar equation in terms of signal to noise ratio can be seen below. This equation can be used to predict performance of a bistatic PCL system.

$$\frac{P_r}{P_n} = \frac{P_t G_t}{4\pi r_1^2} * \sigma_b * \frac{1}{4\pi r_2^2} * \frac{G_r \lambda^2}{4\pi} * \frac{1}{kT_0 B_s F} * L_s \tag{2.1}$$

Where:

$P_r =$ received signal power

P_n = receiver noise power

P_t = transmit power

G_t = transmit antenna gain

r_1 = transmitter to target range

σ_b = target bistatic radar cross section

r_2 = target to receiver range

G_r = receive antenna gain

λ = signal wavelength

G_t = transmit antenna gain

k = Boltzmann′s constant

T_0 = noise reference temperature

B_s = receiver effective bandwidth

F = receiver effective noise figure

L_s = system losses (power ratio < 1)

In order to accurately predict PCL system performance using the bistatic range equation, each parameter must be well understood. The transmit power P_t can be significant for PCL systems operating in most urban areas. For example, the area of San Diego, California hosts several radio

stations with an effective radiated power of 100kW or less [17]. Broadcast digital television stations in the same region radiate 1 MW or less [18]. The radiation patterns for both is omni-directional in the horizontal plane, with tailored beams in the vertical plane to avoid wasting energy. HF signals of interest in the region include Coastal Ocean Dynamics Applications Radar (CODAR) and HF chirp sounders which typically emit 50W or less [19].

One advantage to bistatic radar systems is the increased potential for signal reflection due to bistatic geometry. PCL systems inherently take advantage of this concept by means of a receiver/antenna combination being installed separately from the transmitter of opportunity. One advantage of PCL systems is their inherent ability to take advantage of a target's bistatic radar cross section (RCS), which is usually greater than the same target's monostatic RCS [20]. This is dependent on signal frequency, aspect angel, and target geometry.

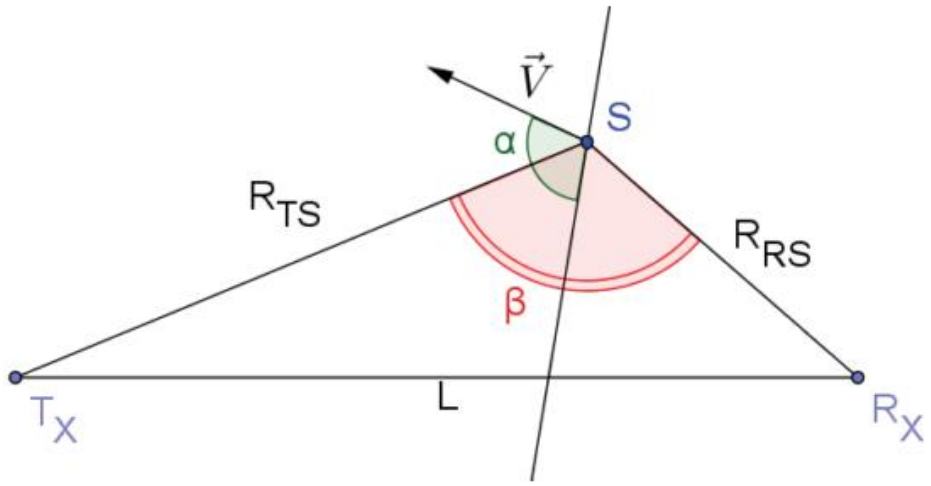

Figure 2.11: Illustration of Bistatic Angle β. This figure was obtained from [21].

Generic equations for bistatic scattering cross section are given below where R is the range between the target scatterer and receiving system.

$$\sigma_b = \lim_{R_2 \to \infty} 4\pi R_2^2 \left(\frac{Power\ per\ unit\ area\ in\ total\ scattered\ wave\ at\ receiving\ antenna}{Power\ per\ unit\ area\ in\ the\ wave\ of\ the\ incident\ target} \right) \quad (2.2)$$

$$\sigma = \lim_{R \to \infty} 4\pi R_2^2 \frac{|E^{SC}|^2}{|E^{in}|^2} \quad (2.3)$$

According to [3], there are three regions for bistatic radar cross section which are defined by the bistatic angle. The first region is the pseudo-monostatic RCS region. The basis of this region is the Crispin and Siegal monostatic-bistatic equivalence theorem which states that the monostatic and bistatic RCS for smooth targets and small wavelengths is the same. This also describes the case in which the bistatic angle β is between 0 and 40-90°. The extents of the pseudo-monostatic region are influenced by the complexity of target structure. The reflection of more complex targets reduces the actual allowed bistatic angle for this region.

The next region is known as the bistatic RCS region. This area of bistatic operation describes the condition in which the bistatic and monostatic RCS begin to disagree. From [3], Kell identifies three sources for bistatic RCS divergence from the monostatic condition. The first source is a “change in relative phase between discrete scattering centers” [3]. The second source is from reflected energy levels fluctuating due to target geometry. The third source is complete

disappearance of reflected energy from previously visible scattering centers. The second two sources describe changes in aspect angle with respect to the target, transmitter, and receiver.

The third bistatic RCS region

For a forward scatter condition, that in which the bistatic angle is 180°, the equation can be simplified to

$$\sigma_b = \frac{4\pi R^2}{\lambda^2} \tag{2.4}$$

In the forward scatter region, target reflections are potentially increased. This concept is described by Babinet's principle, which states that forward scatter from an energy absorbing target acts as an identically sized aperture [12]. Figure 2.9 below illustrates variations in the bistatic angle and bistatic radar cross section for varying frequencies in a forward scatter condition.

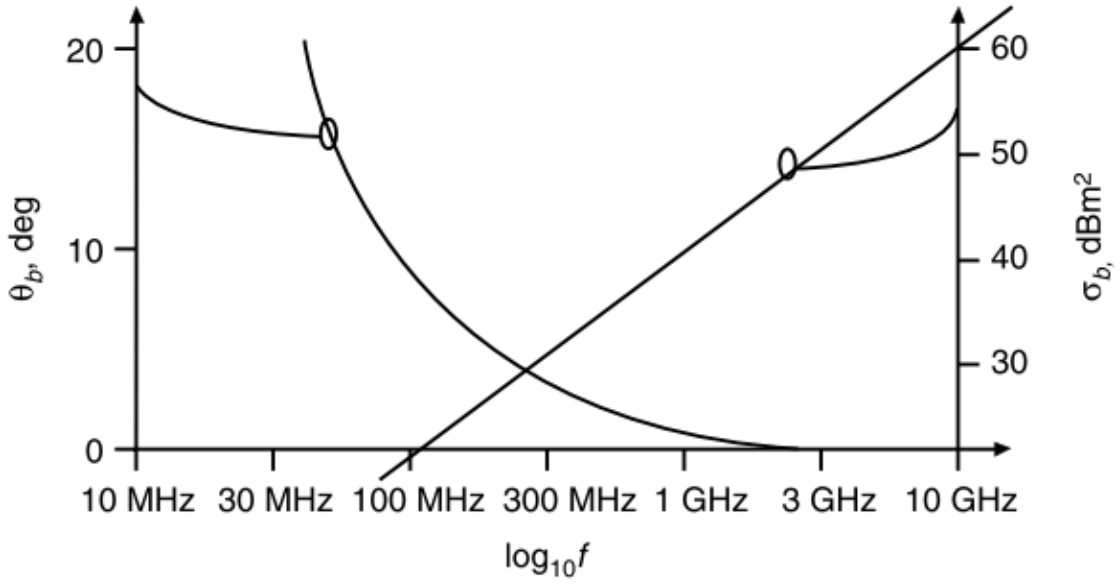

Figure 2.12: Variations of bistatic RCS and bistatic angle for a 10m^2 target versus frequency. This figure was obtained from [12].

The PCL receiver hardware and antenna also contribute to the bistatic radar equation by providing signal gain through antenna characteristics and signal processing gain. However both the receiver and antenna induce noise into the equation. For example, the noise figure of a receiver is increased as its bandwidth increases, the same can be said for an antenna. These gains and losses must be properly identified to accurately predict PCL system performance.

By rearranging terms of the bistatic radar equation in 2.1, adding terms such as integration time t_0 and solving for bistatic range, the expression can be seen in the equation below [3]:

$$(R_T, R_R)max = \left(\frac{P_t t_0 G_t G_r \lambda^2 \sigma_b}{(4\pi^3) k T_0 \left(\frac{S}{N}\right) B_s L_s}\right)^{\frac{1}{2}} \tag{2.5}$$

Where the term $(R_T R_R)max$ describes the maximum distance in which the signal is transmitted, reflected from an object, and received by a receiver geographically separated from the transmitter.

Another useful visualization of bistatic radar performance is calculation of ovals of Cassini. These shapes illustrate the maximum detection range for a bistatic radar system taking into account signal to noise ratio and assuming a constant radar cross section. If we let constant K represent the bistatic radar equation constant given in equation (2.2):

$$K = \frac{P_T G_T G_R \lambda^2 \sigma_B}{4\pi^3 k T_s B_s L_s} \tag{2.6}$$

We can then re-write equation (2.2) as

$$(R_T R_R)^2_{max} = {K}\Big/{\left(\frac{S}{N}\right)_{min}} \tag{2.7}$$

Next we convert R_T and R_R into polar coordinates:

$$R_T^2 = \left(r^2 + \frac{L^2}{4}\right) + rLcos(\theta) \tag{2.8}$$

And

$$R_R^2 = \left(r^2 + \frac{L^2}{4}\right) + rLcos(\theta) \tag{2.9}$$

Combining equations (2.5) and (2.6) results in

$$(R_T R_R)^2 = \left(r^2 + \frac{L^2}{4}\right)^2 - r^2 L^2 \cos^2\theta \tag{2.10}$$

Where the term L is the baseline length between transmitter and receiver, and angle θ is the incident angle at the target between transmit and receive beams. Rearranging terms in equation (2.4) and solving for constant signal to noise ratio yields

$$\left(\frac{S}{N}\right) = \frac{K}{\left(r^2 + \frac{L^2}{4}\right)^2} - r^2 L^2 \cos^2\theta \tag{2.11}$$

Equation (2.8) can be used to plot ovals of Cassini for constant SNR and RCS, and can be seen in Figure 2.10.

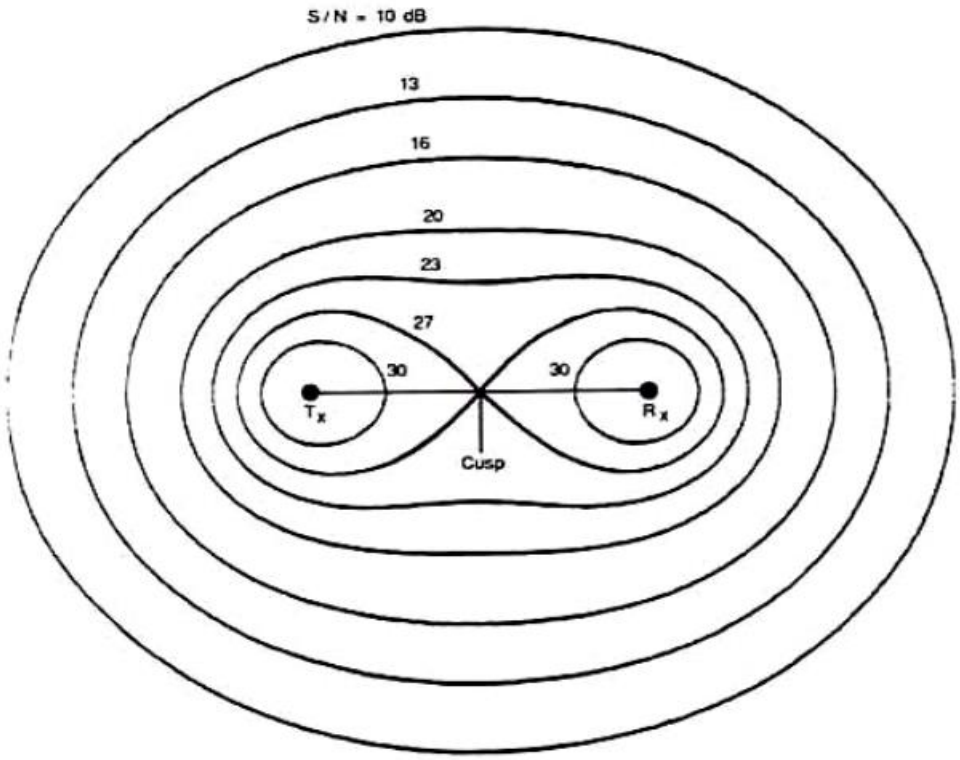

Figure 2.13: Ovals of Cassini for Constant SNR. This figure was taken from [22].

From Figure 2.10 it can be seen that there are three distinct regions of bistatic radar operation:

1. One oval (co-site): $L < 2\sqrt{K}$,
2. Two ovals (transmitter/receiver centered): $L > 2\sqrt{K}$
3. Lemniscate: $L = 2\sqrt{K}$

When the target is located between the transmitter and receiver, the bistatic angle β = 180°. This orientation is known as forward scatter [3] for both target and clutter reflections. For this

condition, target and clutter scattering differ greatly from those of other bistatic geometries, also negatively affecting precision of range and Doppler measurements. From [22], it is noted that normal bistatic radar operation is excluded from 10°-20° from the forward scattering condition. This information can be used for optimal placement of the receiving antenna in a PCL system, and will be discussed in further detail in Chapter 6.

2.2.2 PCL Signals of Opportunity and Expected Performance

There has been a fair amount of research on PCL systems using various signals. Through a search of conference proceedings, journal articles, and textbooks, it seems that broadcast FM radio and digital television are the most common illuminators of opportunity for PCL. However other signals such as GSM, HF CODARs and Sounders, and GPS have been used. This section will highlight the benefits and challenges for various signals that have been used for PCL. Table 2-1 below highlights signals parameters for several different signals often used for PCL.

Table 2-1: Parameters for PCL Signals of Opportunity [12].

Transmission	Frequency	Modulation, bandwidth	$P_t G_t$	Power density (Wm^{-2}) $\Phi = (P_t G_t)/4\pi r_1^2$
HF broadcast	10–30 MHz*	DSB AM, 9 kHz	50 MW	–67 to –53 dBW m^{-2} at r_1 = 1000 km
VHF FM (analogue)	~ 100 MHz	FM, 50 kHz	250 kW	–57 dBW m^{-2} at r_1 = 100 km
UHF TV (analogue)	~ 550 MHz	vestigial-sideband AM (vision); FM (sound), 5.5 MHz	1 MW	–51 dBW m^{-2} at r_1 = 100 km
Digital audio broadcast	~ 220 MHz	digital, OFDM 220 kHz	10 kW	–71 dBW m^{-2} at r_1 = 100 km
Digital TV	~750 MHz	digital, 6 MHz	8 kW	–72 dBW m^{-2} at r_1 = 100 km
Cellphone basestation (GSM)	900 MHz, 1.8 GHz	GMSK, FDM/TDMA/FDD 200 kHz	100 W	–81 dBW m^{-2} at r_1 = 10 km
Cellphone basestation (3G)	2 GHz	CDMA 5 MHz	100 W	–81 dBW m^{-2} at r_1 = 10 km

One of the most commonly used signals for PCL is broadcast FM radio. The FM radio band in the United States occupies the electromagnetic spectrum from 88 to 108 MHz. The effective radiated power from each transmit sites varies, but on average can be measured in the San Diego area at 100kW [17]. Each channel is allocated 200 kHz of bandwidth, however the actual bandwidth varies with signal content and typically occupies no more than 100 kHz [14]. As mentioned in [13] and [23], FM radio channel bandwidth varies with the type of content. For example the bandwidth of a radio station with mostly speech content will exhibit poor ambiguity while an FM station with jazz or similar fast temp music will have a more defined ambiguity function. This means that the best possible range resolution for a radio signal will be 750m at 200kHz bandwidth. A more reasonable figure for range resolution would be 1500-3000m for the case of 50-100 kHz bandwidth. This concept can be seen in the figures below.

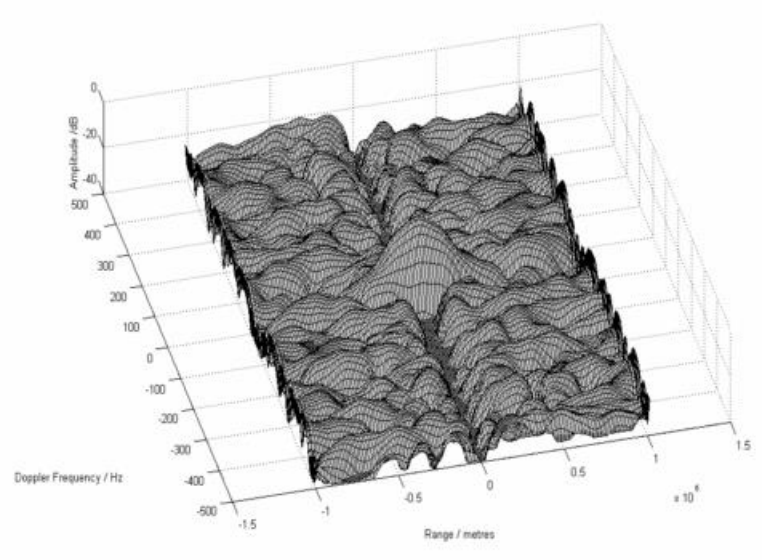

Figure 2.14: Ambiguity function for BBC radio. This figure was taken from [23].

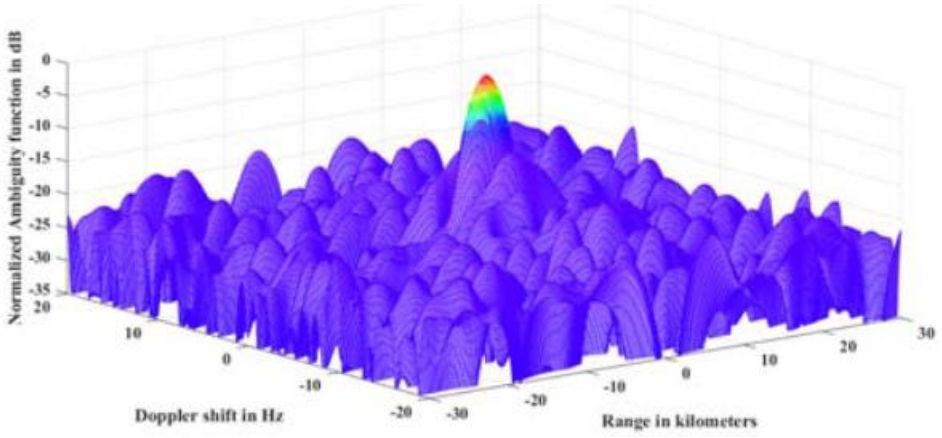

Figure 2.15: Ambiguity function for a FM radio 98.8 MHz in San Diego, CA.

Another useful signal for PCL is broadcast digital television. Digital television signals in the United States use the Advanced Television Systems Committee (ATSC) standard. The signal has a 6MHz bandwidth, and modulation depends on transmission medium. For broadcast digital

TV signals the waveform modulation is 8-level vestigial sideband (VSB). For PCL signal processing we're not concerned with modulation content, but the modulation artifacts play a role in the ambiguity function. In an ATSC broadcasting stream, there exists repetitive signals that help the 8-level VSB receiver locate and demodulate the signal. These "helper" signals include the ATSC pilot, segment sync, and field sync. In the figure below, the ambiguity function for ATSC station 494 MHz exhibits evidence of the sync signals along the range axis at zero Doppler. Another artifact of the sync lines can be seen in the Doppler axis as sidelobes at zero time delay (range). The expected range resolution for a 6 MHz ATSC signal is 25m.

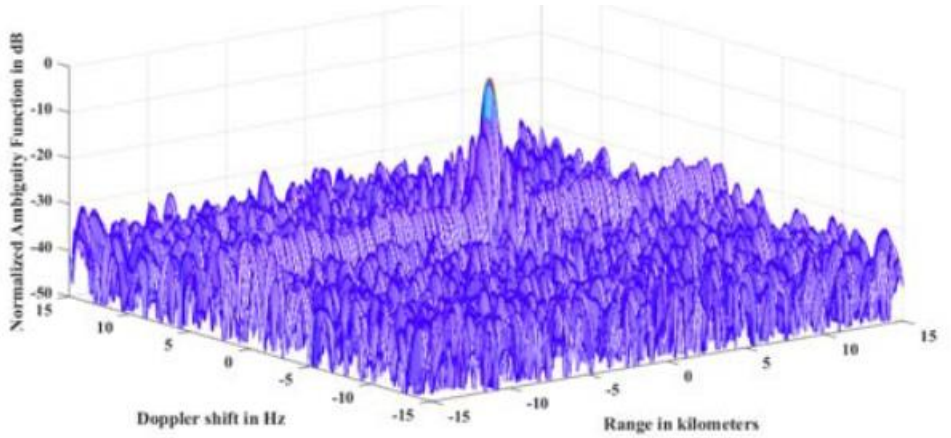

Figure 2.16: Ambiguity function for TV Station 494 MHz in San Diego, CA.

Other signals used for PCL experiments have included GSM cell phone signals [24][25] and GPS [26] [5]. The GSM based passive radar in [25] was able to exploit the 935-960 MHz GSM signal is Singapore to detect sea targets out to a range of 1km and air targets at 3.5km. The

low detection distance was cited due to low power of local tower-based GSM transmitters. The work in [24] gives more information on GSM signals near the Warsaw University on the Polish coast of the Baltic Sea. The paper lists GSM transmitter power at 100W or less with a bandwidth of 200kHz. A similar issue of using low-power emitters for PCL is documented in [5], which cites GPS power received at the earth's surface is typically -160dB. Using an aerial target RCS of 20dBsm, the authors suggest using a GPS signal for PCL is plausible. However they also mentioned that the expected signal is 18-22dB below the expected clutter. A final mention of GPS for PCL is in [26], in which the author provides further information on the 1.2 and 1.5 GHz signal. They also provide a link budget study which results in an expected received power density of GPS signals to be -117dBW/m^2. They further assume a target with 0.1 m^2 RCS 100m from the PCL receiver, which results in an expected power of -178 dBW. One final conclusion is that the receiver capable of performing PCL with GPS signals would need a sensitivity of -160 dBW.

One final signal set of discussion for consideration in PCL is HF coastal ocean dynamics applications radar (CODAR) and HF sounders. HF CODARs are typically used for ocean current measurements, and are prevalent along United States Pacific, Atlantic, and Gulf of Mexico coastlines. The signal frequency depends on the specific emitter, but generally occupies 25-100 kHz of bandwidth between 3-30 MHz. The waveform is frequency modulated continuous wave (FMCW). The ambiguity function for an HF CODAR operated by Scripps Institute of Oceanography can be seen in the figure below. The signal is at 17.6 MHz with a bandwidth of 75 kHz.

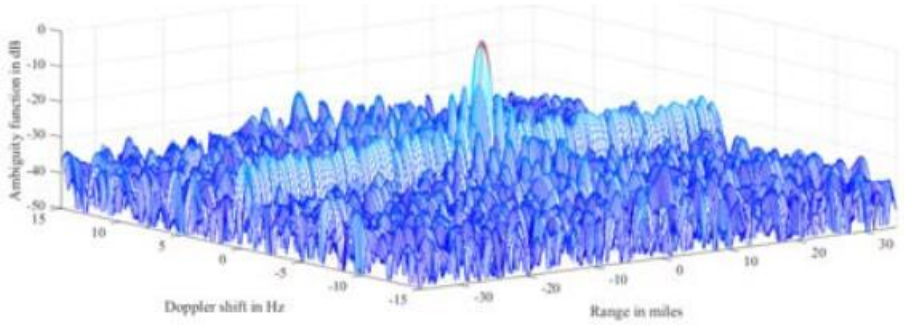

Figure 2.17: Ambiguity function for HF CODAR at 17.6 MHz in San Diego, CA.

Another group of HF signals of interest are HF sounders, which are typically used for monitoring sky-wave HF radars that reflect off of the ionosphere. They are also FMCW waveforms in the HF frequency band. Because of the small bandwidths, these HF signals give less than ideal range resolutions on the order of kilometers.

2.2.3 PCL Signal Processing

This section describes the signal processing necessary in a PCL system to detect targets. Much like monostatic radar, PCL signal processing relies on sufficient signal to noise ratios to detect targets. This can be difficult when relying on commercial non-cooperative, geographically separated transmitters with power lower than typical monostatic radars. Another similarity to monostatic radar is the process for determining range and Doppler frequency of a target, which will be discussed later in this section. One major difference between monostatic radar and PCL processing is the necessity for adaptive cancellation. Because PCL systems rely on a direct-path antenna and receiver, that signal must be removed from the surveillance channel before potential

targets can be identified. Much of this section will be dedicated to describing the different methods used to suppress unwanted signals.

The first step in PCL signal processing involves adaptively filtering the signal of opportunity being exploited. This is necessary due to the unwanted reference channel signal being present in the surveillance channel, likely at a higher amplitude than the target reflection. According to [14], cross-correlation processing would suppress the direct-path signal and restrict it to the zero range and Doppler bin. However this would not be sufficient to remove all unwanted signal content in the sidelobes. This paper also mentions that the amount of direct path signal that can be found in the surveillance channel is up to 90dB greater than the surveillance signal. Another mention of adaptive cancellation in PCL systems is in [27], which indicates the ratio of direct signal to detection signal in the surveillance channel is -74.9dB. The paper goes on to discuss that by using a least-mean-squares filter, they can recover approximately 45dB by suppressing the direct path signal. This concept is illustrated in the figure below.

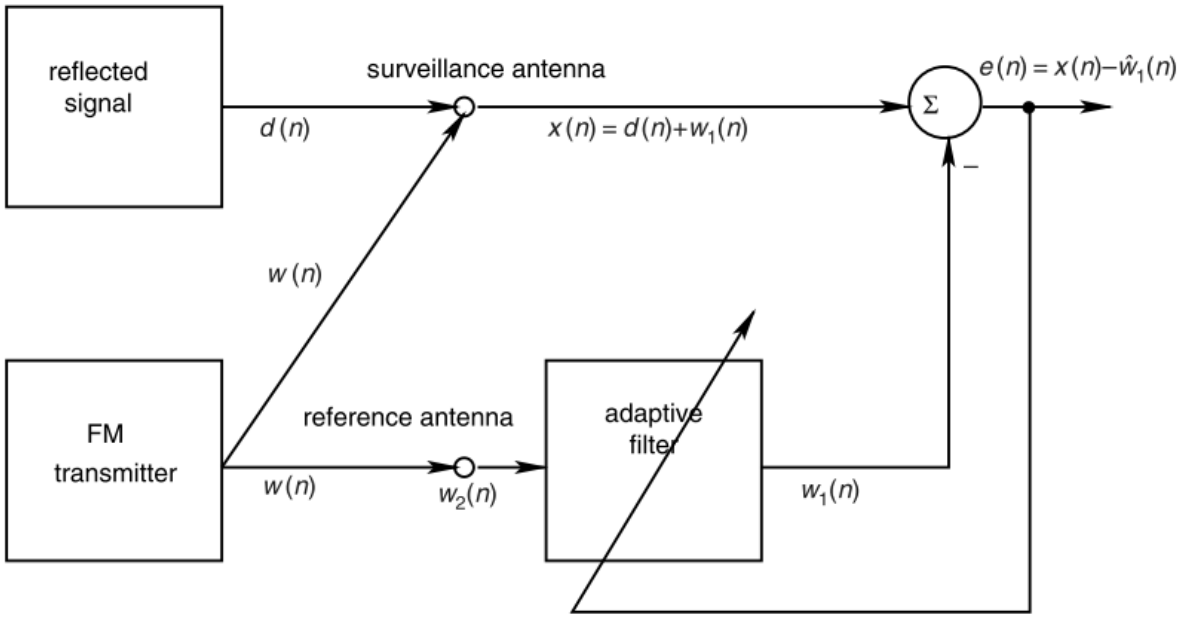

Figure 2.18: Adaptive Cancellation Diagram. This figure was obtained from [14].

There are many recursive adaptive signal processing algorithms similar to the least-mean-squares (LMS) approach, and several papers reviewed for this work indicate use of the LMS filter [28][29][30][31]. The LMS filter is categorized as a stochastic gradient method because it continuously updates the filter statistics. However in the case of PCL, both the signal and interference are measured and quantified. The research in [32] and [33] outline several potential methods for interference cancellation in PCL systems with experimental data for each.

Once the direct path signal has been suppressed to sufficient level, detection of potential targets can begin. In order to determine range of a potential target, a PCL system uses the bistatic radar range equation which can be seen below.

$$R_R = \frac{(R_T+R_R)^2-L^2}{2(R_T+R_R+Lsin\theta_R)} \tag{2.12}$$

$R_R =$ range from target to receiver

$R_t =$ range from target to transmitter

$L =$ baseline length

$\theta_R =$ angle between receiver and target

The bistatic range relationship takes into account the distance from transmitter to target and target to receiver, as well as the bistatic angles formed by those objects. For a PCL system to determine accurate range of a target, it must know when a signal was transmitted. For this reason PCL systems typically rely on a reference antenna focused on the transmitter to provide waveform timing information. This will be further discussed later in this section.

Determining a target's Doppler frequency in a PCL system involves knowing the transmitter and receiver locations, as well as the frequency of the transmitted signal. Assuming both the transmitter and receiver systems are stationary, a target's bistatic doppler is given by the relationship below.

$$f_B = \left(\frac{2V}{\lambda}\right)\cos\delta\cos\left(\frac{\beta}{2}\right) \tag{2.13}$$

$f_B =$ target bistatic doppler

$V =$ target velocity

$$\delta = \text{target aspect angle}$$

$$\beta = \text{bistatic angle}$$

In practice, a cross-correlation scheme may be implemented to determine range and Doppler of a potential target. This concept was taken from [14] and can be seen in figure 2.19 below. The idea is that the signals from both the reference and surveillance channels are cross-correlated, resulting in a spike at the target's range and Doppler frequency. However before this can happen, multiple copies of the reference channel are duplicated at different Doppler-shifted frequencies. If a target is present, the correlation properties of the surveillance channel and Doppler-shifted reference channel create a strong correlation peak corresponding to the target's range and velocity.

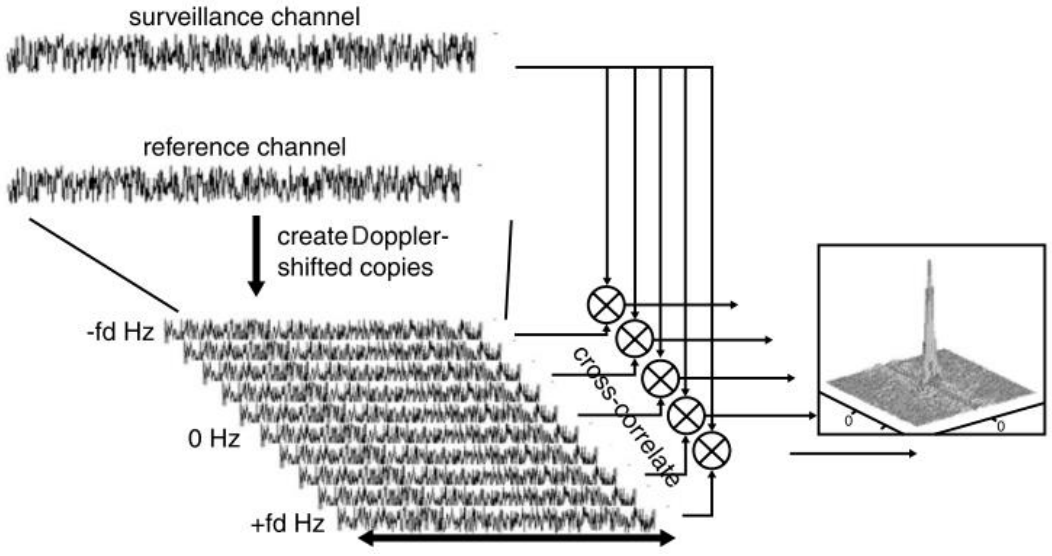

Figure 2.19: Cross Correlation to determine range and doppler. This figure was obtained from [14]

2.2.4 PCL Ambiguity Function

The ideas in this section describing the ambiguity function and data collection for PCL were originally published in [34]. The ambiguity function is a useful tool for determining the behavior of a signal with respect to sidelobe levels, channel bandwidth, and resolution in both range and Doppler [35]. It is typically used in traditional radar waveform applications as a measure of capabilities in terms of object detection, rejection of clutter, range and Doppler resolution, accuracy of measurements, and overall ambiguity [4] [15]. However in passive radar systems, several of these features can be determined in near real-time through calculation of a signal's ambiguity function. To increase the chances of detection and discrimination of closely-spaced targets, a radar waveform designer defines qualitative traits as range resolution, peak-to-sidelobe ratio, and integrated sidelobe ratio [13].

The calculation of an ambiguity function is performed by passing a waveform through its own matched filter. In the case of passive radar, we define this as autocorrelation because we correlate a signal of interest with itself. For the monostatic case, the ambiguity function is defined in [24] as

$$|X(\tau, f)^2| = \left|\int_{-\infty}^{\infty} s_t(t) s_t^*(t-\tau) e^{j2\pi f t} dt\right|^2 \tag{2.14}$$

where $X(\tau, f)$ is the ambiguity function dependent on time delay (τ) and Doppler frequency (f), and s*(t)* represents a complex baseband signal.

In [36], Tsao formulates a different equation for the bistatic case, making the argument that time delay and Doppler frequency are not linear functions of range and velocity because of geometric considerations. His proposed ambiguity function is

$$|X(R_{RH}, R_{Ra}, V_a, \theta_R, L|^2 \tag{2.15}$$

$$= \left| \int \tilde{f}\big(t - \tau_a(R_{Ra}, \theta_R, L)\big)\tilde{f}'(\big(t - \tau_a(R_{Ra}, \theta_R, L)\big) exp\big[-j\big(\omega_{DH}(R_{RH}, V_H, \theta_R, L) - \omega_{DA}(R_{Ra}, V_a, \theta_R, L)\big)t\big]dt \right|^2$$

which incorporates bistatic range, angles, and radial velocities from the positions of both the transmitter and receiver. Tsao also shows through simulation that the bistatic ambiguity function shape is dependent on the bistatic geometry, meaning that range and Doppler resolutions will also vary. Taking into account bistatic geometry is important for characterizing situations when tracking or searching for a target, or when using multiple geographically separated transmitters of opportunity. For this section we rely on the monostatic ambiguity function calculation due to the fact that we are not performing target detection, only analyzing a signal based on its autocorrelation function.

The most obvious characteristic when searching for useful signals is amplitude. The amplitude of the calculated ambiguity function can be increased by lengthening the coherent processing interval (CPI). It can be seen in Figure 3 below that doubling the number of samples used in the autocorrelation increases the amplitude by 3dB. The disadvantage of increasing the CPI is the chance that a fast moving target will migrate through range bins quicker than a detection can be made.

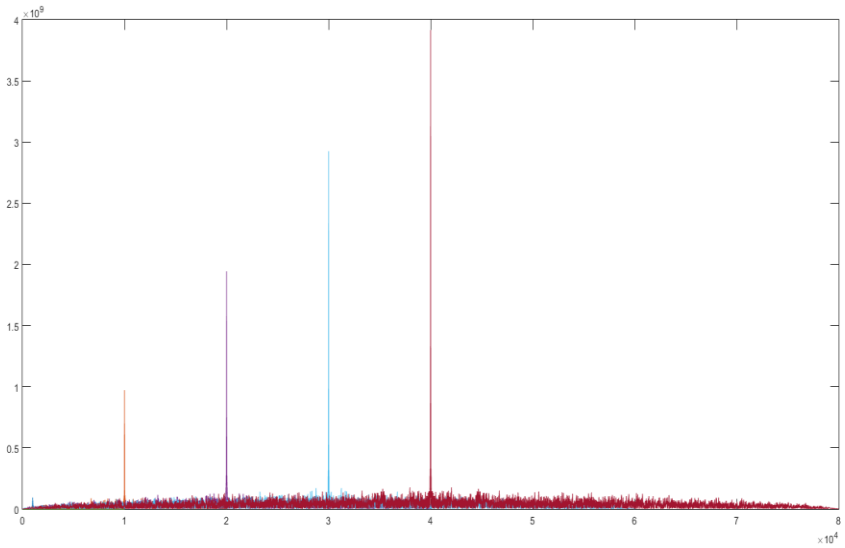

Figure 2.20: Comparison of increasing ambiguity function amplitude for 1000, 10,000, 20,000, 30,000, and 40,000 samples

Another feature that must be studied is the leakage of direct path signal into the surveillance channel. For this reason we can use an adaptive filter to cancel the unwanted signal. However at some azimuths within 90° of the transmit location, it may be difficult to remove the direct path signal without physical isolation between receive antennas.

Another feature that can be derived from the ambiguity function is range resolution. The range resolution τ for a given signal of opportunity is determined by the relationship given in (3):

$$\Delta R = \frac{c}{2B} \tag{2.16}$$

where c equals the speed of light and B is the signal bandwidth. For example, the majority of FM radio channels are allocated 200 kHz of bandwidth. This corresponds to a relative range resolution of 750 meters. However in reality most FM channels do not use all 200 kHz of bandwidth constantly, so the range resolution will vary in time with respect to modulation of the channel. Results presented in [9] illustrate this concept.

The Doppler resolution in a PCL system is largely dependent on the frequency of the signal and is given by the relationship

$$\Delta f = \frac{2v}{c} * f_c \tag{2.17}$$

The Doppler resolution is also dependent on the modulation content of the signal. Depending on the application, a more realistic approach may be to consider integration time t_i instead of frequency. In that case we can use the relationship from [24] seen below for velocity resolution calculation.

$$\Delta v = \frac{2\lambda}{t_i} = \frac{2c}{t_i f} \tag{2.18}$$

The sidelobe levels of the ambiguity function will indicate a signals ability to resolve a target response in both the range and Doppler dimensions. Two metrics we will use to characterize a signal's abilities are peak to sidelobe ratio (PSLR) and integrated sidelobe ratio (ISLR). PSLR shows a signals ability to resolve targets with various amplitude responses in the same range bin. ISLR indicates a signal's ability to resolve multiple targets in the same range cell. The equations for PSLR and ISLR are given below [37]:

$$PSLR = \frac{1}{A_0^2}\max\{A_n^2\}, n \neq 0 \tag{2.19}$$

$$ISLR = \frac{1}{A_0^2}\sum_{n=1}^{N}\{A_n^2\} \tag{2.20}$$

The first set of ambiguity functions for analysis are from the local HF CODAR. The calculated ambiguity function for these signals are presented in Figures 4 and 5. The 5.3 MHz CODAR signal has a bandwidth of 25 kHz, compared to the 17.6 MHz signal bandwidth of 75 kHz. This means that the 17.6 MHz CODAR will have a better range resolution (2 km) compared to the 5.3 MHz signal (6 km). Also, by using the HF signals, we are able to resolve target velocities between approximately 6 and 28 m/s.

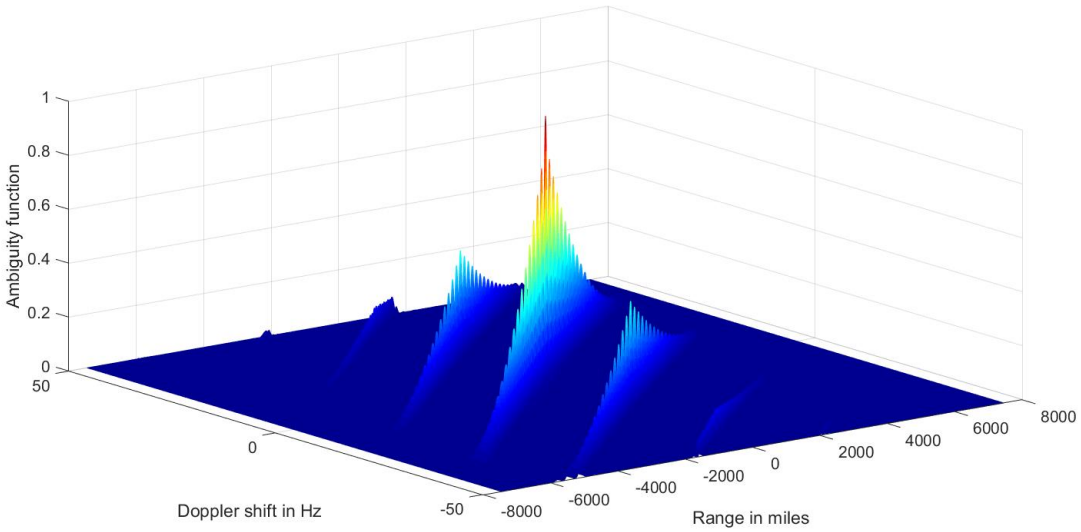

Figure 2.21: Ambiguity function for HF CODAR at 5.3 MHz in San Diego, CA.

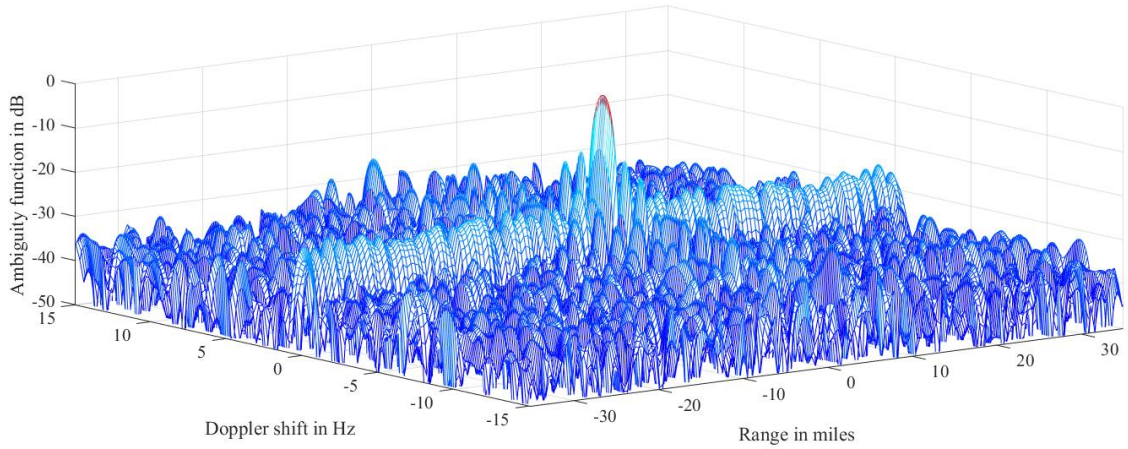

Figure 2.22: Ambiguity function for HF CODAR at 17.6 MHz in San Diego, CA.

The next set of signals collected were broadcast FM radio signals. The ambiguity functions for two FM radio signals can be seen in Figures 6 and 7. Both of these channels are allocated 200 kHz bandwidth, however the most we observed was roughly 100 kHz. This corresponds to a range resolution span of 750-1500m.

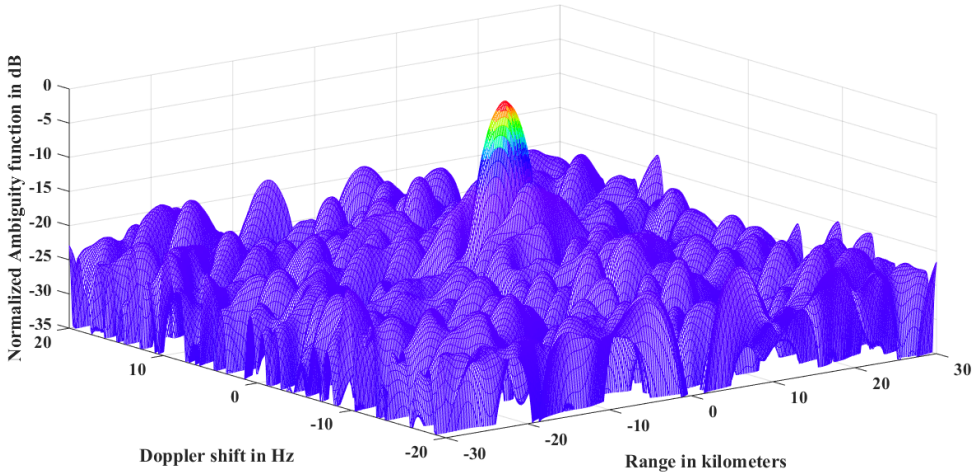

Figure 2.23: Ambiguity function for FM Radio 98.8 MHz in San Diego, CA.

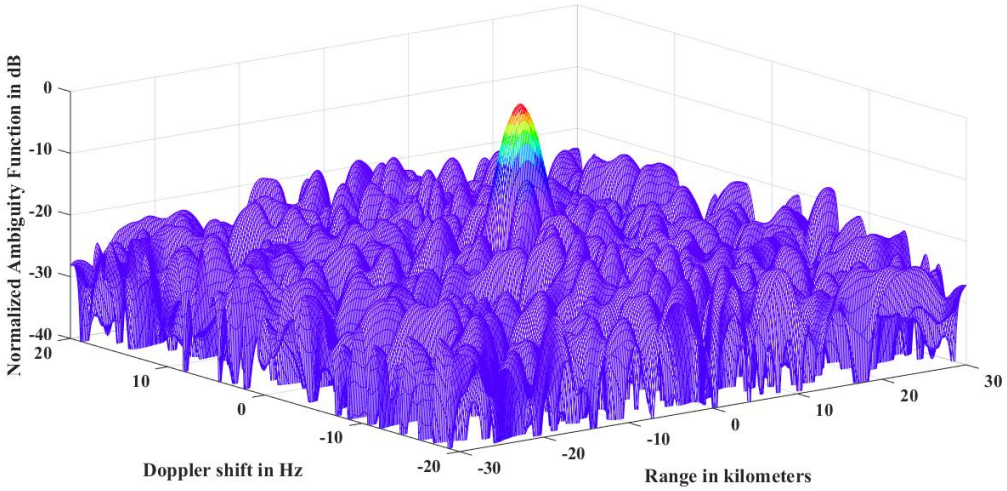

Figure 2.24: Ambiguity function for FM Radio 101.5 MHz in San Diego, CA.

The last set of collected signals were broadcast HDTV channels. The ambiguity functions can be seen in Figures 8 and 9. The allocated bandwidth of an HDTV channel is 6 MHz. This corresponds to a best possible range resolution of 25m.

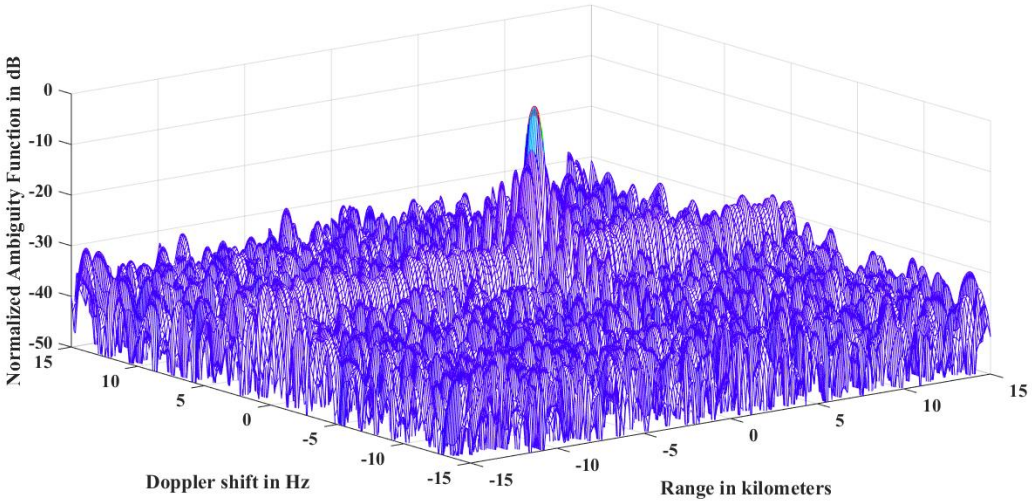

Figure 2.25: Ambiguity function for HDTV Station 494 MHz in San Diego, CA.

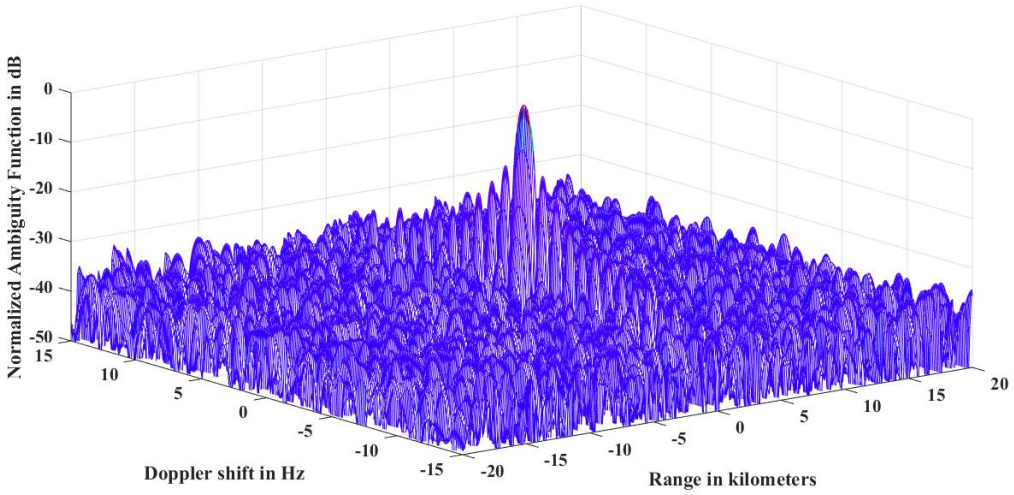

Figure 2.26: Ambiguity function for HDTV Station 500 MHz in San Diego, CA.

Table II summarizes the characteristics of each collected signal. It can be seen that the main driver for range and Doppler resolution for this signal set is frequency.

Table 2-2: Comparison of PCL signals' ambiguity functions.

Features	5.3 (HF)	17.6 (HF)	98.8 (FM)	101.5 (FM)	495 (HDTV)	500 (HDTV)
Range Resolution (m)	6000	2000	750	750	25	25
Velocity Resolution (m/s)	28.3	5.88	1.52	1.48	0.30	0.3
PSLR (range dimension)	.97	.95	1.25	1.23	1.17	1.19
ISLR (range dimension)	0.9	0.89	1.43	1.45	1.52	1.53

2.2.5 PCL Hardware and Antennas

This section describes the necessary hardware to perform PCL processing using methods described previously in this chapter. Relying on the fact that PCL requires at least two antennas, and that we are interested in resolving targets in time, frequency, and spatial domains, the antenna network must have a somewhat directional quality. This could be a circular array to direction-find the target or two directional antennas with sufficient gain to discriminate targets.

The antenna requirement for a PCL system can vary with the intended application. Several commercial PCL systems such as those from Thales, Selex, and Lockheed Martin use a circular array [8] for 360 degree coverage. Other experimental systems such as the ones described in [28] and [38] utilize two directional antennas with high directivity. The circular array would be more suitable for an operational PCL system in which full coverage was desired. This would allow for a more broad selection of transmitters and surveillance area.

The receiver system for performing PCL has several requirements based on a literature search and prior experience designing and building a PCL system. A first requirement is the ability to tune to the appropriate frequency, while adequately filtering out of band signals. Several papers including [31] and [39] describe the use of commercial software defined radios as a receiver system. Others such as [40] and [41] outline the design of specialized receivers and processors for PCL.

CHAPTER 3: PCL DATA COLLECTION AND ANALYSIS

In this chapter we present several recorded signals including HF CODAR, FM radio, and HDTV and their corresponding ambiguity functions. We will individually analyze each one to illustrate the effects each signal has on target detection capabilities. Features to be examined include range, Doppler resolution, peak side-lobe level ratio (PLSR) and integrated sidelobe ratio (ISLR). Lastly, we demonstrate a target response within an implemented PCL system. Parts of this chapter were previously published by Johnson et al in [34].

The scenario geometry for the proposed PCL system is depicted in Fig. 1. The collection site is located on the cliffs of Point Loma peninsula, located in San Diego. The sets of transmitted signals and their locations are also depicted in the figure. The first set of signals to be captured are from two local, high-frequency (HF) coastal ocean dynamics applications radars (CODAR) controlled by Scripps Institute of Oceanography. These signals were recorded at 5.3 (SDSL) and 24 MHz (SDPL). The second signals came from the FM Radio Stations 98.8 and 101.5 MHz, which are located 25 miles southeast of the collection site. The Effective Radiated Power for both is 50 kW and each has an omni-directional pattern. The broadcast TV stations at 497 MHz and 500MHz are located 18 miles directly east of the collection site which has a broadcast ERP of 355 and 328kW, respectively. At the collection site, two directional antennas were utilized. One antenna was pointed toward 135° (SE) and the other toward 80° (ENE). Collections were performed in clear weather conditions during the daytime.

Figure 3.1: PCL geometry for signal collection in San Diego, CA. Map data taken from 2016 INEGI, SIO, NOAA, U.S. Navy, NGA, GEBCO, 2016 Google, USGS.

3.1 Prototype PCL System

The data for this section was collected using two software defined radios (SDR) and a pair of matched log-periodic antennas. The SDRs were GPS synchronized during RF data collection. Figure 3.2 shows the schematic for signal collection ad PCL processing using one signal. Figure 3.3 illustrates the hardware schematic used for multiple signal PCL processing.

For the signal collections, we utilized two Channel Master CM3016 log periodic antennas with a 75 Ohm balun (300-75 ohms), matched to 50 Ohms (Pasternak). The matched Antennas were then connected to an SDR Ettus URSP N210 with a Basic RX daughterboard and GPS. The SDRs were connected via gigabit Ethernet to a Linux PC (Ubuntu 14.04) and GPS antenna. A python/C++ script acted as a trigger synchronizing the GPS and the PC clock. The triggered collections were stored on the PC for post processing, See Table 3-1 for Hardware and software specifications.

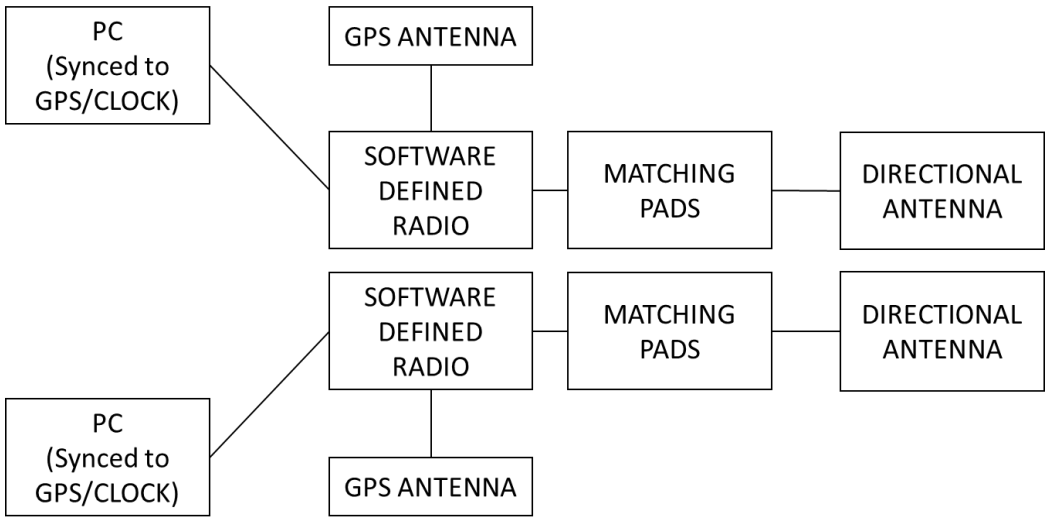

Figure 3.2: Experimental PCL system block diagram – one signal.

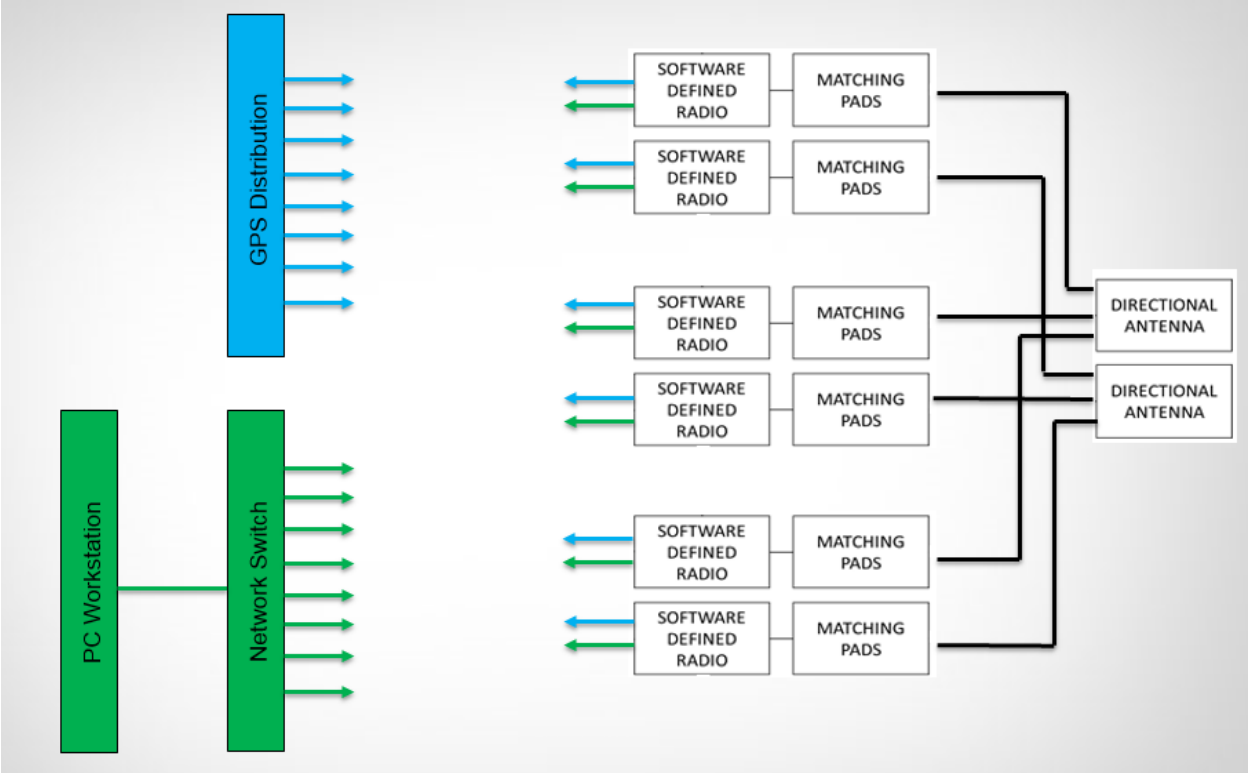

Figure 3.3: Experimental PCL system block diagram-three signals.

The selected sample rate for the synchronous FM collections were 2.4 mega samples per second at FM frequencies of 101.1 MHz and Bandwidth of 2.4MHz, the durations of collections ranged from 20-30 seconds.

Table 3-1: Experimental PCL system hardware and software.

HARDWARE	
Device	**Model**
Software Defined Radio (2)	USRP N210/BasicRx/GPS
Antenna (2)	Channel Master, CM3016
PC (2) – Lu	Intel NUC i7
Matching Pads (2)	75-50 Pasternak
GPS Antennas (2)	GPS-00464 (Sparkfun)
Cables (2)	RG-9 Coax Cable
SOFTWARE	
GNU RADIO, C, Python, OCTAVE, MATLAB OS: Ubuntu 14.04	

Once the data were collected for all signals of interest, analysis was performed with post-processing methods including calculation and analysis of each signal's ambiguity function.

In order to verify potential target information, another software defined radio was used to capture automatic dependent surveillance broadcast (ADS-B) information from aircraft in the San Diego area. The ADS-B feed provides information such as altitude, speed, heading, position, and other identifying features such as carrier and flight number. A sample of ADS-B data is shown in the figure below. The data is decoded using commercially available software and displayed on Google Maps.

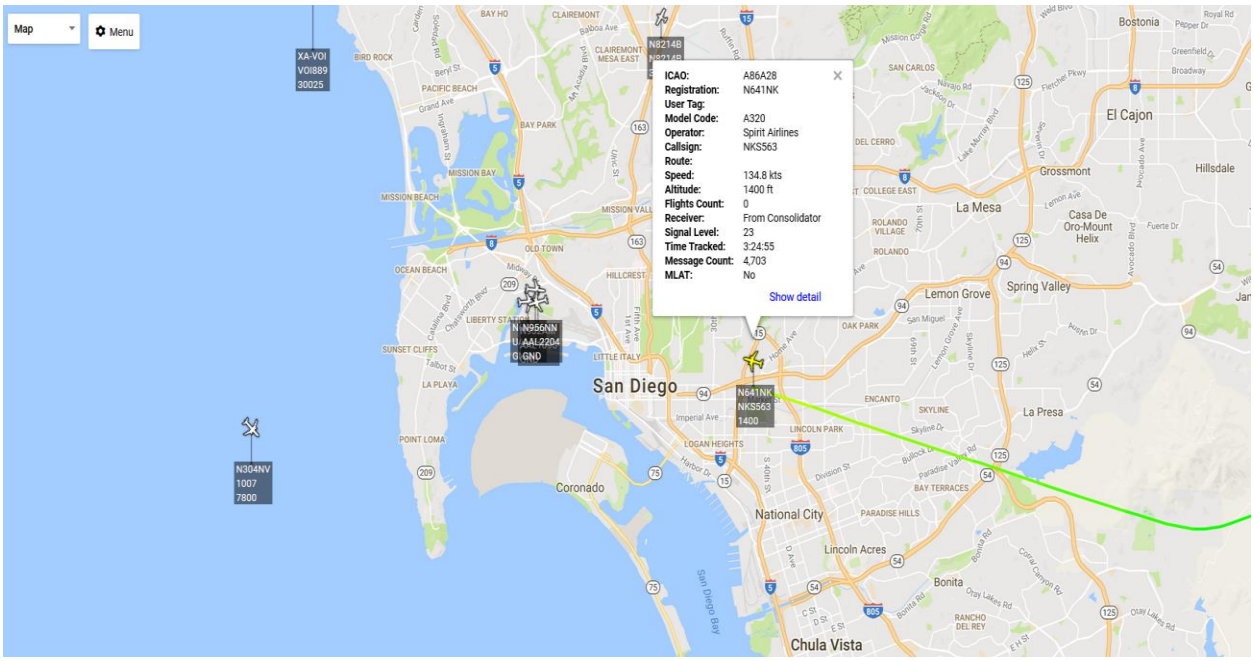

Figure 3.4: ADS-B data captured in San Diego, CA. Map data taken from 2017 Google.

To obtain information on signals of opportunity, data were captured from several sources. For HF CODAR and Sounder data including transmit sites, frequencies, radiated power, and coverage, data were recorded from the website at [19]. For similar information on FM radio signals, data were captured from the website at [17]. Further information on FM radio and digital TV transmitters was found at [42].

3.2 PCL Signal Collection and Ambiguity Function Analysis

The ambiguity function is used in traditional radar waveform applications as a measure of capabilities in terms of object detection, rejection of clutter, range and Doppler resolution, accuracy

of measurements, and overall ambiguity [1, 12]. However in passive radar systems, several of these features can be determined in near real-time through calculation of a signal's ambiguity function. To increase the chances of detection and discrimination of closely-spaced targets, a radar waveform designer defines qualitative traits as range resolution, peak-to-sidelobe ratio, and integrated sidelobe ratio [13].

The calculation of an ambiguity function is performed by passing a waveform through its own matched filter. In the case of passive radar, we define this as autocorrelation because we correlate a signal of interest with itself. For the monostatic case, the ambiguity function is defined in [15] as

$$|X(\tau, f)^2| = \left|\int_{-\infty}^{\infty} s_t(t) s_t^*(t-\tau) e^{j2\pi f t} dt\right|^2 \tag{3.1}$$

where $X(\tau, f)$ is the ambiguity function dependent on time delay (τ) and Doppler frequency (*f*), and s*(t)* represents a complex baseband signal.

In [6], Tsao formulates a different equation for the bistatic case, making the argument that time delay and Doppler frequency are not linear functions of range and velocity because of geometric considerations. His proposed ambiguity function is

$$|X(R_{RH}, R_{Ra}, V_a, \theta_R, L|^2 \tag{3.2}$$

$$= \left| \int \tilde{f}\big(t - \tau_a(R_{Ra}, \theta_R, L)\big)\tilde{f}'(\big(t - \tau_a(R_{Ra}, \theta_R, L)\big) exp\big[-j\big(\omega_{DH}(R_{RH}, V_H, \theta_R, L) - \omega_{DA}(R_{Ra}, V_a, \theta_R, L)\big)t\big]dt \right|^2 \tag{3.3}$$

which incorporates bistatic range, angles, and radial velocities from the positions of both the transmitter and receiver. Tsao also shows through simulation that the bistatic ambiguity function shape is dependent on the bistatic geometry, meaning that range and Doppler resolutions will also vary. Taking into account bistatic geometry is important for characterizing situations when tracking or searching for a target, or when using multiple geographically separated transmitters of opportunity. For this section, we rely on the monostatic ambiguity function calculation due to the fact that we are not performing target detection, only analyzing a signal based on its autocorrelation function.

The most obvious characteristic when searching for useful signals is amplitude. The amplitude of the calculated ambiguity function can be increased by lengthening the coherent processing interval (CPI). It can be seen in Figure 3.5 below that doubling the number of samples used in the autocorrelation increases the amplitude by 3dB. The disadvantage of increasing the CPI

is the chance that a fast moving target will migrate through range bins quicker than a detection can be made.

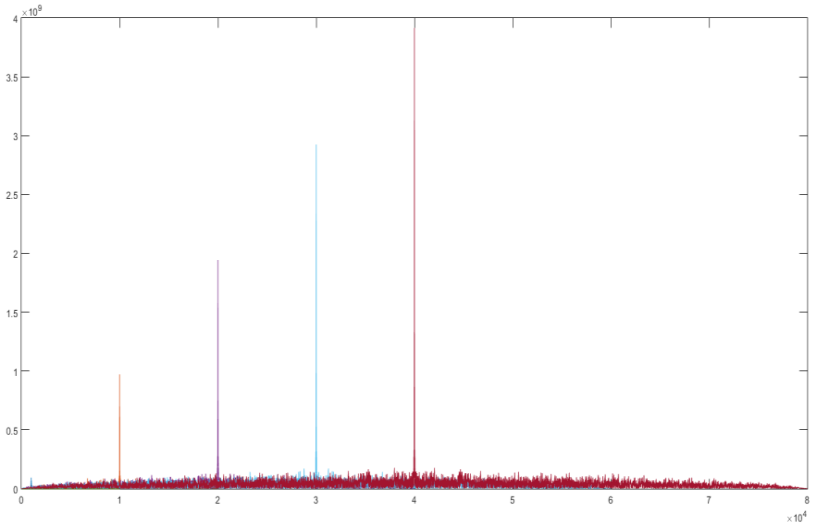

Figure 3.5: Comparison of increasing ambiguity function amplitude for 1000, 10,000, 20,000, 30,000, and 40,000 samples.

3.3 PCL System Target Detection Experiments

The PCL system described in sections 3.1 and 3.2 was used to detect commercial airline traffic landing at San Diego International Airport (SAN). The map in figure 3.6 below shows the geometry of the prototype PCL system, FM radio transmitter location, antenna boresights, and flight path of aircraft. Note the transmitter location was chosen based on its ideal geometry for PCL target detection, which will be discussed in Chapter 4.

Figure 3.6: PCL experiment geometry. Map data taken from 2016 INEGI, SIO, NOAA, U.S. Navy, NGA, GEBCO, 2016 Google, USGS.

The predicted SINR plots are shown in figure 3.7. This illustrates the concepts of ovals of Cassini mentioned in Chapter 2. From the figure, it can be seen that the highest levels of SINR are in locations near the FM transit tower and the PCL system.

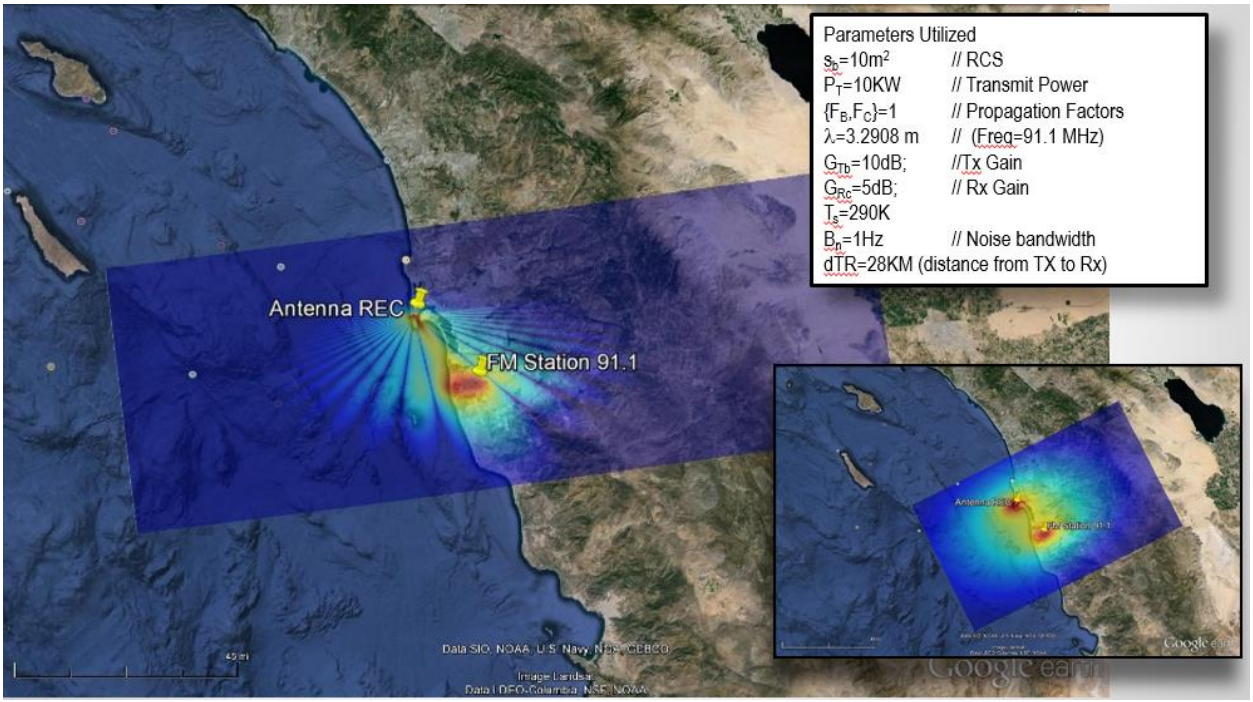

Figure 3.7: SINR map for San Diego PCL collection. Map data taken from 2016 INEGI, SIO, NOAA, U.S. Navy, NGA, GEBCO, 2016 Google, USGS.

Prior to attempted detection of targets, the bistatic radar equation was used to predict the received power levels from targeted aircraft. The parameters in the table below indicate parameters of the PCL system, FM and digital TV transmitters, and assumptions for losses and target RCS. The FM radio and TV data were taken from [17]. Assumed target RSC data were taken from [3]. The target range estimate was taken from ADS-B flight data.

Table 3-2: Calculated values using the bistatic radar equation.

	$P_t G_t$ (dB)	G_r (dB)	λ^2	σ_1 (dBsm)	R_t	R_r	*Cable Loss (dB)*	P_r *(dB)*
FM 91.1 MHz	50	30	11	16	30km	25km	2	-24.2
TV 497 MHz	49	30	0.4	16	30km	25km	4.5	-41.1

The target detection for an aircraft landing at San Diego International airport using FM radio station 91.1 MHz can be seen in figures 3.8 and 3.9 below.

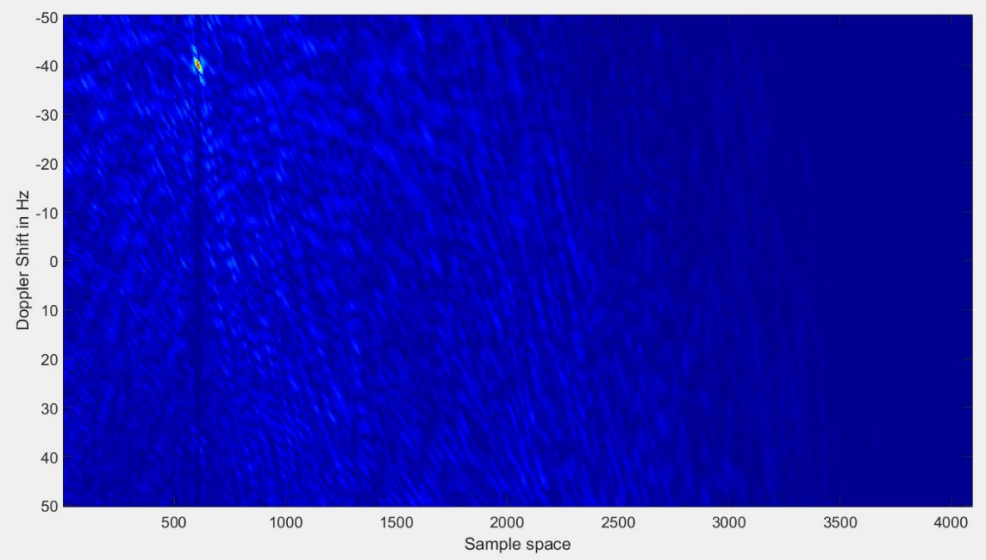

Figure 3.8: Range/Doppler response for aircraft landing at San Diego International Airport using FM 91.1 MHz.

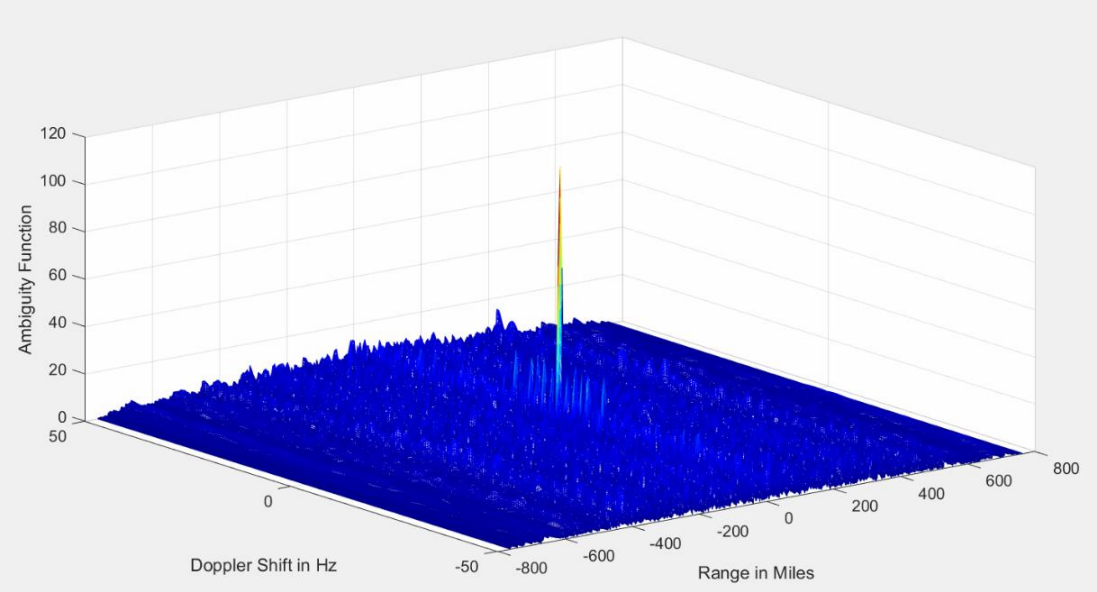

Figure 3.9: Range/Doppler response for aircraft landing at San Diego International Airport using FM 91.1 MHz.

The target detection for an aircraft landing at San Diego International airport using digital TV station 497 MHz can be seen in figures 3.10 and 3.11 below.

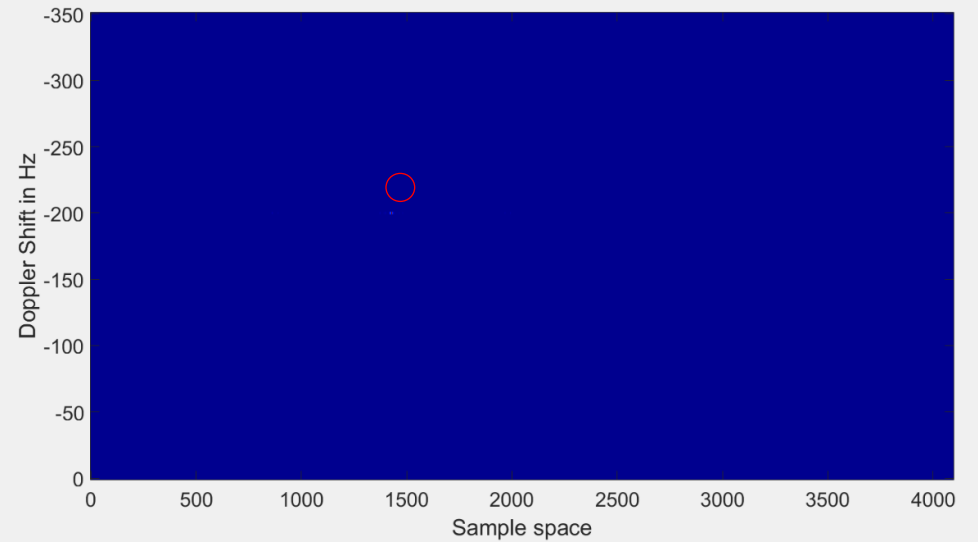

Figure 3.10: Range/Doppler response for aircraft landing at San Diego International Airport using digital TV 497 MHz.

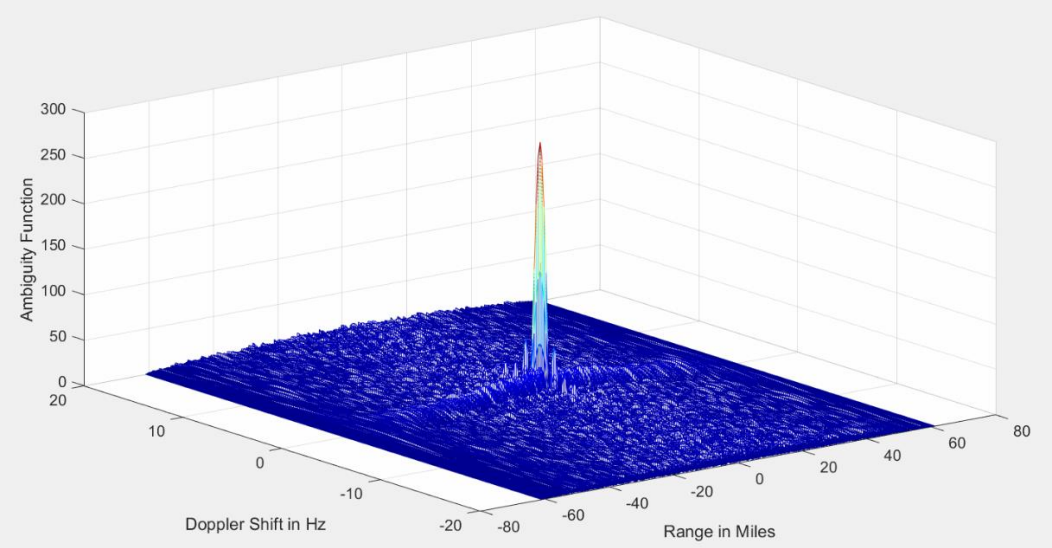

Figure 3.11: Range/Doppler response for aircraft landing at San Diego International Airport using digital TV 497 MHz.

Once actual data were received for this experiment, they were recorded in table 3-3 and compared to the theoretical data from table 3-2. The reason for discrepancies between actual and calculated received power is due to actual system and atmospheric losses as well as actual versus assumed target radar cross section.

Table 3-3: Actual values for PCL target detection.

	Bandwidth	t_i	*Surveillance Channel* $Gain = Bt_i$ *(dB)*	*Power Received (dB)*	*Power Expected (dB)*
FM 91.1	50kHz	25ms	31	-28.7	-24.2
TV 476	6MHz	1ms	37.8	-46.3	-41.1

This experiment was a demonstration of the designed and developed prototype PCL system that will be used for experiments in chapters 4, 5, and 6. This shows that this prototype PCL system can collect FM radio and digital TV signals and detect targets within theoretical expectations.

CHAPTER 4: GEOMETRIC CONSIDERATIONS FOR PCL SYSTEMS

In [43], Jackson defines the geometry for bistatic radar systems and mentions several advantages and disadvantages due to the geometry. He discusses the derivations for constant range and echo power, effects of beamwidth on range resolution cells and pulse repetition frequency (PRF), and the problem of using separated transmitters and receivers to detect targets. He concludes that the main driver of bistatic system performance is the angle between the transmitter, target, and receiver.

In [36], [44] and [45], Tsao et al discuss geometric considerations for a bistatic radar system using a Gaussian pulsed waveform. He gives a mathematical formulation for bistatic range and Doppler calculation. He goes beyond the traditional bistatic range and Doppler equations to include geometric relationships between transmitter, receiver, and airborne targets. He further defines his method for detecting a target using his formulated bistatic ambiguity function with several examples.

Following Tsao, Chen et al expand on the bistatic ambiguity function in [46] to include examples of a square pulse. He experimented with multiple geometries between transmitter, receiver, and target to illustrate the non-linear effects of bistatic geometry on range and Doppler.

In this chapter, we expand on this previous work to further define the bistatic ambiguity function for PCL systems. The novelty of this approach is the fact that PCL systems generally rely on continuous wave (CW) signals, as opposed to pulsed signals shown by Tsao and Chen. We formulate mathematical relationships that show linear and non-linear detection zones for range and

Doppler. We also show the ambiguity function for several cases in which the bistatic angle is varied. Finally we present a graphical representation of linear and non-linear regions for relationships between bistatic range, angle, and Doppler frequency.

4.1 Range Ambiguity of PCL Systems

In a monostatic radar system an object's range (R) is a linear relationship to the radar signal's two-way propagation time delay, τ.

$$\tau = \frac{2R}{c} \tag{4.1}$$

As shown in Figure 2, for the bistatic case, geometry between transmitter, receiver, and target must be considered.

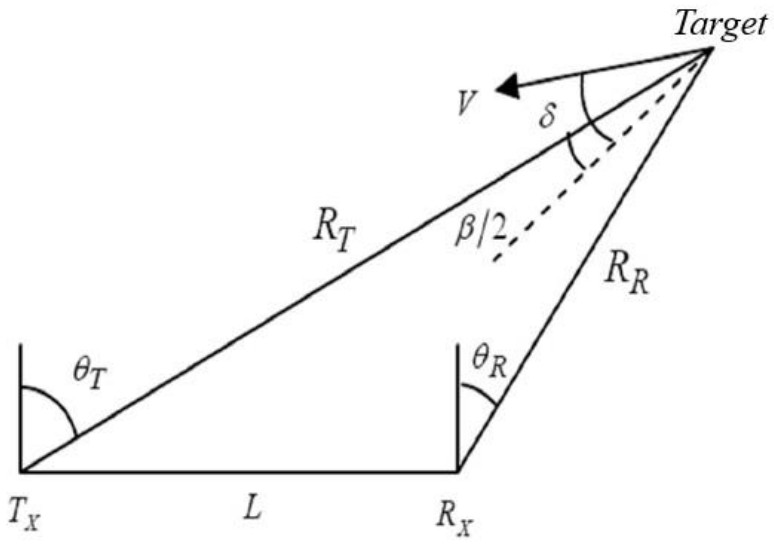

Figure 4.1: Two-Dimensional Bistatic Radar Geometry [3]

As a result, the relationship between time delay and range becomes non-linear due to the addition of several terms. In the following discussions, we speak of linear and non-linear terms. The linear case describes bistatic time delay τ_b as it varies linearly with range R, baseline L and angle θ. The non-linear case is the condition in which the terms beneath the radical become dominant, resulting in a non-linear relationship between τ_b and the remaining terms.

$$\tau_b = \frac{R_R + \sqrt{R_R^2 + L^2 + 2R_R L\, sin\theta}}{c} \tag{4.2}$$

The bistatic range equation consists of a linear term, R, and a non-linear term under the radical that includes R, baseline length L, and the angle θ. It can be seen that as the angle θ changes, the relationship between range and time delay become more complex.

To define the location of each zone we will analyze the deviation of time delay as a function of $R \in [0,\infty]$ and $\theta \in [-\frac{\pi}{2}, \frac{\pi}{2}]$.

For $\theta = -\frac{\pi}{2}$: (4.3)

$$\tau_b = \frac{\left(R + \sqrt{R^2 + L^2 + 2.R.L.\sin\left(-\frac{\pi}{2}\right)} \right)}{c}$$

$$= \frac{\left(R + \sqrt{R^2 + L^2 - 2.R.L} \right)}{c}$$

$$= \frac{\left(R + \sqrt{(R-L)^2} \right)}{c} = \frac{(R + |R-L|)}{c}$$

$$if\ R < L \Rightarrow \tau_b = \frac{L}{c}$$

$$if\ R \geq L \Rightarrow \tau_b = \frac{2.R - L}{c}$$

In this case where R is greater than L, the target is located between the transmitter and receiver, and will most likely not be detected. If R is greater than L, the delay τ_b is a linear function of R, and the resulting ambiguity function is similar to the monostatic case.

For $\theta = 0$: (4.4)

$$\tau_b = \frac{\left(R + \sqrt{R^2 + L^2 + 2.R.L.\sin(0)} \right)}{c}$$

$$= \frac{\left(R + \sqrt{R^2 + L^2} \right)}{c}$$

For the case in which $\theta = 0$, it can be seen that the time delay has two regions. If $R \in [0, L]$ the nonlinear term under the radical is dominant, but if $R \in [L, \infty[$ the linear term R will be dominant.

For $\theta = \frac{\pi}{2}$: : (4.5)

$$\tau_b = \frac{\left(R + \sqrt{R^2 + L^2 + 2RL \sin\left(\frac{\pi}{2}\right)} \right)}{c}$$

$$= \frac{\left(R + \sqrt{R^2 + L^2 + 2RL} \right)}{c}$$

$$= \frac{\left(R + \sqrt{(R + L)^2} \right)}{c} \qquad = \frac{(R + R + L)}{c}$$

$$\tau_b = \frac{(2R + L)}{c}$$

The figure below shows the variation of time delay as a function of $R \in [0, L]$ for different values of $\theta \in [-90^{\circ}, 90^{\circ}]$ in steps of 5°.

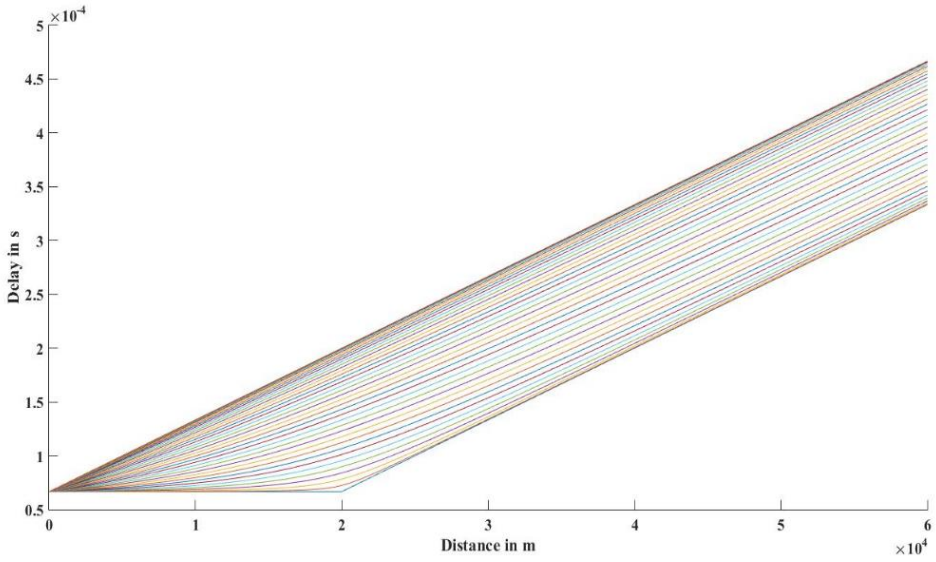

Figure 4.2: Variations of Time Delay as Functions of R and θ

Figure 4 illustrates the three zones calculated from Equation 2. The first zone for θ ∈ [20°, 90°] is a linear zone for all values of $R \in [0, \infty]$. This zone is similar to the general condition of a monstatic radar measuring range related to time delay. The second zone for θ ∈ [-45°, 15°] is linear for R > L, but non-linear for $R \in [0, L]$. The third zone is a non-detection zone for $R \in [0, L]$, but the relationhip becomes linear for R > L.

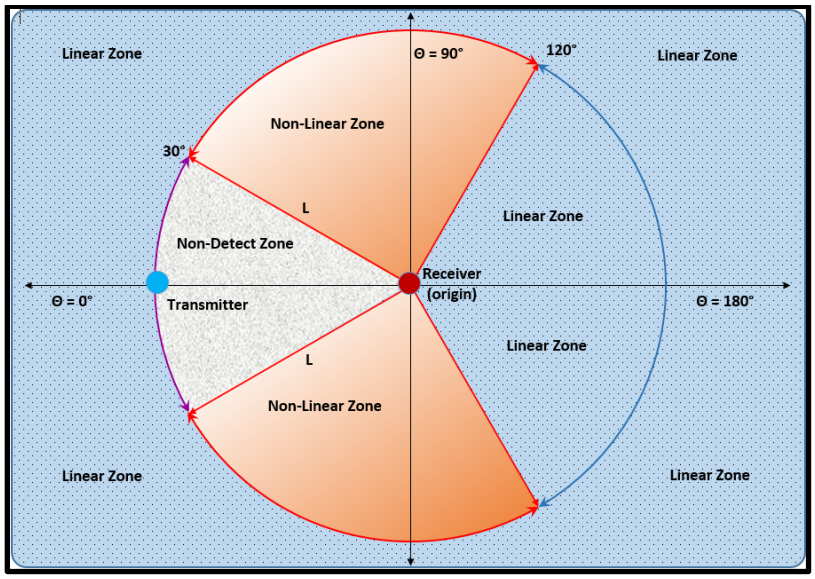

Figure 4.3: Visualization of linear and non-linear range/time delay zones due to bistatic geometry.

4.2 Doppler Ambiguity of PCL Systems

In a monostatic radar system the Doppler shift is a constant value for a target with constant speed, given by the equation below.

$$f_d = \pm \frac{2.v}{c} f_0 cos\theta \tag{4.6}$$

For the bistatic case, the formula includes terms for the range R, baseline L, and angle θ.

$$f_d = \pm \frac{2f_0}{c}\left(v.cos\Phi\sqrt{\frac{1}{2}+\frac{R+L.sin\theta}{2\sqrt{R^2+L^2+2.R.L.sin\theta}}}\right) \tag{4.7}$$

The figure below shows the variation of Doppler shift with the target position residing at $R \in [0, L]$ and θ ∈ [-90°, 90°].

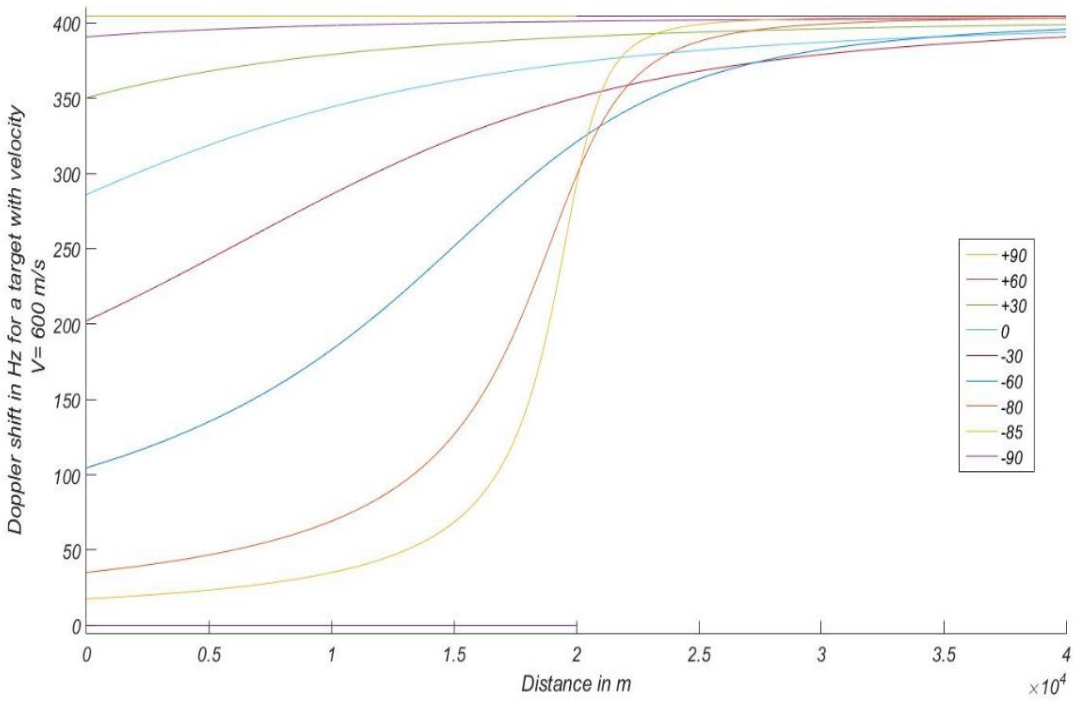

Figure 4.4: Variations of Doppler shift as a function of R and θ.

From calculations of Equation (4), we establish three major zones. The first zone is a linear region for θ ∈ [30°, 90°] in which Doppler shift is non-linear for R ≤ L, and becomes linear for R > L. If θ = 90°, the Doppler shift is constant for all values of R. The second zone is for θ ∈ [-90°, 30°]. In this zone we have two areas, a linear area for R ≤ L and a non-linear area for R > 1.25L. If θ = -90°, the Doppler shift has two constant values:

$$f_d = \begin{cases} 0 \;\; if \;\; R \leq L \\ cte \;\; if \; R > L \end{cases}$$

The following figure illustrates the two zones previously described.

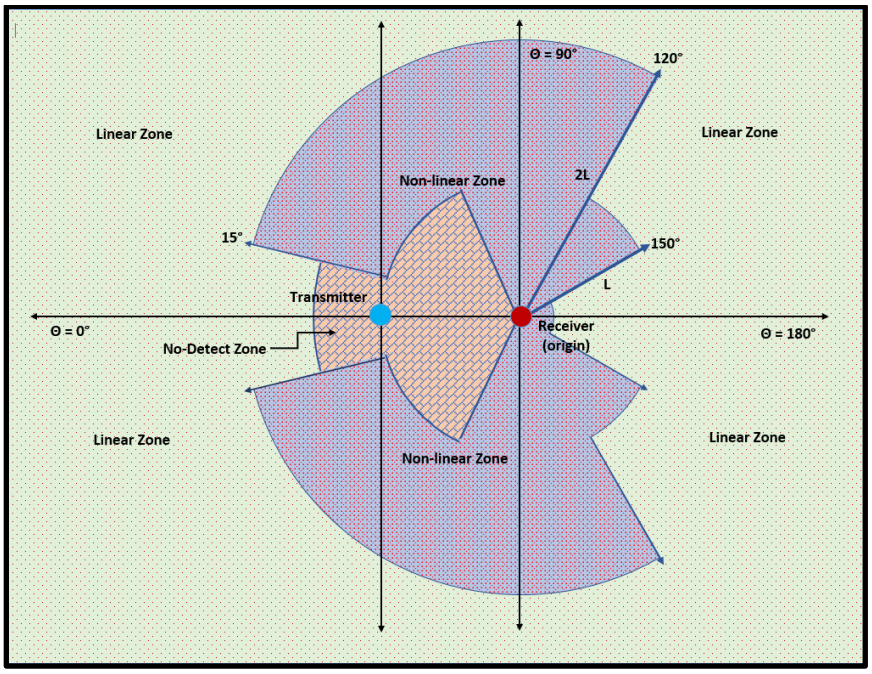

Figure 4.5: Visualization of linear and non-linear doppler zones due to bistatic geometry.

4.3 Bistatic Effects on the Ambiguity Function

It can be inferred from the last two sections that range and Doppler frequency are dependent on the geometry of bistatic systems. As a result, the bistatic ambiguity function is affected. By using Tsao's derivation of the bistatic ambiguity function in [36] and [44], we can visualize the effects of linear and non-linear geometric zones. The bistatic ambiguity function relationship is shown in equation 5.

$$|X(R_{RH}, R_{Ra}, V_a, \theta_R, L|^2 \tag{4.8}$$

$$= \left| \int \tilde{f}\big(t - \tau_a(R_{Ra}, \theta_R, L)\big)\tilde{f}'(\big(t - \tau_a(R_{Ra}, \theta_R, L)\big) exp\big[-j\big(\omega_{DH}(R_{RH}, V_H, \theta_R, L) - \omega_{DA}(R_{Ra}, V_a, \theta_R, L)\big)t\big]dt \right|^2$$

Using the relationships defined in the previous sections and Tsao's bistatic ambiguity function formula, we show the bistatic ambiguity functions for two angles. The first ambiguity function shown in Figure 7 is for θ = 60°. It can be seen that range axis is capable of high resolution, while the Doppler axis has a wider shape. The next ambiguity function in Figure 8 is for θ = 89°. In contrast to the previous instance, the Doppler axis exhibits high resolution, while the range axis has become indiscernible.

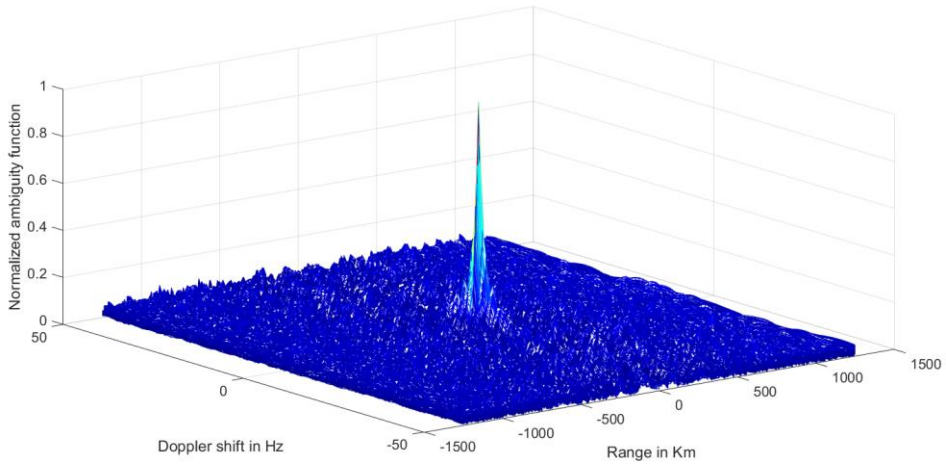

Figure 4.6: Bistatic ambiguity function for θ=60°.

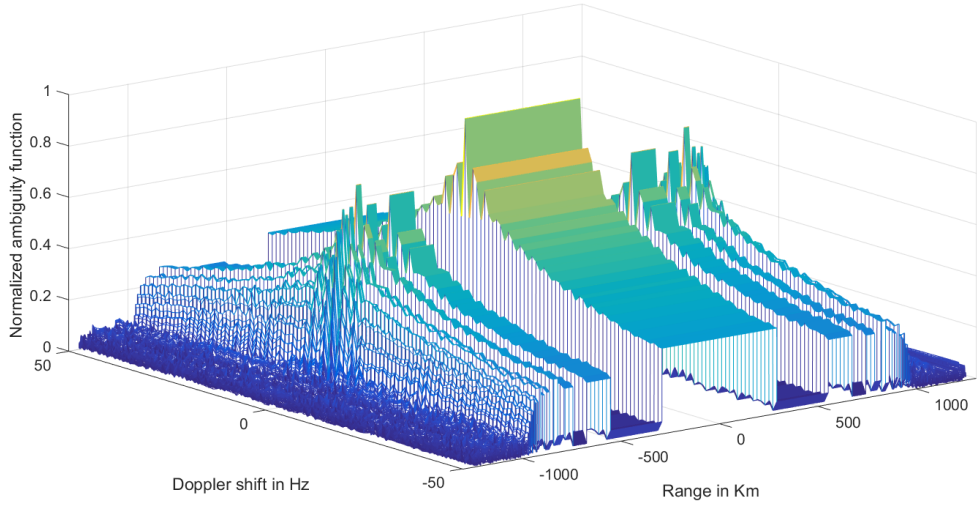

Figure 4.7: Bistatic ambiguity function for θ=89°.

4.4 PCL Geometry Experiment

In an effort to prove the concepts presented in this chapter, an experiment was arranged to show changes in a signal's ambiguity function and target response as a target migrates towards the San Diego International airport. Figure 4.8 indicates locations of the PCL system, target flight path, antenna boresights, and FM radio tower location in San Diego, CA.

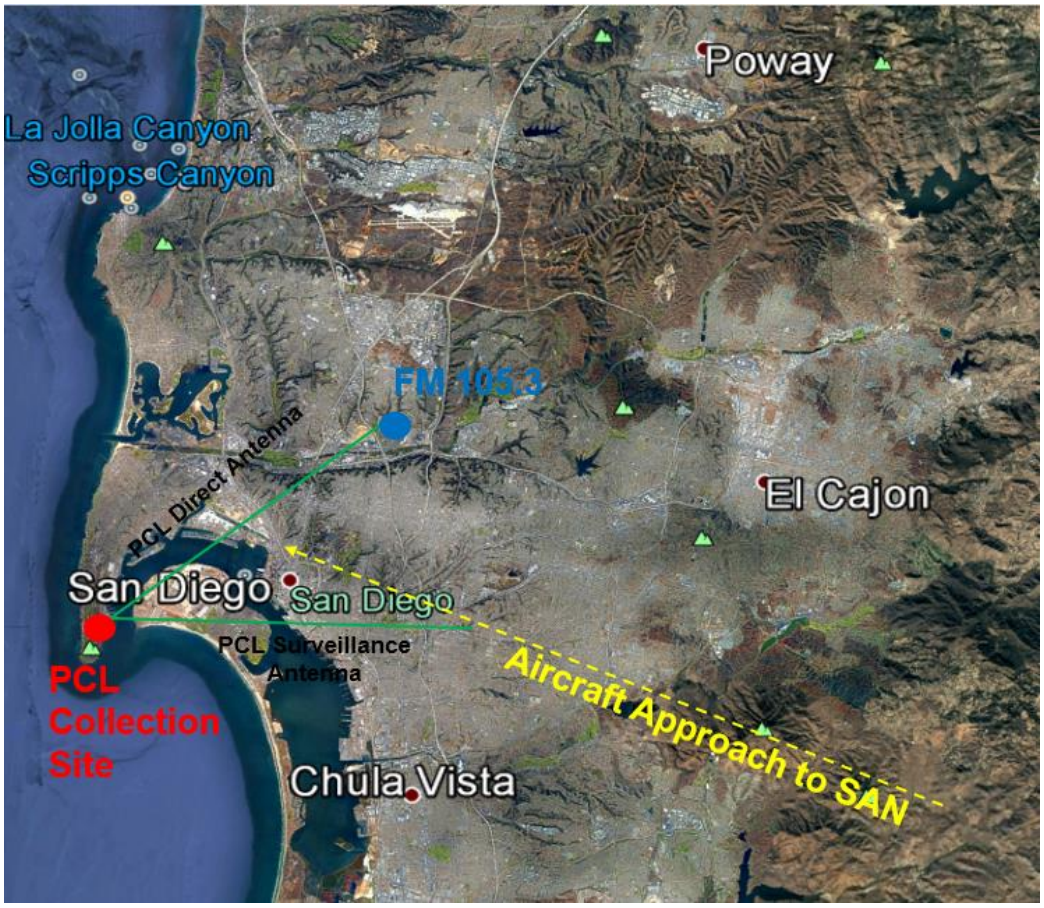

Figure 4.8: Geometry for bistatic ambiguity function experiments. Map data taken from 2016 INEGI, SIO, NOAA, U.S. Navy, NGA, GEBCO, 2016 Google, USGS.

Using ADS-B flight data, it was possible to estimate the bistatic angle. The following figures illustrate the progression of a target towards the San Diego airport, with data captured at bistatic angles of 60, 70, 80, and 85 degrees.

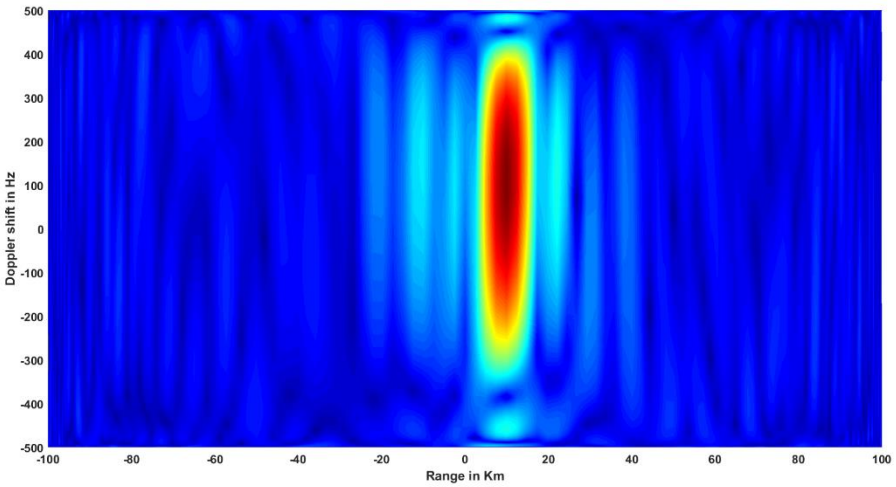

Figure 4.9: Target range/Doppler response for bistatic angle =60°.

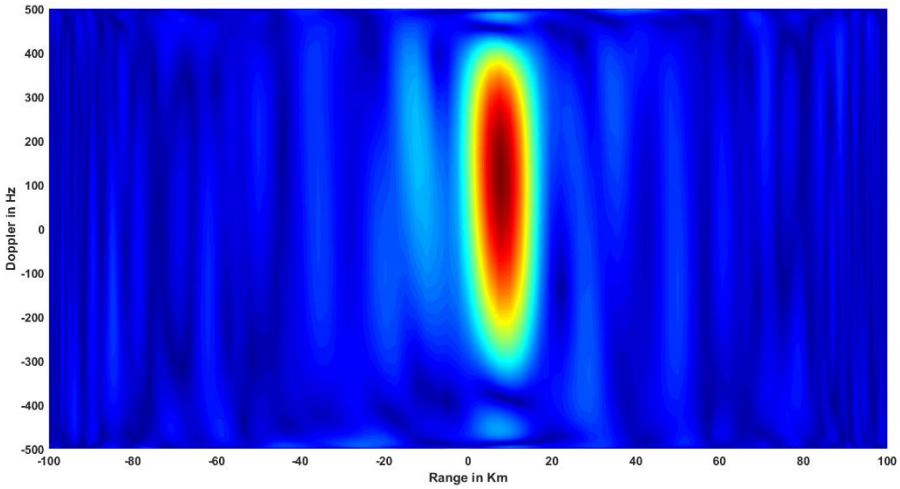

Figure 4.10: Target range/Doppler response for bistatic angle =70°.

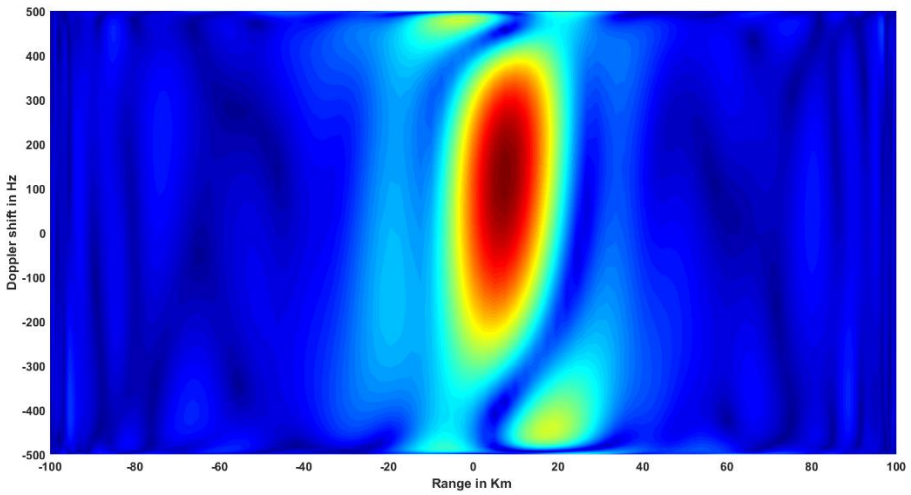

Figure 4.11: Target range/Doppler response for bistatic angle =80°.

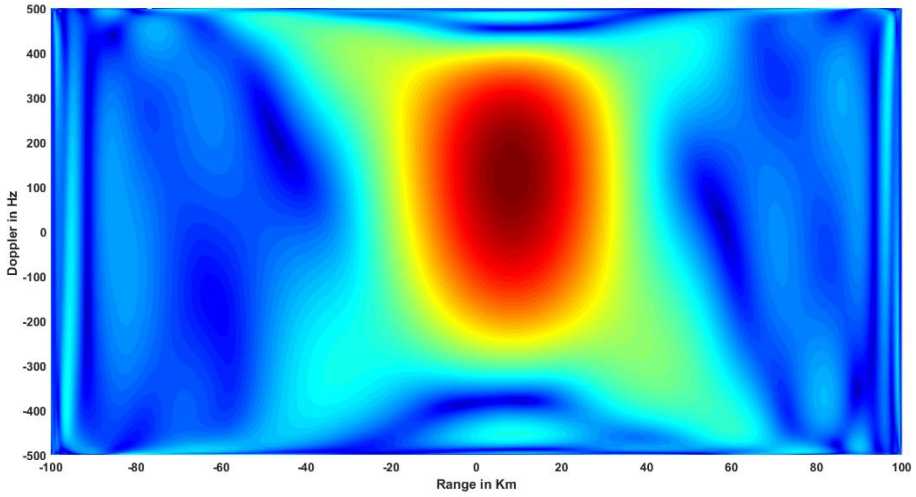

Figure 4.12: Target range/Doppler response for bistatic angle =85°.

From these figures it can be illustrated that the concepts mentioned previously in this chapter hold true for this experiment. The initial target response at 60° indicate smearing in the Doppler axis and poor resolution on the range axis. This effect seems to grow exponentially as we reach angles of 80° and 85°, where the resolution is lowered by approximately 400% in the range dimension.

In this chapter we have shown that geometric considerations for bistatic PCL systems can have dramatic effects on range and Doppler relationships. There are certain bistatic angles for the transmitter, target, and receiver that force an unpredictable condition of the ambiguity function in which velocity and range cannot be surmised by traditional equations. We have also shown a graphical representation of the linear and non-linear zones, which could be useful when planning and implementing a PCL system. Finally, an experiment provided proof that range and Doppler ambiguity worsen at bistatic angles that approach 90°.

CHAPTER 5: PCL SIGNAL CHARACTERIZATION

A passive radar system can be thought of as an atypical radar system, performing traditional radar processing functions by exploiting co-located cooperative or non-cooperative transmitters of opportunity. The general premise is that broadcasted signals that are reflected off of objects can be received and processed to detect and track objects of interest. These signals of opportunity have traditionally included FM radio [47][39], DAB/DVB [48], GSM [24], and GPS [5], among several others. The passive radar receiving sub-system can be in either a bistatic or multi-static configuration. For this section, only the bistatic case will be considered. The receiver is typically designed for operation with a specific signal set or frequency range of interest. Using current technology, a fairly wideband receiving system could be realized using several antennas, tuners, and channelized receivers, each optimized for a particular frequency band. This type of system would give access to a large number of signals present in the electromagnetic spectrum (EMS) at any given time. This chapter begins to address the enhanced capabilities of such a system to analyze the EMS, determine a useful set of signals, and employ them for passive detection and tracking. Portions of this chapter were previously published by Johnson et al in [34].

Recent work by Griffiths [35] has illustrated the dynamic nature of ambiguity functions calculated for FM radio and DVB signals. One reason for this is the dynamic modulation content of the signal, as well as any signal specific anomalies such as the sync pulses in typical digital TV signals. If a passive radar system were designed to operate only on a single signal or frequency, it could prove to be unreliable. For this reason it is important to have the flexibility to employ any broadcast channel to achieve the best detection capability. This chapter presents a novel approach

to characterize those signals present in the EMS based on features of its ambiguity function. The goal is to provide a method of signal selection for PCL that is more effective than choosing signals based solely on received signal strength.

5.1 Ambiguity Function Characteristics

In traditional radar systems, a transmit waveform is chosen based on its capabilities in regards to object detection, range and Doppler resolution, accuracy of measurements, rejection of clutter, and overall ambiguity [49]. Several of these features can be determined through calculation of a signal's ambiguity function (AF). The authors in [37] define qualitative traits for a signal's ambiguity function as range resolution, peak-to-sidelobe ratio, and integrated sidelobe ratio. Following this criteria increases the chances of detection and discrimination of closely-spaced targets.

The calculation of an ambiguity function is performed by passing a waveform through its own matched filter. For the monostatic case, the ambiguity function is defined in [13] as

$$|X(\tau, f)^2| = \left|\int_{-\infty}^{\infty} s_t(t) s_t^*(t-\tau) e^{j2\pi f_t} dt\right|^2 \tag{5.1}$$

where $X(\tau, f)$ is the ambiguity function dependent on time delay (τ) and Doppler frequency (f), and s(t) represents a complex baseband signal. Figures 5.1 and 5.2 illustrate the ambiguity function for an ideal rectangular pulse of unit amplitude and pulse width equal to 5×10^{-5}.

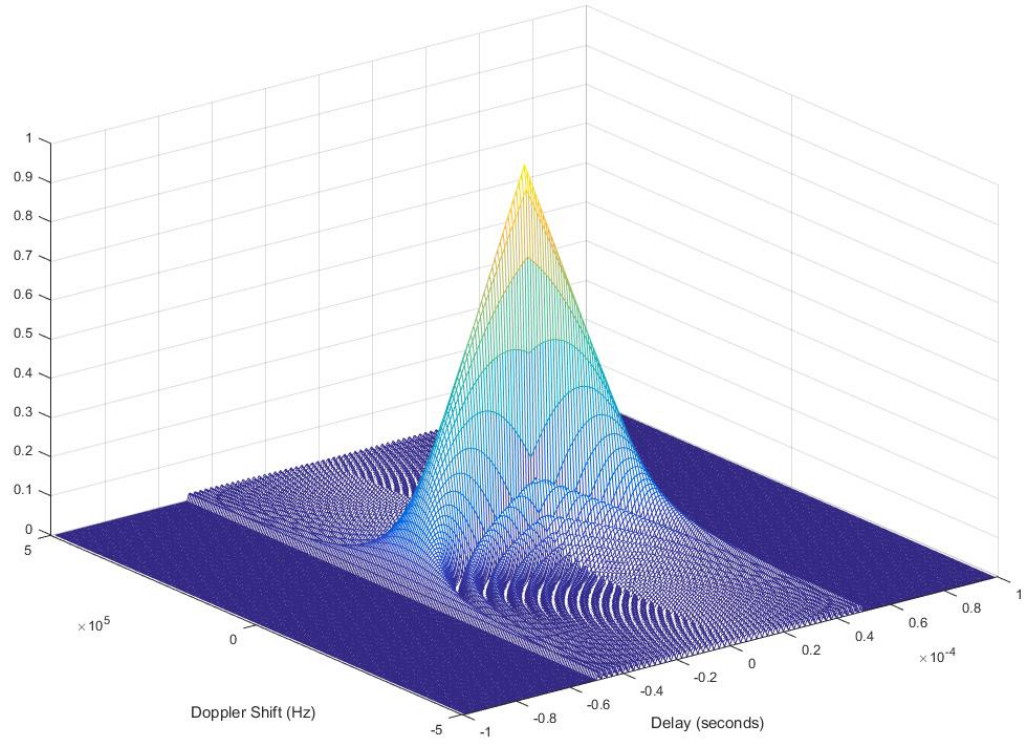

Figure 5.1: Ambiguity Function for an Ideal Rectangular Pulse.

For the bistatic case, Tsao [36] formulates a different equation, making the argument that geometry plays an important role due to the fact that time delay and doppler frequency are not linear functions of range and velocity, respectively. His proposed ambiguity function is

$$|X(R_{RH}, R_{Ra}, V_a, \theta_R, L|^2 \tag{5.2}$$

$$= \left| \int \tilde{f}\big(t - \tau_a(R_{Ra}, \theta_R, L)\big)\tilde{f}'\big(\big(t - \tau_a(R_{Ra}, \theta_R, L)\big)exp\big[-j\big(\omega_{DH}(R_{RH}, V_H, \theta_R, L) - \omega_{DA}(R_{Ra}, V_a, \theta_R, L)\big)t\big]dt \right|^2$$

which incorporates bistatic range, angles, and radial velocities from the positions of both the transmitter and receiver. Tsao also shows through simulation that the bistatic ambiguity function shape is dependent on the bistatic geometry, meaning that range and Doppler resolutions will vary with geometry. Taking into account bistatic geometry is important for characterizing situations when tracking or searching for a target, or when using multiple geographically separated transmitters of opportunity. However for the case of characterizing a signal prior to any targeting functions, assuming a single transmit site, we are confident in relying on the traditional monostatic equation for creating the ambiguity function.

Another determining factor of an ambiguity function's shape in both the monostatic and bistatic case is the signal bandwidth [35]. For example, a broadcast FM radio channel's assigned spectrum bandwidth is ~200kHz. At any instant in time, the actual channel bandwidth will vary based on the modulation content. Results presented in [23] show that signals with content such as plain speech are worse performers than that of jazz or rock music for this reason. This is the motivation for using the ambiguity function as an indication of a signal's usefulness to passive target detection. An experimental collection of FM radio signal 91.1 MHz illustrates the concept of a dynamic ambiguity function due to changes to the channel's modulation and noise content and can be seen in the figures below. Figure 5.2 indicates a moderately clean channel with little noise, most likely a bandwidth approaching the channel maximum of 200 kHz. The ambiguity function in figure 5.3 shows a degraded ambiguity function of the same signal. This may indicate change in channel content to commercial or other speech broadcast that occupies far less bandwidth than that of figure 5.2.

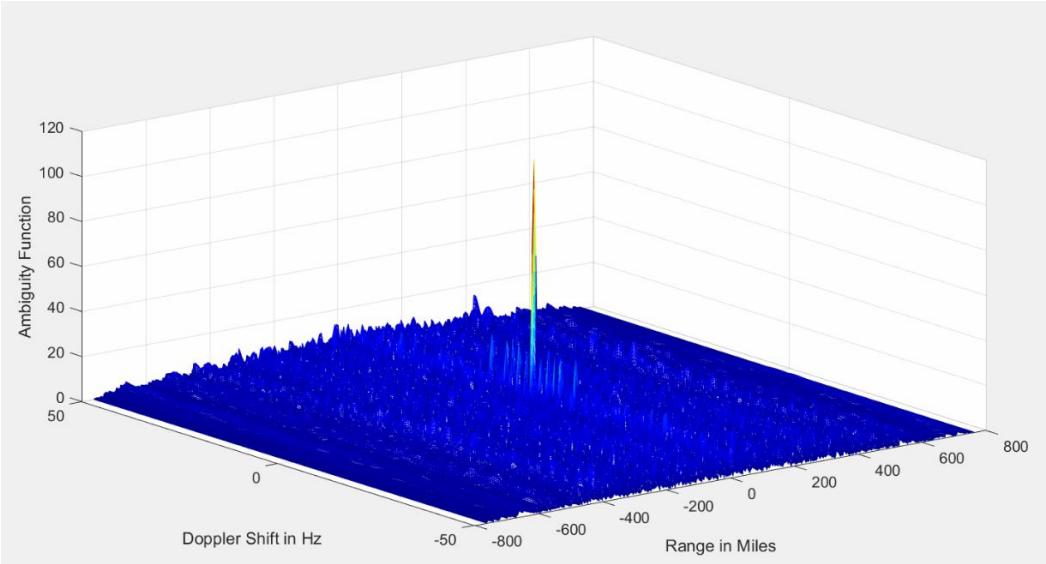

Figure 5.2: Ambiguity Function for FM 91.1 MHz.

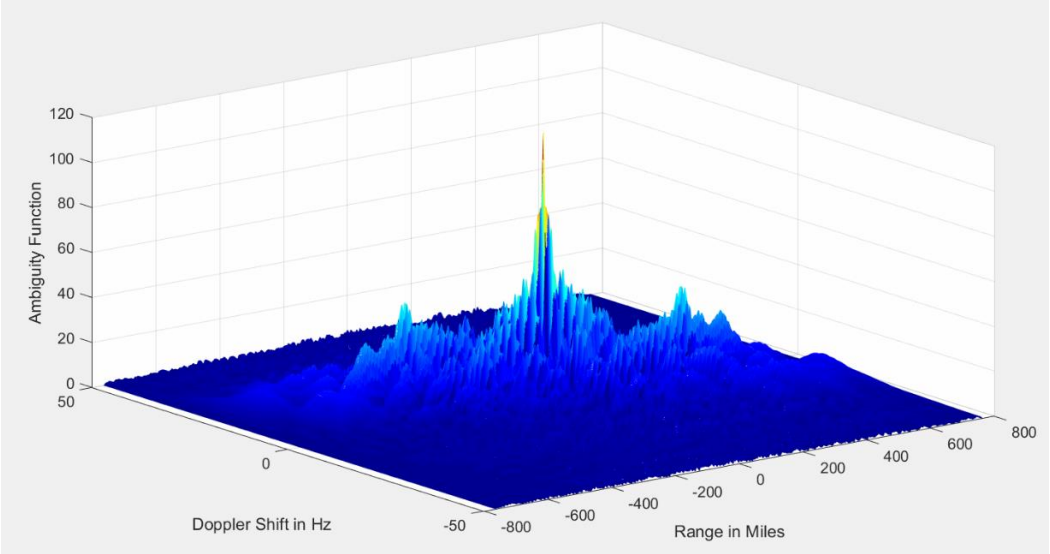

Figure 5.3: Ambiguity Function for FM 91.1 MHz.

When choosing a signal for PCL, the system operator should be aware of expected signal parameters for each signal set potentially used for PCL. The table below shows expected performance of HF, FM radio, and digital TV signals for PCL.

Table 5-1: Notable signal features for PCL [35].

	Typical ERP	**Frequency Range**	**Maximum Channel Bandwidth**	**Best Possible Range Resolution**	**Best Possible Velocity Resolution ($t_i = 1s$)**
HF	10's kW	3-30 MHz	20 kHz	7500 m	20 m/s
FM Radio	50-100kW	88-108 MHz	200 kHz	750 m	6 m/s
HDTV	50-100kW	470-890 MHz	6 MHz	30 m	0.67 m/s

5.2 Autonomous Evaluation of the Ambiguity Function

We are interested in characterizing signals for use in a passive radar system by following the previously mentioned criteria of range and doppler resolution, sidelobe levels, and signal-to-noise-ratio (SNR), all determined autonomously from the ambiguity function. We will also experiment with distance metric functions to evaluate similarity between a pre-defined ideal ambiguity function and those calculated from collected signals. For this section, we will bound this problem to HF, broadcast FM, and digital TV signals (VHF/UHF frequencies).

Our first task is to collect a set of signals and calculate their ambiguity functions. Using software defined radios, two signals were collected for a duration of 250ms. Each signal's ambiguity function was generated using an integration time of 500ms. Figures 5.3 and 5.4 below show the calculated ambiguity function for a collected broadcast (analog) FM signal operating at 91.1 MHz. Figures 5.5 and 5.6 show the calculated ambiguity function for a collected broadcast (digital) TV signal operating at 497 MHz.

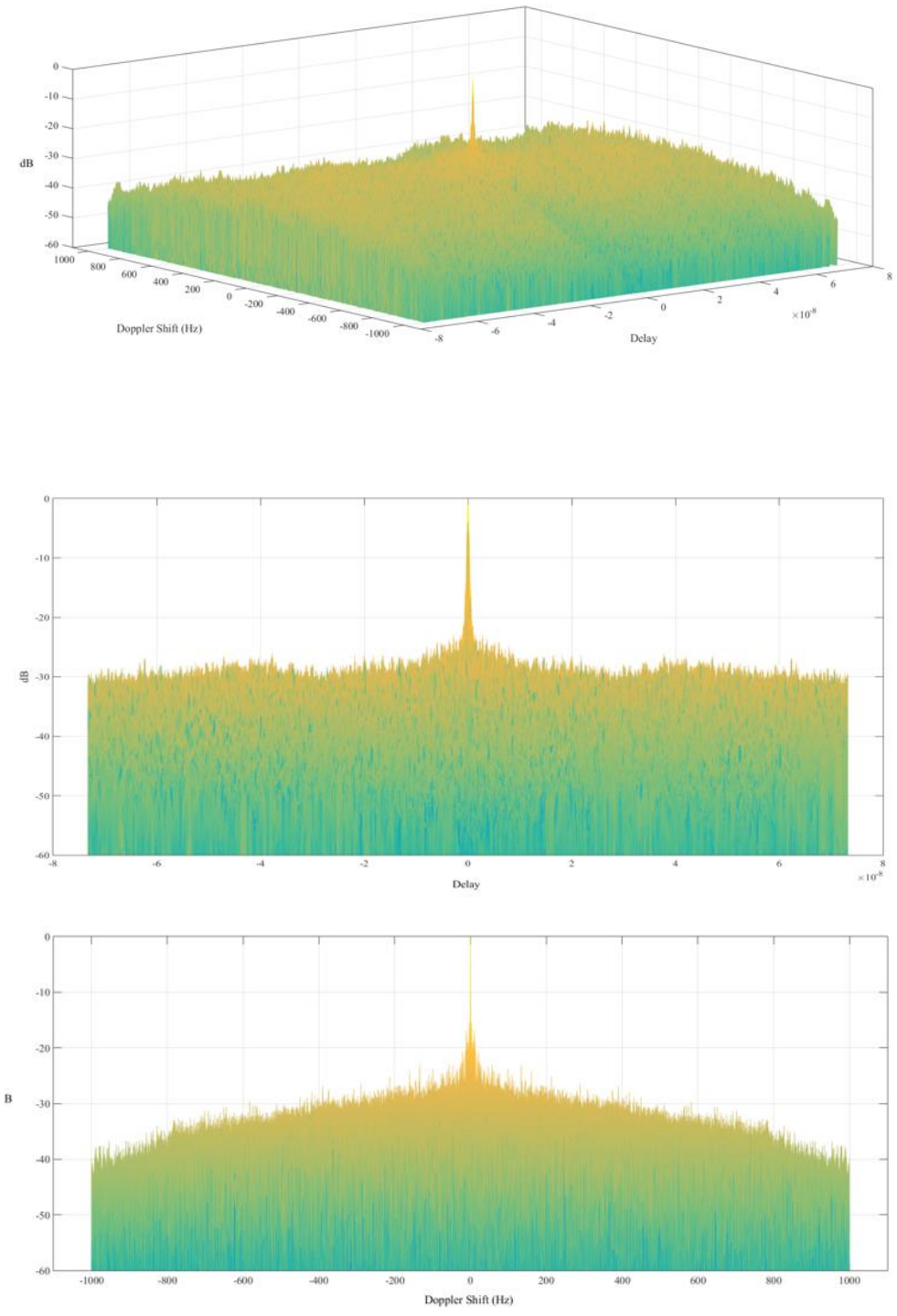

Figure 5.4: Calculated Ambiguity Function for FM Radio Station 91.1 MHz

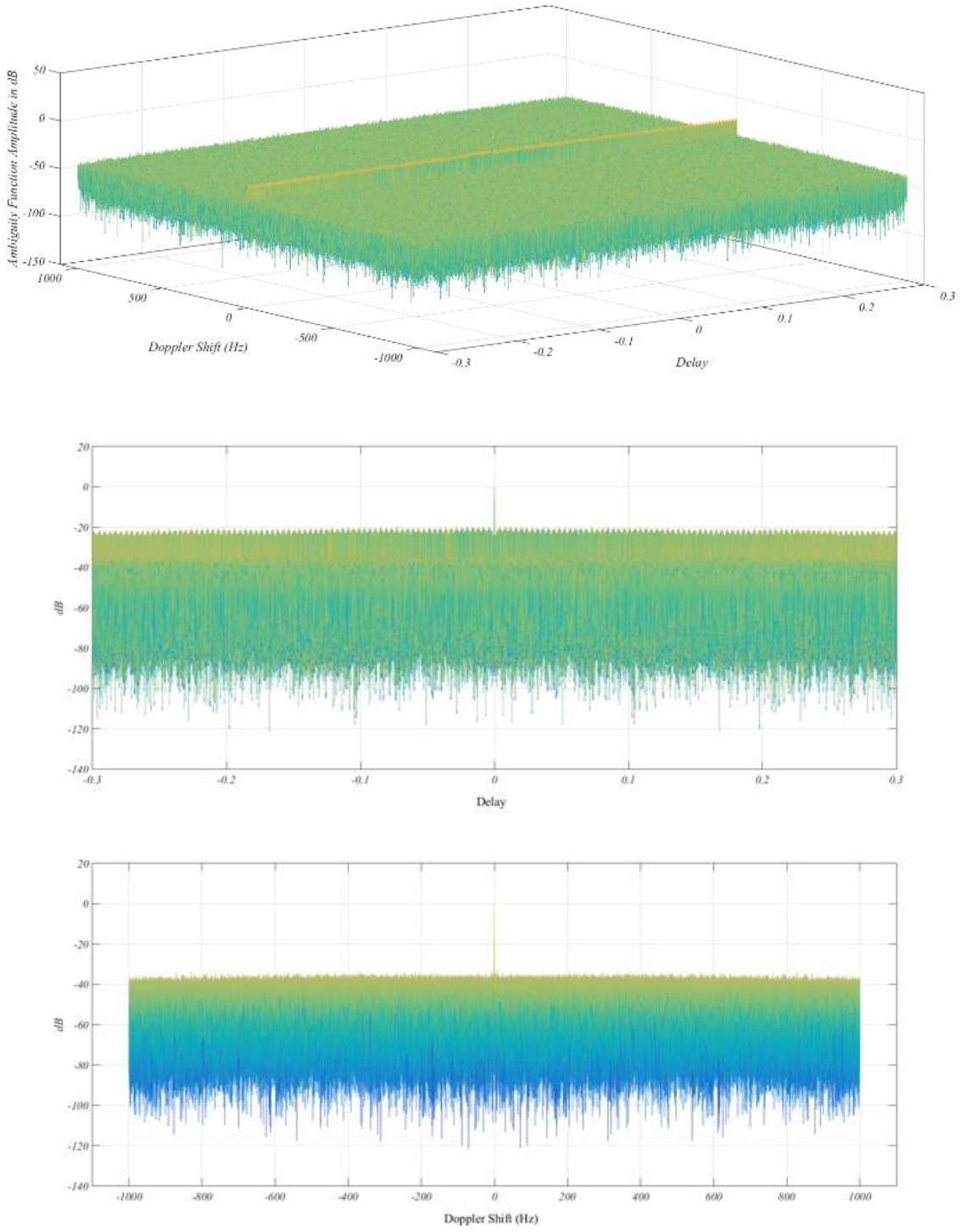

Figure 5.5: Calculated Ambiguity Function for Digital TV Station 497 MHz

Next, we smooth the data using an FIR filter and implement a computationally efficient peak-finding algorithm for locating the index and value of the main peak and sidelobes. The peak-finding algorithm creates a function parallel to the actual AF and determines the locations of peak values using a comparative difference function. Starting at the index of the max value of the main lobe, this algorithm makes a comparative note of which indexes the original function is increasing in time. Also at each iteration, it calculates the difference between the two functions. When the difference is greater than zero, the function is increasing, less than zero indicates the function is decreasing. The algorithm notes the index at which this change occurs and declares presence of a peak value. Figure 5.7 below illustrates this concept, and in this case, the function starts at t = 0. At t = 1, the "peak finder" function is enabled, tracking the original function delayed by one time sample.

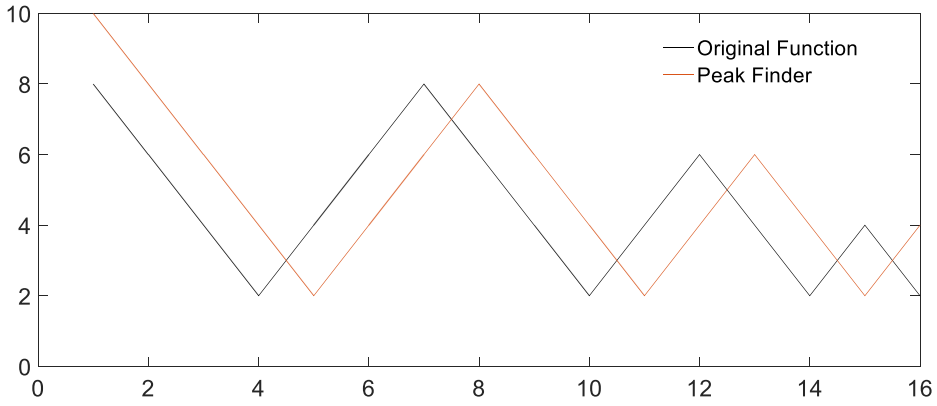

Figure 5.6: Peak Finding Algorithm Illustration.

Once identified, the peak values are used to calculate the peak-to-sidelobe-ratio (PSLR) using the following equation from [37], where A_n is the amplitude of the nth sidelobe and $A_0$is the peak. This metric will be used for determining the signal's ability to detect two targets with various amplitudes in the range dimension only.

$$PSLR = \frac{1}{A_0^2}\max\{A_n^2\}, n \neq 0 \tag{5.3}$$

In addition, we can also calculate the integrated sidelobe ratio (ISLR), where N equals the number of sidelobes in the ambiguity function's range dimension. The ISLR will be used to characterize a signal's detection capability when multiple targets are in the same range profile.

$$ISLR = \frac{1}{A_0^2}\sum_{n=1}^{N}\{A_n^2\} \tag{5.4}$$

Next, the range and Doppler resolution metrics are evaluated. We assume that the main lobe of the ambiguity function is the largest peak identified by the peak-finding algorithm that is nearest to the origin, and the -3dB width of the main lobe defines the resolution. Also, due to channel modulation, it is expected that the range resolution will change in time. Conversely the Doppler resolution is a function of integration time, which will remain constant.

One final measure used to evaluate the ambiguity function was through the use of distance metric functions. In preparation for a proper comparison, it is necessary to normalize each ambiguity function. Our approach was to identify the minimum value, then scale the entire function to make that value equal to zero. Next, we can generate an ideal ambiguity function, which is widely considered to be a single large spike at range and Doppler equal to zero. This large spike and the lack of sidelobes indicates a perfect correlation between two functions. In practice

however, it was found that a tall cube was a more reasonable approach. This is due to the varying geometry of the ambiguity function matrix resulting from different sample sizes. In addition, a cube allows for a shape equivalent to the main lobe width at the -3dB points to be generated. The height of the cube was determined by the amplitude of the ambiguity function for each signal. Additionally, the rest of the matrix values are uniform, calculated by averaging the noise floor of the normalized ambiguity function. The ideal ambiguity function generated for the previously mentioned FM signal is shown in Figure 5.8.

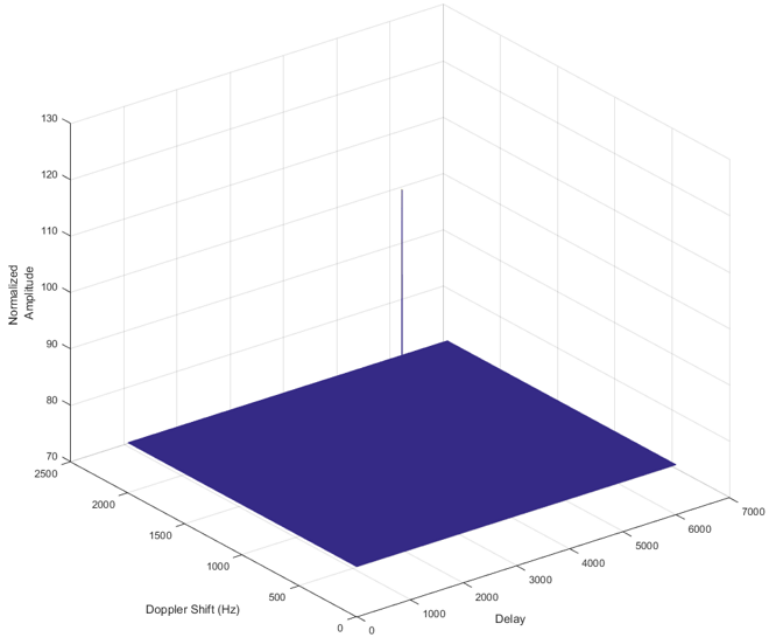

Figure 5.7: Ideal Ambiguity Function Calculated for the Collected FM Signal 91.1 MHz.

The first distance metric applied to this problem is known as the sum of absolute difference method, which is simply the absolute value of the difference between two points as shown in (5).

$$d_{SD}(p,q) = \sum_{i=1}^{n} \|p_i - q_i\| \tag{5.5}$$

The results in Figure 5.9 show the error between the ideal ambiguity function and that for the collected FM signal.

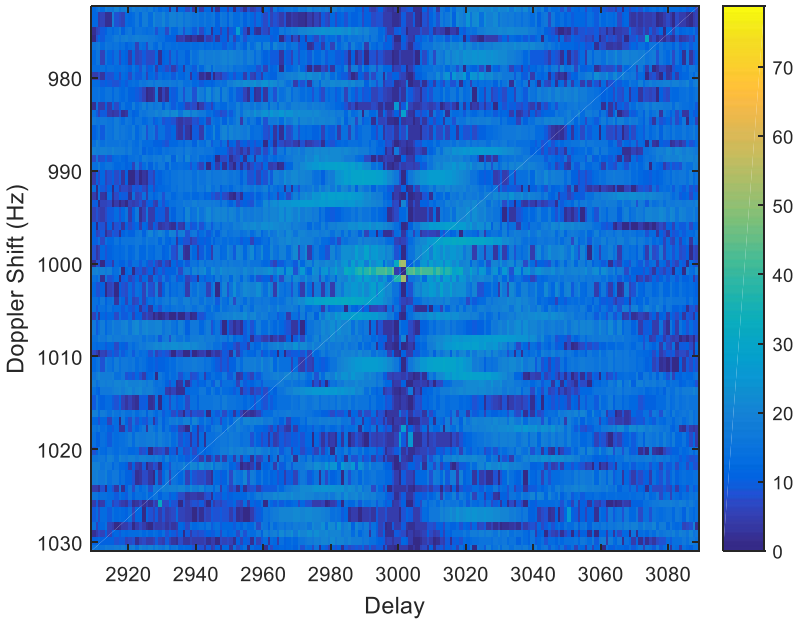

Figure 5.8: Error Calculated using the Absolute Difference Method.

The second distance metric used was the mean-squared error performed between each point of the ideal and actual ambiguity functions, calculated using the equation (6) with results shown in Figure 5.10.

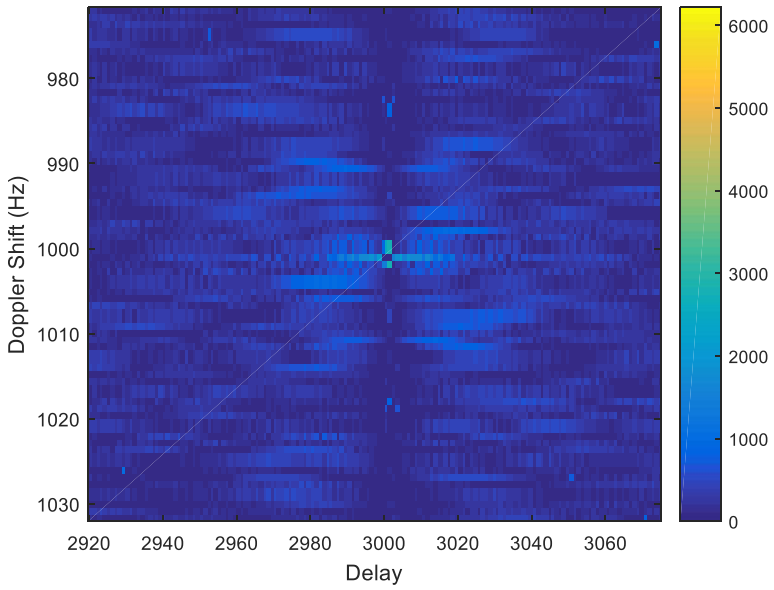

Figure 5.9: Error Calculated using the Mean Squared Error Method.

Table 5-2 summarizes the findings from analyzing the FM radio and TV signals. It can be seen that through analysis of the ambiguity function, signals can be characterized in preparation for evaluation and ranking.

Table 5-2: Comparison between Collected FM Radio and TV Signals.

	Analog FM Radio Station 91.1 MHz	**Digital TV Station 497 MHz**
Signal Strength	-40	-45
Delay Resolution	360m	48m
Doppler Resolution	1 Hz	1 Hz
PSLR (range dimension)	1.23	1.21
ISLR (range dimension)	1.48	1.51
Distance Metric (Sum of Absolute Difference Method)	8.05×10^7	7.93×10^7
Distance Metric (Mean Square Error Method)	8.54×10^8	6.73×10^8

5.3 Ambiguity Function Evaluation and Characterization Experiments

In order to demonstrate and prove effectiveness of the proposed PCL signal ambiguity function characterization method, an experiment was conducted using six signals of opportunity in the San Diego, CA area. Using the prototype PCL system described in chapter 2, two signals were collected from HF band, FM radio band, and digital TV band. The signals were chosen based on their respective transmitter locations in reference to the PCL system and expected target location. Autocorrelation was performed on each signals, resulting in ambiguity functions which can be seen in the following figures.

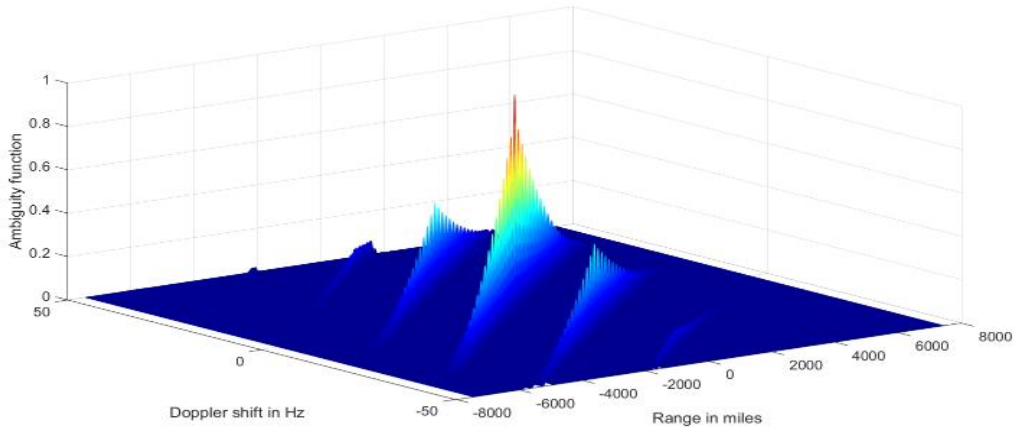

Figure 5.10: Ambiguity function for HF Sounder 5.3 MHz.

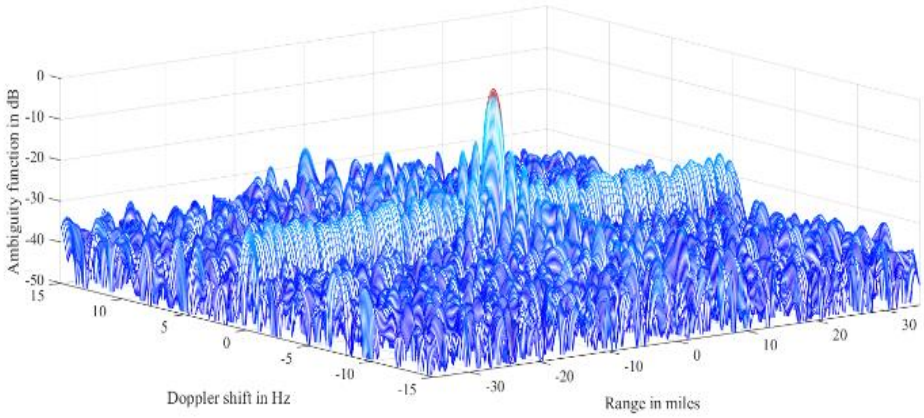

Figure 5.11: Ambiguity function for HF CODAR 17.6 MHz.

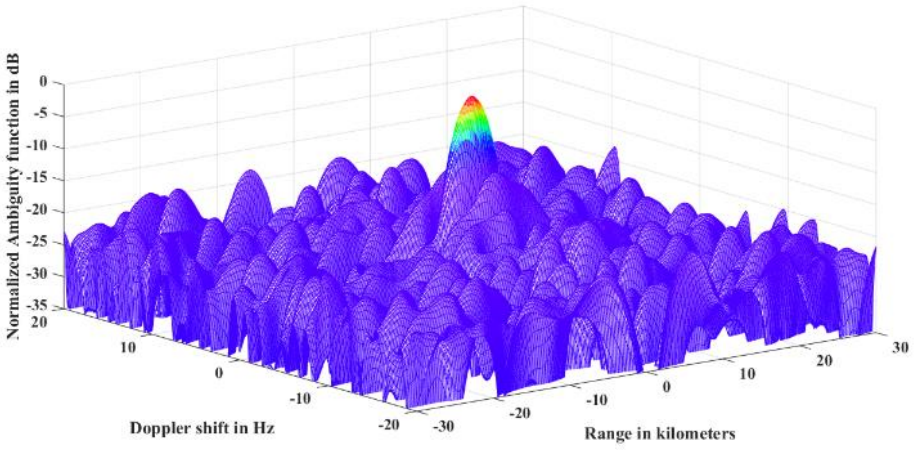

Figure 5.12: Ambiguity function for FM radio 98.8 MHz.

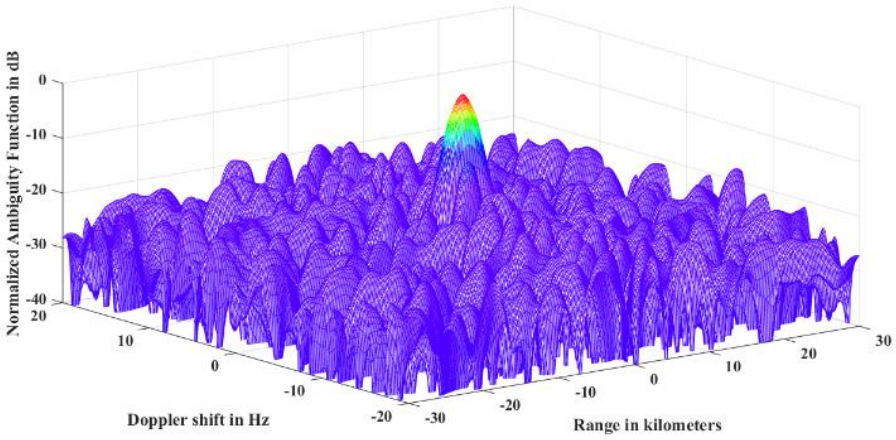

Figure 5.13: Ambiguity function for FM radio 101.5 MHz.

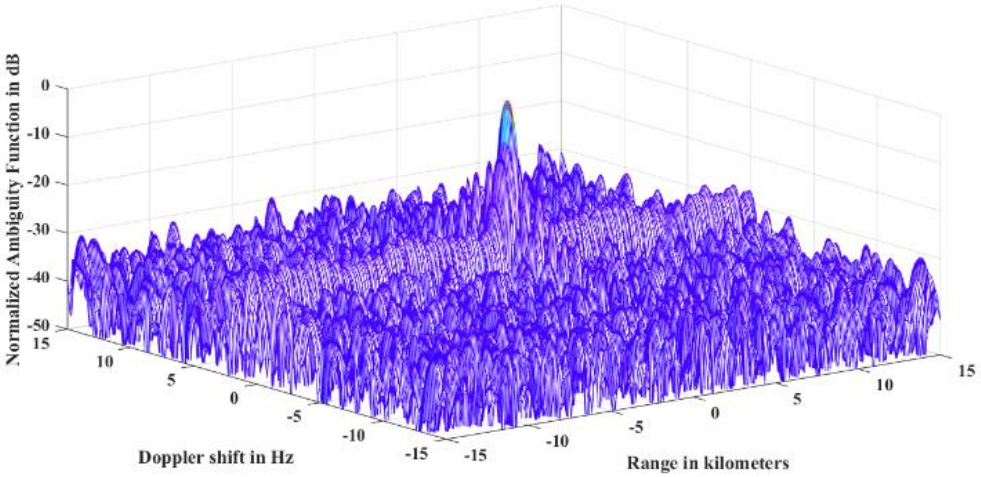

Figure 5.14: Ambiguity function for digital TV station 494 MHz.

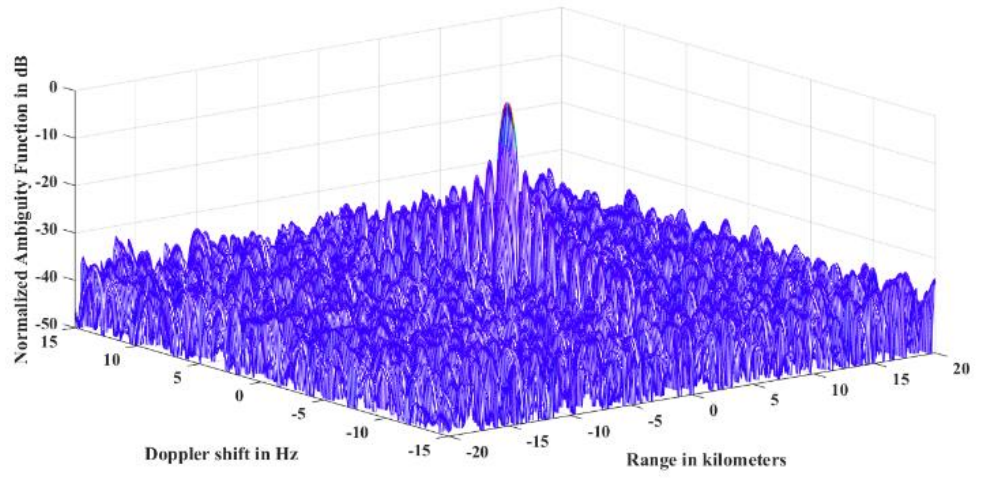

Figure 5.15: Ambiguity function for digital TV station 500 MHz.

Following realization of each ambiguity function, the autonomous characterization and evaluation algorithm was implemented. The results are captured in the table below.

Table 5-3: Results of autonomous signal characterization.

Features	5.3 (HF)	17.6 (HF)	91.1 (FM)	101.5 (FM)	497 (DTV)	500 (DTV)
Signal Strength (dBm)	-72	-67	-40	-41	-45	-42
Range Resolution (m)	15000	12000	1500	2800	25	25
Velocity Resolution (km/s)	128	11.6	0.433	0.349	0.0147	0.0144
PSLR (range dimension)	0.97	0.95	1.25	1.17	1.17	1.19
ISLR (range dimension)	0.9	0.89	1.43	1.45	1.52	1.53
Distance Metric	$4.05\ x10^9$	$3.22\ x10^9$	$8.54\ x10^8$	$6.73\ x10^8$	$6.88\ x10^7$	$5.43\ x10^7$

In this case, the presence of three signal types shows the variety of signal parameters one could expect. It is obvious from the results that digital TV signals would most likely always be chosen over HF and FM radio signals for PCL. Looking at each signal set (HF, FM, and digital TV), the value of autonomous characterization becomes more apparent. For example, if a PCL system operator were to arbitrarily choose FM radio 101.5 MHz, he will most likely achieve less than ideal results compared to the potential use of FM radio 91.1 MHz.

The next experiment uses only FM radio signals captured from a transmitter tower in Tijuana, Mexico. The experiment geometry can be seen in figure 5.16. The resulting ambiguity functions can be seen in figures 5.17, 5.18, and 5.19.

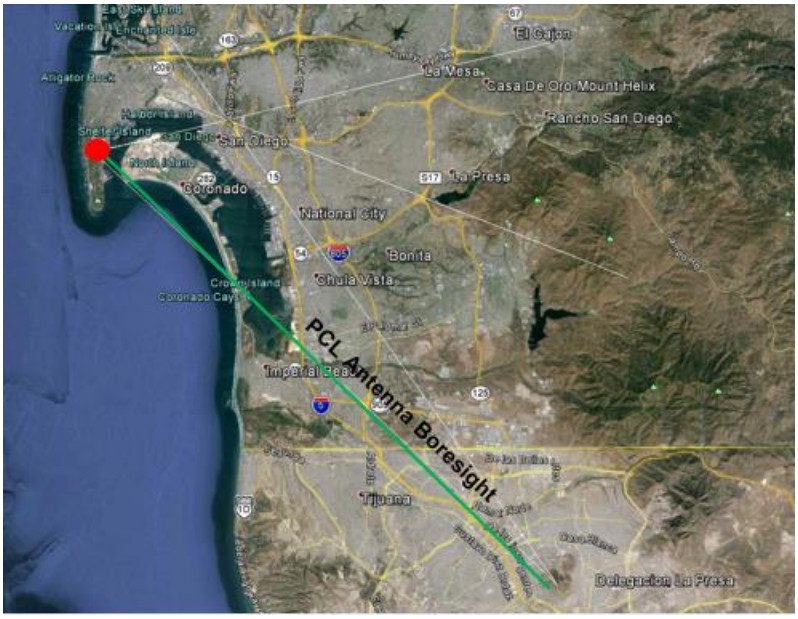

Figure 5.16: Experiment geometry for collection of Tijuana FM radio signals. Map data taken from 2016 INEGI, SIO, NOAA, U.S. Navy, NGA, GEBCO, 2016 Google, USGS.

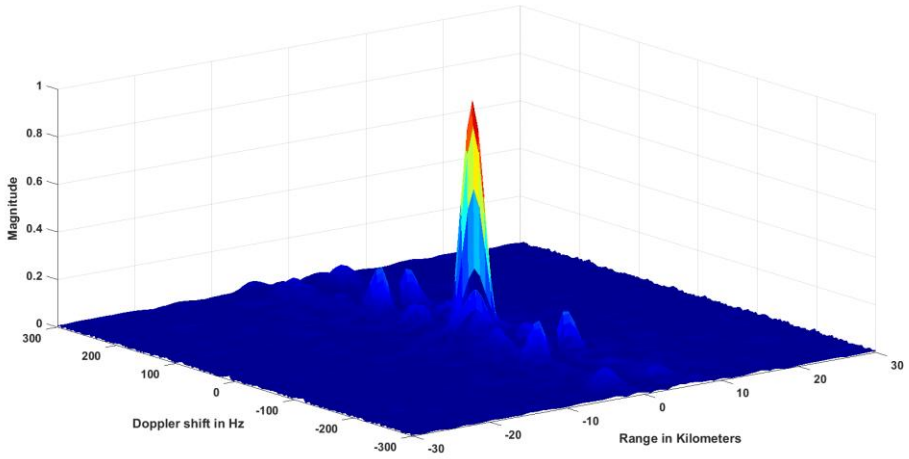

Figure 5.17: Ambiguity function for FM radio 91.1 MHz.

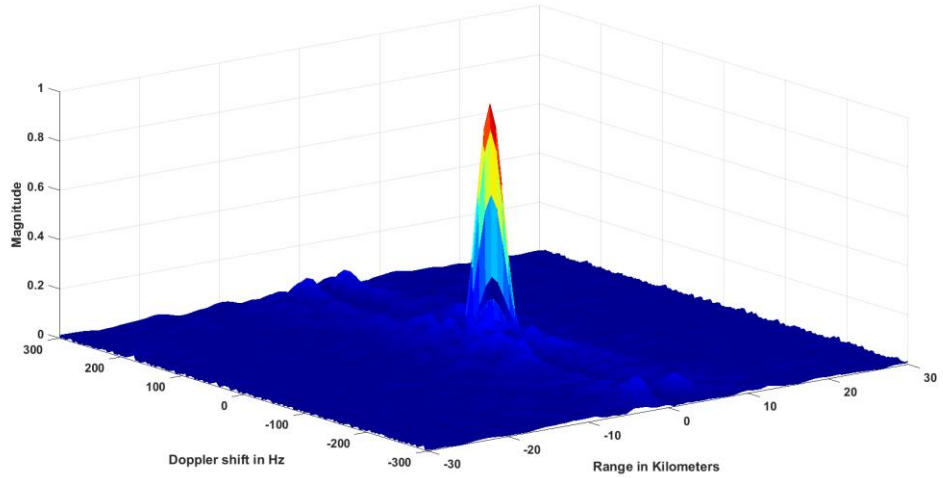

Figure 5.18: Ambiguity function for FM radio 98.9 MHz.

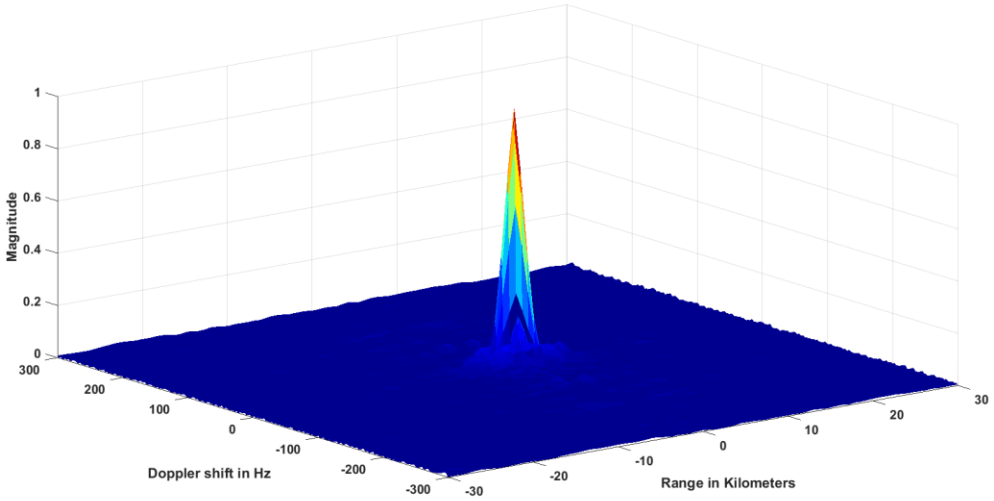

Figure 5.19: Ambiguity function for FM radio 99.7 MHz.

The output of the autonomous signal characterization algorithm applied to FM radio stations 91.1, 98.9, and 99.7 can be seen in table 5.4

Table 5-4: Results of autonomous signal characterization.

Features	91.1	98.9	99.7
Signal Strength (dBm)	-43	-47	-46
Range Resolution (m)	2100	2100	2100
Velocity Resolution (km/s)	6	6	6
PSLR (range dimension)	8.48	10.38	10.12
ISLR (range dimension)	15.01	15.17	13.89
Distance Metric	0.001887	0.001931	0.001895

This experiment indicates that for a PCL system, FM radio signal 91.1 MHz is superior based on its range and Doppler resolution, low sidelobe levels, and overall low noise and interference in the channel as indicated by the distance metric. This is another example that illustrates the superiority of this method over choosing signals based solely on amplitude.

One final experiment for the autonomous signal characterization method involved recording signals transmitted from San Diego, CA. According to concepts presented in chapter 4,

these transmitters are not ideal for detecting targets landing at San Diego International Airport. However for experimental purposes, these signals were collated solely for analysis of their ambiguity functions. The experiment geometry can be seen in figure 5.20 below, followed by calculated ambiguity functions for FM radio stations 93.3, 97.3, and 101.5 MHz (figures 5.21 – 5.23).

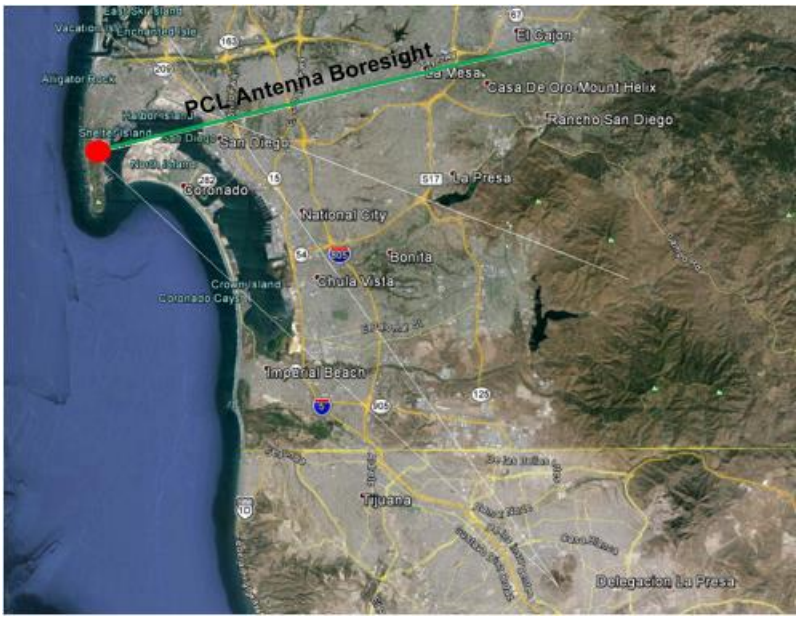

Figure 5.20: Experiment geometry for collection of San Diego FM radio signals. Map data taken from 2016 INEGI, SIO, NOAA, U.S. Navy, NGA, GEBCO, 2016 Google, USGS.

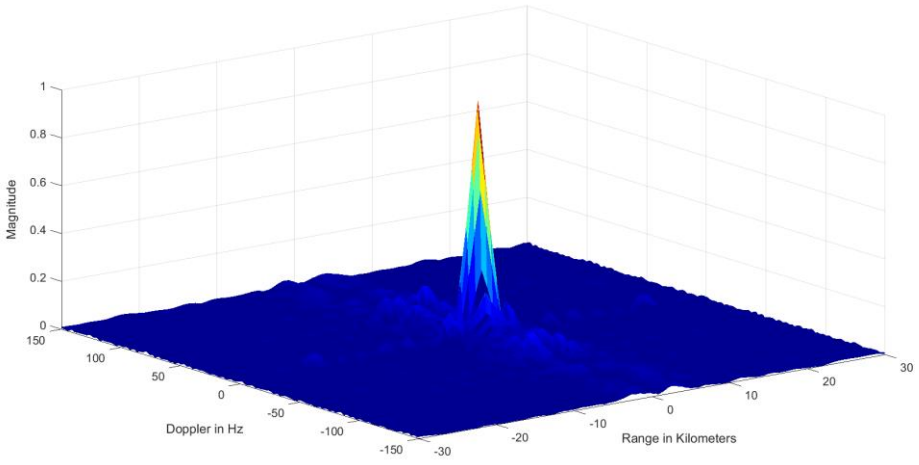

Figure 5.21: Ambiguity function for FM radio 93.3 MHz.

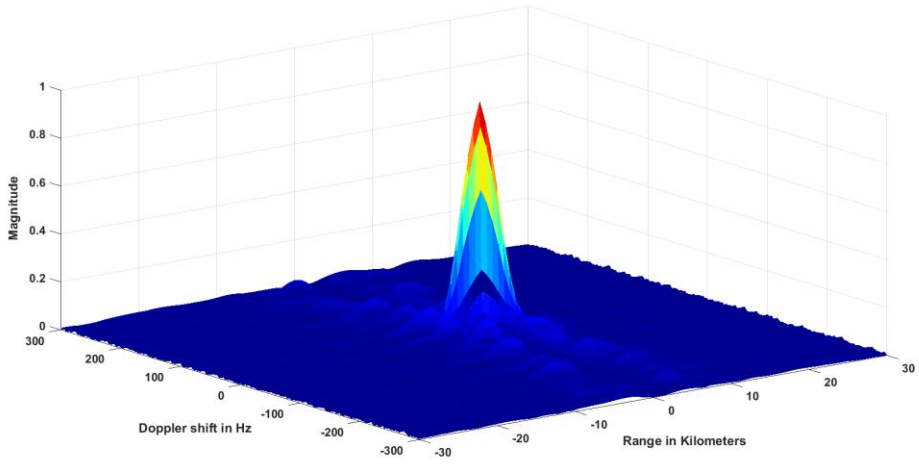

Figure 5.22: Ambiguity function for FM radio 97.3 MHz.

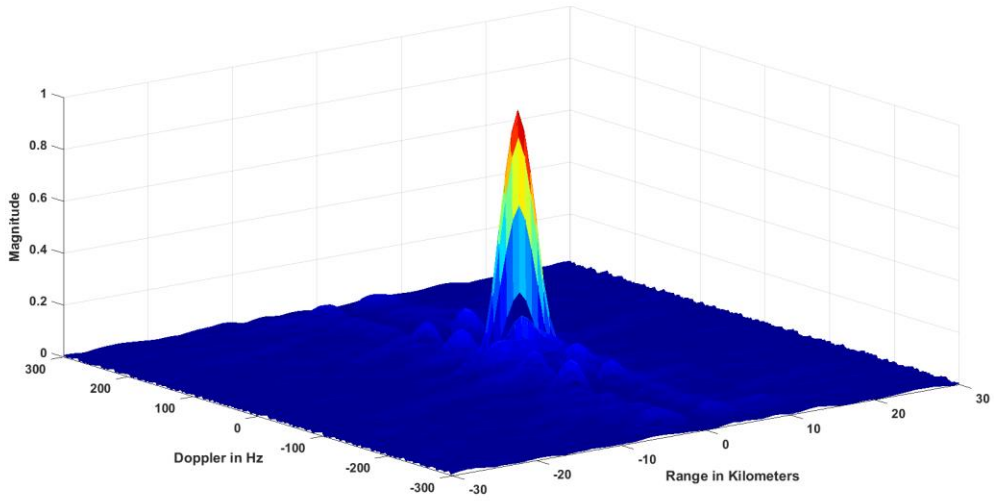

Figure 5.23: Ambiguity function for FM radio 101.5 MHz.

The results of this experiment can be seen in table 5-5. It can be seen that FM radio signal 93.3 MHz is the superior signal for PCL based on its features derived from the ambiguity function.

Table 5-5: Results of autonomous signal characterization.

Features	101.5	97.3	93.3
Signal Strength (dBm)	-42	-42	-41
Range Resolution (m)	2700	2100	2100
Velocity Resolution (km/s)	6	6	6
PSLR (range dimension)	7.95	11.93	7.16
ISLR (range dimension)	15.39	18.99	15.63
Distance Metric	0.002222	0.002038	0.001882

5.4 Ambiguity Function Evaluation and Characterization Conclusions

This section presents a novel method for characterizing a signal through features obtained by autonomously evaluating its ambiguity function. We have established the need for such a technology by describing a passive detection system capable of employing many signals and the need to rank those signals. With that motivation, we have developed an intelligent method for determining the range and Doppler resolution, SNR, and sidelobe levels. This method considers features such as resolution, PSLR, ISLR, and metrics derived from employing distance functions. The next step of this research will expand this work taking into account the bistatic ambiguity function developed by Tsao [36]. Although it is not considered in the scope of this work, it will be

beneficial for scenarios in which a target is present and multiple geographically separated transmitters exist. We also plan to define another qualitative measure of a signal by analyzing changes in its ambiguity function over time. As signal strength and modulation changes, the signal quality reflected in the ambiguity function will change as well.

CHAPTER 6: PCL MULTI-SIGNAL DETECTION

Passive coherent location (PCL) and passive bistatic radar (PBR) describe target detection and ranging systems capable of exploiting existing third party transmitters [3]. A passive radar system is cheaper to be implemented, lighter in weight, and requires far less power than a traditional active radar system. For those reasons, passive radar systems have received increasing interest among academic, industry, and government research over the last several years. However, the design of PCL systems is also faced with a number of challenges. Specifically, some transmitters usually employ omnidirectional antennas to cover a wide area, which might bring strong direct signals, clutter, and multi-path signals into the surveillance channel. In addition, the locations and waveforms used by the transmitters are no longer under control. All of those factors and others influence the detection capabilities of passive radar systems, and at the same time, these systems often require additional measures to improve the detection capacity which is a crucial factor in the success and reputation of this technology.

However, there are many techniques to overcome PCL detection limitations. One such method is frequency diversity, which is a simple technique that significantly improves detection performance for PCL under adverse weather conditions [1]. It is based on two or more conventional radar transceivers which are combined through a common antenna, in a multiplexed arrangement on the same RF transmission channel. Some advantages of frequency diverse radars are [2] more received total power, greater continuity of detection, reduced RCS fluctuations, and lessened effects of clutter.

Besides frequency diversity, the use of a radar sensor network or multiple receivers has advantages compared to a single radar system in improving the system sensitivity, reducing obscuration effects and vulnerability as well as increasing the detection performances [2]. In this section, we present and simulate a PCL architecture in which we achieve frequency diversity with a multi-sensor configuration. It is shown that through these methods, we realize improved target detection by enhancing the probability of detection, as well as a reduced required SNR per channel. We also show an experiment in which a binary detection scheme was applied a three-channel PCL system. The designed system is based on a multi-channel receiver, which uses commercial broadcast channels (including FM Radio, VHF TV, and digital TV channels) for target detection.

6.1 Traditional Binary Detection Methods

Binary integration is the final step of a detection process, which follows coherent or non-coherent integration [49]. The output of binary integration is one of two choices, which for radar purposes are "target present" and "no target present". It is also known that each decision of target present or not present will have a probability if detection and probability of false alarm. According to [49], there are two methods for binary detection. The first method known as the cumulative detection, can be used when the probability of detection and probability of false alarm are equal across multiple systems or channels for non-fluctuating (Swerling 0) targets. The binary probability of detection for a Swerling 0 target is given by the following equation.

$$P_{BD} = 1 - (1 - P_D)^N \tag{6.1}$$

This relationship shown in [49] also notes that the "1 of N" rule reduces the required signal to noise ratio to achieve a desired probability of detection. One critical note about cumulative detection is that this rule holds true for probability of false alarm as well.

$$P_{BFA} = 1 - (1 - P_{FA})^N \tag{6.2}$$

This means that by increasing the number of systems or channels N, both expressions for P_{BD} and P_{BFA} increase.

The author in [49] asserts that a better scheme for binary detection is the M of N method, in which a target is declared if a detection is made in M systems or channels out of N trials. To determine the ideal value of M, the author in [50] derives the equation below.

$$M_{opt} = 10^b N^a \tag{6.3}$$

Values are also listed for a and b given different ranges of N. As an approximation, the following equation is also given.

$$M_{opt} = 1.5\sqrt{N} \tag{6.4}$$

The author in [50] also gives a set of relationships for signal to noise ratio required to achieve a certain probability of detection, given N channels. Figure 6.1 note fig call outs for other fgis in this chapter are missing! shows the probability of detection P_d as a function of SNR and $P_{fa} = 10^{-6}$ with different values of N for non-fluctuating targets (Swerling 0). This figure was created using the equation below.

$$P_d = e^{-\frac{V_t}{(1+SNR)}} \tag{6.5}$$

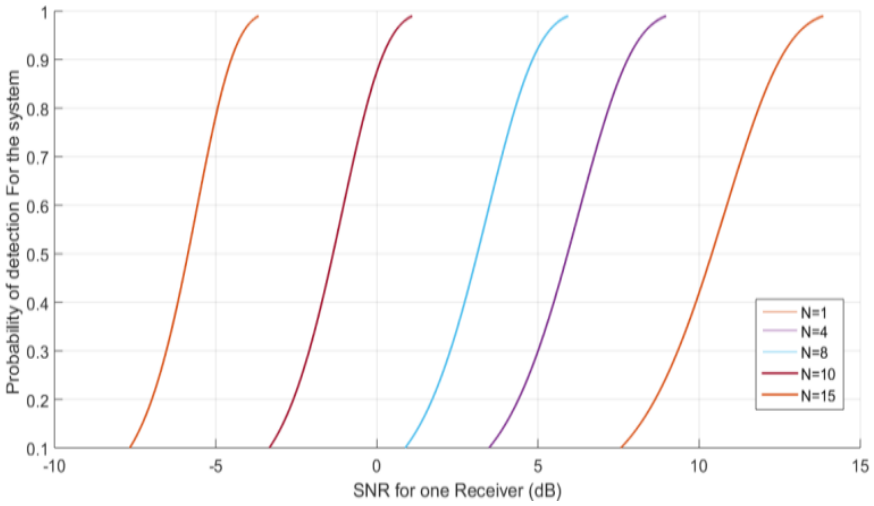

Figure 6.1: Variations of Probability of Detection versus SNR for N channels for $P_{fa} = 10^{-6}$ for a Swerling 0 target.

In an effort to show the value for M of N detection in multi-channel PCL systems, an experiment was conducted using three FM radio signals. The experiment geometry is shown below Fig call out. The FM signals are transmitted out of Tijuana, Mexico, potential targets are landing at San Diego International Airport, which provides ideal geometry for linear range and Doppler relationships. Target data was verified by a live ADS-B feed.

Figure 6.2: Multi-channel PCL experiment geometry. Map data taken from 2016 INEGI, SIO, NOAA, U.S. Navy, NGA, GEBCO, 2016 Google, USGS.

Three trials were setup so that the SNR could be varied for each set of FM signals detecting a target. Assuming a non-fluctuating or slowly fluctuating target (Swerling 0, 1), from [49] the optimum M was calculated to be 2.59, rounded up to 3.

$$For\ N = 3, M_{optimum} = 1.5\sqrt{N} = 2.59 \tag{6.6}$$

The initial experiment's SNR was recorded as 16dB. Once this data was recorded, further noise was added via simulation in Matlab.

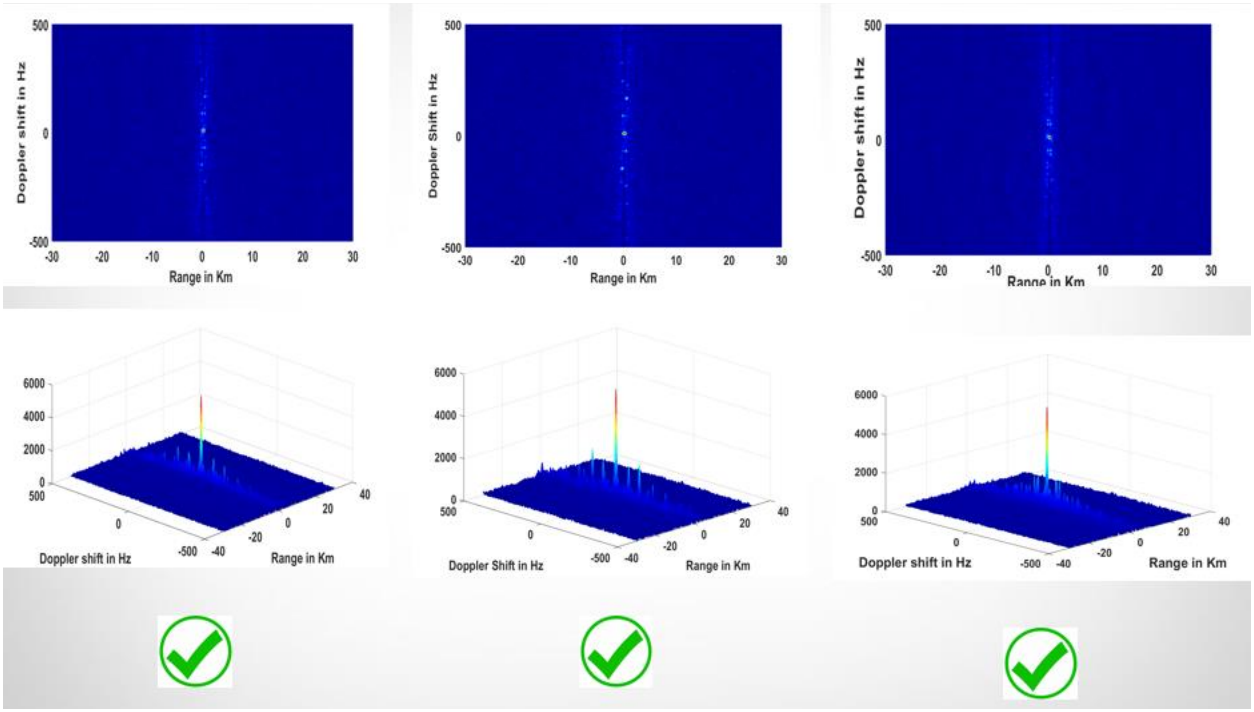

Figure 6.3: Multi-channel PCL target detection with SNR=16dB.

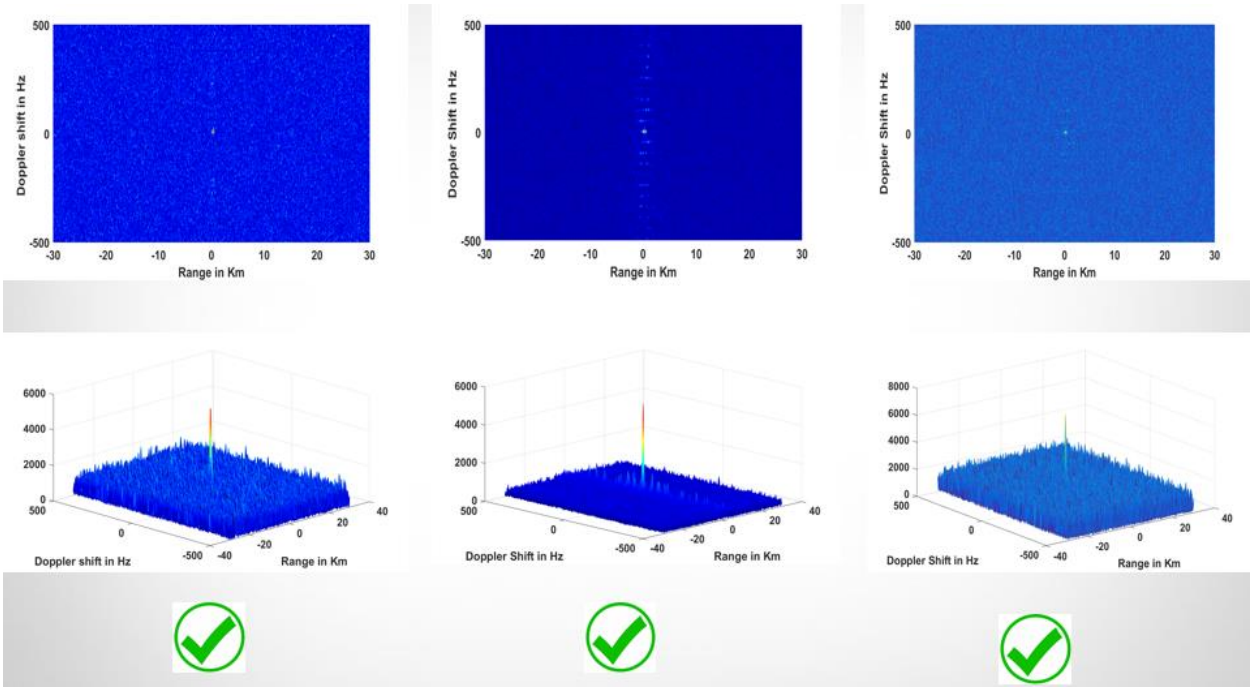

Figure 6.4: Multi-channel PCL target detection with SNR=6dB.

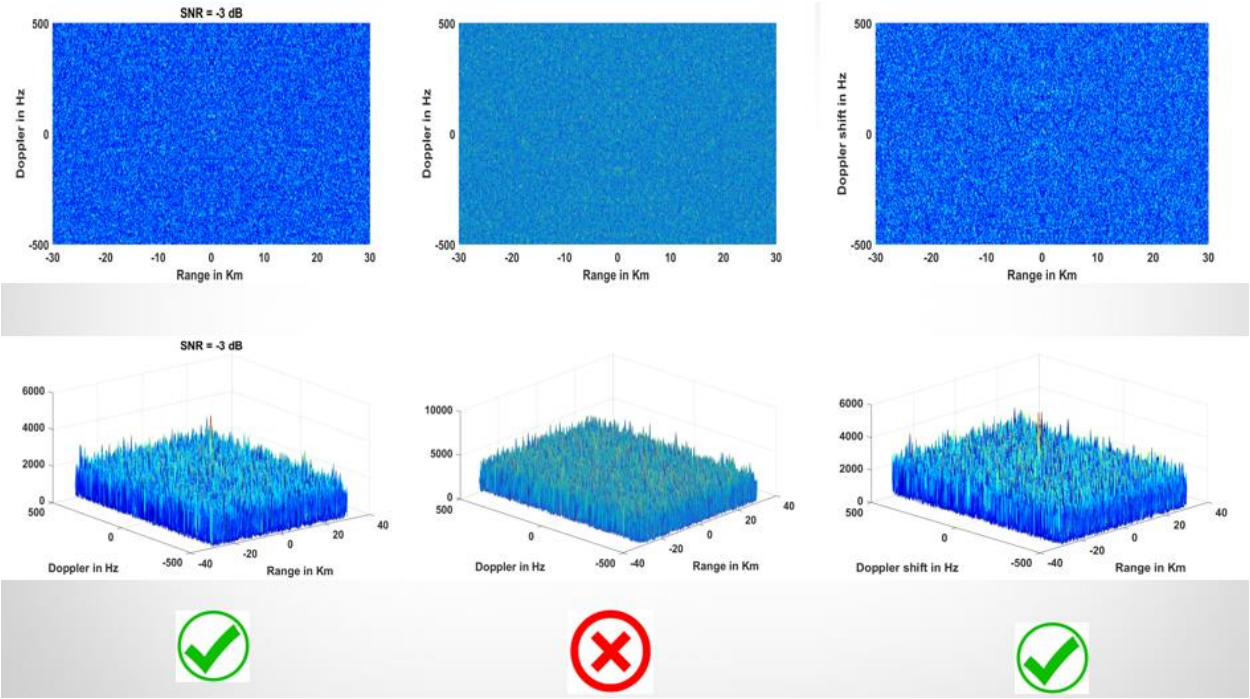

Figure 6.5: Multi-channel PCL target detection with SNR= - 6dB.

The results of this experiment indicate that the optimal M of N criteria that was calculated is in agreement with actual results. Detections were made for M=N=3 for SNR equal to 16dB and 6dB. For the experiment with SNR=-6dB, detections were made in 2 out of three channels, not meeting optimum M requirement of 2.59 (3). This case resulted in a missed detection. However Monte Carlo trials are necessary to increase confidence in this method.

6.2 Passive Coherent Location Binary Detection Algorithm Conclusions

In this section it has been shown that traditional methods for binary integration can be applied to multi-channel PCL systems. Theoretically the required SNR per channel can be reduced

by employing multiple signals. The experiment also shows that M of N detection is potentially a solution for combining detections from multiple channels to increase confidence in the system. However this idea needs to be further proven with Monte Carlo trials for complete assurance in this method.

CHAPTER 7: CONCLUSIONS AND FUTURE WORK

This work has produced several innovations for PCL systems. The first material presented in this work expands bistatic radar relationships to address geometric considerations. This chapter illustrates the area in which a bistatic PCL system can operate with linear relationships in time delay, target range, and Doppler frequency. It was also shown that large areas of non-linear zones exist in which the expected values o target range and velocity will likely not be realized in these areas.

Secondly, we have developed a novel method for characterizing and evaluating signals of opportunity. With an overwhelming number of signals in an urban environment, our algorithm enables a PCL system to decide which signal set is best for a specific application. The signal characterization method takes into account amplitude, bandwidth, sidelobe ratios, and includes a distance metric comparison with an ideal ambiguity function. The output of this characterization over iterations on multiple channels is compiled into a best to worst listing of available signals.

The final innovation we presented was the concept of using multiple signals to increase signal to noise ratio for target detection. Following the first concept of identifying, characterizing, and evaluating multiple signals, we can use those best suited for an application in concert to improve target detection capability. Through the use of a modified binary integration scheme

7.1 Future Work

Future work will focus on adaptive processing for PCL detection. Limitations still exist with PCL systems that make them less attractive than traditional active radar. The main challenges

of PCL detection still remain, which revolve around low signal to noise ratios due to unstable commercial transmitters and interference. In this vein, current state-of-the-art methods for monostatic radar may potentially have use in passive bistatic systems. Techniques such as Space Time Adaptive Processing (STAP), adaptive filtering, and modern thresholding techniques will be inserted into the prototype PCL system for proof of concept.

Another future improvement in PCL is establishing one's own transmitter of opportunity. For example, if a transmitting system were to be established and the PCL system had knowledge of the waveform, a reference channel would no longer be needed. This concept could be expanded to a moving transmitter platform that relays time, space, and position information, along with waveform details.

APPENDIX A: PCL MATLAB CODE

Matlab Code for Data Collection from Ettus N210 SDR

```
usrp210=findsdru;
%usrp_ip=usrp210.IPAddress;
usrp_ip1='192.168.10.201';
usrp_ip2='192.168.10.202';
decimation=4;
bandwidth=1e8/(decimation); %Total bandwidth
FC=501e6; %Center Frequency
gain=30;
N_samples=1024;
hSDRu1 = comm.SDRuReceiver(usrp_ip1,...
   'DecimationFactor', decimation,...
   'Gain',gain,...
   'SampleRate',1e8/decimation, ...
   'FrameLength',N_samples, ...
   'EnableBurstMode',true,...
   'OverrunOutputPort',true,...
   'OutputDataType', 'double',...
   'CenterFrequency',FC);
hSDRu2 = comm.SDRuReceiver(usrp_ip2,...
   'DecimationFactor', decimation,...
   'Gain',gain,...
   'SampleRate',1e8/decimation, ...
   'FrameLength',N_samples, ...
   'EnableBurstMode',true,...
   'OverrunOutputPort',true,...
   'OutputDataType', 'double',...
   'CenterFrequency',FC);
```

Matlab Code for PCL FM Channel Evaluation

```
function [CH]=Channel_Evaluation(y,Fs)
load('filterCoef.mat');
yf = filter(Num,1,y);
AF=my_code1(yf,yf);
RC=abs(xcorr(yf,yf).^2);
k=max(size(AF))-1;
p=(k/2)+1;
DC=abs(AF(:,p));
M=max(RC);
RC=RC./M;
DC=DC./M;
```

```
pksr=findpeaks(abs(RC));
for i=1:length(pksr)
   if pksr(i)>0.9
      pksr(i)=0;
   end
end
MPr=max(pksr);
SLLr=10.*log10(1/MPr);
pksd=findpeaks(abs(DC));
l=0;
for i=1:length(pksd)
   if pksd(i)>0.9
      pksd(i)=0;
   end
end
MPd=max(pksd);
SLLd=10.*log10(1/MPd);
MPdr=max(MPr,MPd);
AFR=abs(AF)/M;
k1=size(AFR);
s=0;
for j=1:k1(1)
   for n=1:k1(2)
      if AFR(j,n)>MPdr
         AFR(j,n)=0;
         s=s+1;
      end
   end
end
Nmean=sum(sum(AFR))/(k1(1).*k1(2));
p=((length(RC)-1)/2);
q=0;
for i=p-250:p+250
   if RC(i)>0.5
      q=q+1;
   end
end
RR=q.*3e8/(2.*Fs);
CH=[SLLr,SLLd,M,RR,Nmean];
```

Matlab Code for PCL FM Channel Selection

```
function []=Channel_Selection(CH1,CH2,CH3)
CHM=[CH1;CH2;CH3];
TM=CHM;
DM=zeros(3,5);
[M g]=max(TM(:,1));
DM(g,1)=1;
[M g]=max(TM(:,2));
DM(g,2)=1;
[M g]=max(TM(:,3));
DM(g,3)=1;
[m g]=min(TM(:,4));
DM(g,4)=1;
[m g]=min(TM(:,5));
DM(g,5)=1;

K1=sum(DM(1,:));
K2=sum(DM(2,:));
K3=sum(DM(3,:));
if (K1>K2)&&(K1>K3)
   'channel 1 is the best'
else
  if (K2>K1)&&(K2>K3)
   'channel 2 is the best'
  else
   'channel 3 is the best'
  end
end
```

Matlab Code for PCL Multi-Channel Processing

```
function varargout = MULTIRADIO(varargin)
% MULTIRADIO MATLAB code for MULTIRADIO.fig
%      MULTIRADIO, by itself, creates a new MULTIRADIO or raises the existing
%      singleton*.
%
%      H = MULTIRADIO returns the handle to a new MULTIRADIO or the handle to
%      the existing singleton*.
%
%      MULTIRADIO('CALLBACK',hObject,eventData,handles,...) calls the local
```

```
%      function named CALLBACK in MULTIRADIO.M with the given input arguments.
%
%      MULTIRADIO('Property','Value',...) creates a new MULTIRADIO or raises the
%      existing singleton*.  Starting from the left, property value pairs are
%      applied to the GUI before MULTIRADIO_OpeningFcn gets called.  An
%      unrecognized property name or invalid value makes property application
%      stop.  All inputs are passed to MULTIRADIO_OpeningFcn via varargin.
%
%      *See GUI Options on GUIDE's Tools menu.  Choose "GUI allows only one
%      instance to run (singleton)".
%
% See also: GUIDE, GUIDATA, GUIHANDLES

% Edit the above text to modify the response to help MULTIRADIO

% Last Modified by GUIDE v2.5 19-Dec-2016 14:49:33

% Begin initialization code - DO NOT EDIT
gui_Singleton = 1;
gui_State = struct('gui_Name',       mfilename, ...
                   'gui_Singleton',  gui_Singleton, ...
                   'gui_OpeningFcn', @MULTIRADIO_OpeningFcn, ...
                   'gui_OutputFcn',  @MULTIRADIO_OutputFcn, ...
                   'gui_LayoutFcn',  [] , ...
                   'gui_Callback',   []);
if nargin && ischar(varargin{1})
   gui_State.gui_Callback = str2func(varargin{1});
end

if nargout
   [varargout{1:nargout}] = gui_mainfcn(gui_State, varargin{:});
else
   gui_mainfcn(gui_State, varargin{:});
end
% End initialization code - DO NOT EDIT


% --- Executes just before MULTIRADIO is made visible.
function MULTIRADIO_OpeningFcn(hObject, eventdata, handles, varargin)
% This function has no output args, see OutputFcn.
% hObject    handle to figure
% eventdata  reserved - to be defined in a future version of MATLAB
% handles    structure with handles and user data (see GUIDATA)
% varargin   command line arguments to MULTIRADIO (see VARARGIN)
```

```
% Choose default command line output for MULTIRADIO


global ABORT
global USRPDETECTION
ABORT=false;

% RADIOS ADDRESS USRP IPs
handles.usrp_ip1='192.168.10.2';
handles.usrp_ip2='192.168.10.202';

handles.usrp_ip3='192.168.10.200';
handles.usrp_ip4='192.168.10.201';

handles.usrp_ip5='192.168.10.202';
handles.usrp_ip6='192.168.10.203';


% handles.usrp_ip7='';
% handles.usrp_ip8='';

% Center Frequencies
handles.FM_FC=92.5e6; %FM Center Frequency
handles.UHF_FC=497e6; %UHF Center Frequency
handles.VHF_FC=294e6; %VHF Center Frequency
handles.HF_FC=17.4E6; % HF Center Frequency


% FM PARAMATERS
handles.FM_decimation=250;
handles.FM_bandwidth=1e8/(handles.FM_decimation); %Total bandwidth
handles.FM_gain=27;
handles.FM_N_samples=1024;
handles.FM_DopplerFreqMin=-50;
handles.FM_DopplerFreqMax=50;
handles.FM_alfa=handles.FM_bandwidth/(2)


% UHF PARAMATERS
handles.UHF_decimation=80;
handles.UHF_bandwidth=1e8/(handles.UHF_decimation); %Total bandwidth
handles.UHF_gain=27;
```

```
handles.UHF_N_samples=1024;
handles.UHF_DopplerFreqMin=-50;
handles.UHF_DopplerFreqMax=50;
handles.UHF_alfa=handles.UHF_bandwidth/(2)

% VHF PARAMATERS
handles.VHF_decimation=80;
handles.VHF_bandwidth=1e8/(handles.VHF_decimation); %Total bandwidth
handles.VHF_gain=27;
handles.VHF_N_samples=1024;
handles.VHF_DopplerFreqMin=-50;
handles.VHF_DopplerFreqMax=50;
handles.VHF_alfa=handles.VHF_bandwidth/(2)

% HF PARAMATERS
handles.HF_decimation=400;
handles.HF_bandwidth=1e8/(handles.HF_decimation); %Total bandwidth
handles.HF_gain=27;
handles.HF_N_samples=1024;
handles.HF_DopplerFreqMin=-50;
handles.HF_DopplerFreqMax=50;
handles.HF_alfa=handles.HF_bandwidth/(2)



handles.output = hObject;

% Update handles structure
guidata(hObject, handles);




handles.output = hObject;

% Update handles structure
guidata(hObject, handles);

% UIWAIT makes MULTIRADIO wait for user response (see UIRESUME)
% uiwait(handles.figure1);


% --- Outputs from this function are returned to the command line.
```

```
function varargout = MULTIRADIO_OutputFcn(hObject, eventdata, handles)
% varargout  cell array for returning output args (see VARARGOUT);
% hObject    handle to figure
% eventdata  reserved - to be defined in a future version of MATLAB
% handles    structure with handles and user data (see GUIDATA)

% Get default command line output from handles structure
varargout{1} = handles.output;


% --- Executes on button press in RUN.
function RUN_Callback(hObject, eventdata, handles)
% hObject    handle to RUN (see GCBO)
% eventdata  reserved - to be defined in a future version of MATLAB
% handles    structure with handles and user data (see GUIDATA)

global ABORT;
usrp210=findsdru;


% FM BLOCK
handles.hSDRu1 = comm.SDRuReceiver(handles.usrp_ip1,...
   'DecimationFactor', handles.FM_decimation,...
   'Gain',handles.FM_gain,...
   'SampleRate',1e8/handles.FM_decimation, ...
   'FrameLength',handles.FM_N_samples, ...
   'EnableBurstMode',true,...
   'OverrunOutputPort',true,...
   'OutputDataType', 'double',...
   'CenterFrequency',handles.FM_FC);

handles.hSDRu2 = comm.SDRuReceiver(handles.usrp_ip2,...
   'DecimationFactor', handles.FM_decimation,...
   'Gain',handles.FM_gain,...
   'SampleRate',1e8/handles.FM_decimation, ...
   'FrameLength',handles.FM_N_samples, ...
   'EnableBurstMode',true,...
   'OverrunOutputPort',true,...
   'OutputDataType', 'double',...
   'CenterFrequency',handles.FM_FC);

% UHF BLOCK
handles.hSDRu3 = comm.SDRuReceiver(handles.usrp_ip3,...
   'DecimationFactor', handles.UHF_decimation,...
```

```
    'Gain',handles.UHF_gain,...
    'SampleRate',1e8/handles.UHF_decimation, ...
    'FrameLength',handles.UHF_N_samples, ...
    'EnableBurstMode',true,...
    'OverrunOutputPort',true,...
    'OutputDataType', 'double',...
    'CenterFrequency',handles.UHF_FC);

handles.hSDRu4 = comm.SDRuReceiver(handles.usrp_ip4,...
    'DecimationFactor', handles.UHF_decimation,...
    'Gain',handles.UHF_gain,...
    'SampleRate',1e8/handles.UHF_decimation, ...
    'FrameLength',handles.UHF_N_samples, ...
    'EnableBurstMode',true,...
    'OverrunOutputPort',true,...
    'OutputDataType', 'double',...
    'CenterFrequency',handles.UHF_FC);


% HF BLOCK
handles.hSDRu5 = comm.SDRuReceiver(handles.usrp_ip5,...
    'DecimationFactor', handles.HF_decimation,...
    'Gain',handles.HF_gain,...
    'SampleRate',1e8/handles.HF_decimation, ...
    'FrameLength',handles.HF_N_samples, ...
    'EnableBurstMode',true,...
    'OverrunOutputPort',true,...
    'OutputDataType', 'double',...
    'CenterFrequency',handles.HF_FC);

handles.hSDRu6 = comm.SDRuReceiver(handles.usrp_ip6,...
    'DecimationFactor', handles.HF_decimation,...
    'Gain',handles.HF_gain,...
    'SampleRate',1e8/handles.HF_decimation, ...
    'FrameLength',handles.HF_N_samples, ...
    'EnableBurstMode',true,...
    'OverrunOutputPort',true,...
    'OutputDataType', 'double',...
    'CenterFrequency',handles.HF_FC);



%%%%% UHF BLOCK
% handles.hSDRu5 = comm.SDRuReceiver(handles.usrp_ip7,...
```

```
%     'DecimationFactor', handles.UHF_decimation,...
%     'Gain',handles.UHF_gain,...
%     'SampleRate',1e8/handles.UHF_decimation, ...
%     'FrameLength',handles.UHF_N_samples, ...
%     'EnableBurstMode',true,...
%     'OverrunOutputPort',true,...
%     'OutputDataType', 'double',...
%     'CenterFrequency',handles.UHF_FC);
%
% handles.hSDRu6 = comm.SDRuReceiver(handles.usrp_ip8,...
%     'DecimationFactor', handles.UHF_decimation,...
%     'Gain',handles.UHF_gain,...
%     'SampleRate',1e8/handles.UHF_decimation, ...
%     'FrameLength',handles.UHF_N_samples, ...
%     'EnableBurstMode',true,...
%     'OverrunOutputPort',true,...
%     'OutputDataType', 'double',...
%     'CenterFrequency',handles.UHF_FC);

%%%%%%%%%%%%%%%%%%%%%%%%%%%%%%%%%%%%%%%%%%%%%%%%%%%%%%%%%%%%%%%%%%%%%%%%%%%%%%%
%%%%%%%%%%%%%%%%%%%%%%%%%%%%%%%%%%%%%%%%%%%


t_FM=1/handles.FM_N_samples:1/handles.FM_N_samples:1;
DopplerFreq_FM=handles.FM_DopplerFreqMin:1:handles.FM_DopplerFreqMax;

t_UHF=1/handles.UHF_N_samples:1/handles.UHF_N_samples:1;
DopplerFreq_UHF=handles.FM_DopplerFreqMin:1:handles.UHF_DopplerFreqMax;

t_HF=1/handles.HF_N_samples:1/handles.HF_N_samples:1;
DopplerFreq_HF=handles.HF_DopplerFreqMin:1:handles.HF_DopplerFreqMax;


FM_Freq=linspace(handles.FM_FC-
handles.alfa,handles.FM_FC+handles.alfa,handles.FM_N_samples);
UHF_Freq=linspace(handles.UHF_FC-
handles.alfa,handles.UHF_FC+handles.alfa,handles.UHF_N_samples);
HF_Freq=linspace(handles.HF_FC-
handles.alfa,handles.HF_FC+handles.alfa,handles.HF_N_samples);

% % % % t_UHF=1/handles.UHF_N_samples:1/handles.UHF_N_samples:1;
% % % %
DopplerFreq_UHF=handles.UHF_DopplerFreqMin:1:handles.UHF_DopplerFreqMax;
```

```
i=0;

while ABORT==false;
      % Just add one more tab per additional set
      USRPDATA= [step(handles.hSDRu1), step(handles.hSDRu2),step(handles.hSDRu3),
step(handles.hSDRu4),step(handles.hSDRu5), step(handles.hSDRu6)];
      USRP1DATA_FM  = USRPDATA(:,1)';
      USRP2DATA_FM  = USRPDATA(:,2)';
      USRP1DATA_UHF = USRPDATA(:,3)';
      USRP2DATA_UHF = USRPDATA(:,4)';
      USRP1DATA_HF  = USRPDATA(:,5)';
      USRP2DATA_HF  = USRPDATA(:,6)';

%%% ASSUMING doppler freq range same accross bands
      for p=1:(2*handles.FM_DopplerFreqMax+1)
         dopplerUSRP1_FM=exp(-2*pi*1i*DopplerFreq_FM(p).*t_FM);
         g_FM=USRP1DATA_FM.*dopplerUSRP1_FM;
         dopplerUSRP3_UHF=exp(-2*pi*1i*DopplerFreq_UHF(p).*t_UHF);
         g_UHF=USRP3DATA_UHF.*dopplerUSRP3_UHF
         dopplerUSRP5_HF=exp(-2*pi*1i*DopplerFreq_HF(p).*t_HF);
         g_HF=USRP5DATA_HF.*dopplerUSRP5_HF
         handles.DETECT_FM(p,:)=xcorr(g_FM,USRP2DATA_FM);
         handles.DETECT_UHF(p,:)=xcorr(g_UHF,USRP4DATA_FM);
         handles.DETECT_HF(p,:)=xcorr(g_HF,USRP6DATA_FM);
         pause (0.5)
         handles.currentdata=abs(handles.DETECT_FM);
         axes(handles.axes1)
         mesh(handles.currentdata),view(2)
         handles.currentdata=abs(handles.DETECT_UHF);
         axes(handles.axes2)
         mesh(handles.currentdata),view(2)
         handles.currentdata=abs(handles.DETECT_HF);
         axes(handles.axes3)
         mesh(handles.currentdata),view(2)
      end
      i=i+1;
      pause(0.5)
end



handles.output = hObject;
% Update handles structure
guidata(hObject, handles);
```

```
% --- Executes on button press in ABORT.
function ABORT_Callback(hObject, eventdata, handles)
% hObject    handle to ABORT (see GCBO)
% eventdata  reserved - to be defined in a future version of MATLAB
% handles    structure with handles and user data (see GUIDATA)
global ABORT;
ABORT=true;


% --- Executes on button press in ANALYSIS.
function ANALYSIS_Callback(hObject, eventdata, handles)
% hObject    handle to ANALYSIS (see GCBO)
% eventdata  reserved - to be defined in a future version of MATLAB
% handles    structure with handles and user data (see GUIDATA)
global ANALYSIS;
ANALYSIS=true;
```

Matlab Code for PCL Geometry

```
% R=((c.*t).^2-L.^2)./(2.*(t.*c+L.*sin(d)));
%v=(c.*fd)./(2.*f0.*(sqrt(0.5+((R1+L.*sin(d)).*(2.*(sqrt(R1.^2+L.^2+2.*R1.*L.*sin(d))))))));
N=1:10001;
c=3e8;
Fs=2.4e6;
R=N.*3e8/Fs;
tet=-90:1:90;
d=tet.*pi/180;
L=1000000;
for i=1:181
   to(i,:)=((R+sqrt(R.^2+L.^2+2.*L.*R.*sin(d(i)))))/c;

fd(i,:)=(101.1e6.*(2.*1.*(sqrt(0.5+((R+L.*sin(d(i))).*(2.*(sqrt(R.^2+L.^2+2.*R.*L.*sin(d(i))))))
)).*c);
end

for i=1:5:180
plot(R,to(i,:))
hold on
end
To=to.*Fs;
nn=round(To);
```

```
mm=nn-min(nn(1,:));
for i=1:10001
kk(10002-i)=-mm(2,i);
end
fd2=-50;
for p=1:101
ff=fd2.*fd(2,:);
jj=ff.*t;
d1=exp(-2*pi*1i*jj);
g=y.*d1;
T(p,:)=cross_corr(y,g,mm(2,:));
fd2=fd2+1;
end
for p=1:101
ff=fd2.*fd(2,:);
jj=ff.*t;
d1=exp(-2*pi*1i*jj);
g=y.*d1;
Tf(p,:)=cross_corr(y,g,kk);
fd2=fd2+1;
end
ss=[Tf T];
fd1=-50:1:50;
cg=max(max(T));
N1=-10000:1:10001;
R1=N1.*3e8/Fs;
mesh(R1/1000,fd1,abs(T/cg))
```

Matlab Code for LMS Filter

```
function e = LMS2(ref,det,mu)
N = max(length(ref)); % number of data samples
w = ones(1,N); % initialize filter coefficient vector
for n = 1:10000
  w1 = w.*ref; % filter output
  e = det - w1; % error
  w = 0.1.*w + mu*sign(ref).*e(n); % update filter coefficients
end
```

Matlab Code for Range Doppler Response

```
function AF=my_code(ref,det)
AF=zeros(1001,8193);
t=0.0:1/4096:1;
fd=-50:0.1:50;

for p=1:1001
   d=exp(-2*pi*1i*fd(p).*t);
   g=ref.*d;
   AF(p,:)=(x_cross_fft(g,det)).^2;
end
```

Matlab Code for Cross Correlation Processing

```
%   Cross-correlation by Using FFT final
function c=x_cross_fft(ref,det)
N=max(size(ref));
d=zeros(1,N);
%ref1=[ref,d];
%det1=[det,d];
R=fft(ref);
D=fft(det);
C=conj(R).*D;
c=fftshift(ifft(C));
```

APPENDIX B: FM RADIO SIGNAL COVERAGE

All coverage patterns listed in Appendix B were taken from [17].

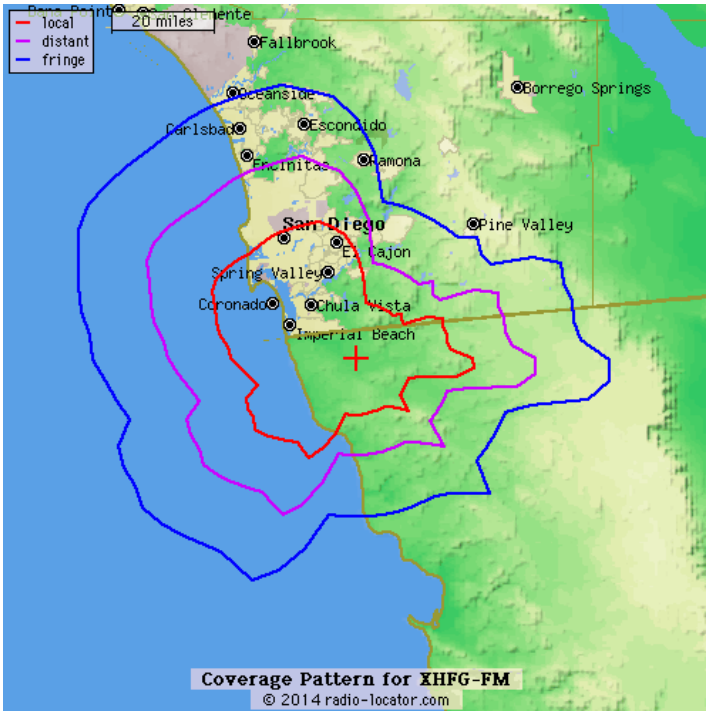

Figure B-1: Signal Coverage for FM Radio 107.3 MHz

Figure B-2: Signal Coverage for FM Radio 91.1 MHz

Figure B-3: Signal Coverage for FM Radio 101.5 MHz

Figure B-4: Signal Coverage for FM Radio 93.3 MHz

Figure B-5: Signal Coverage for FM Radio 97.3 MHz

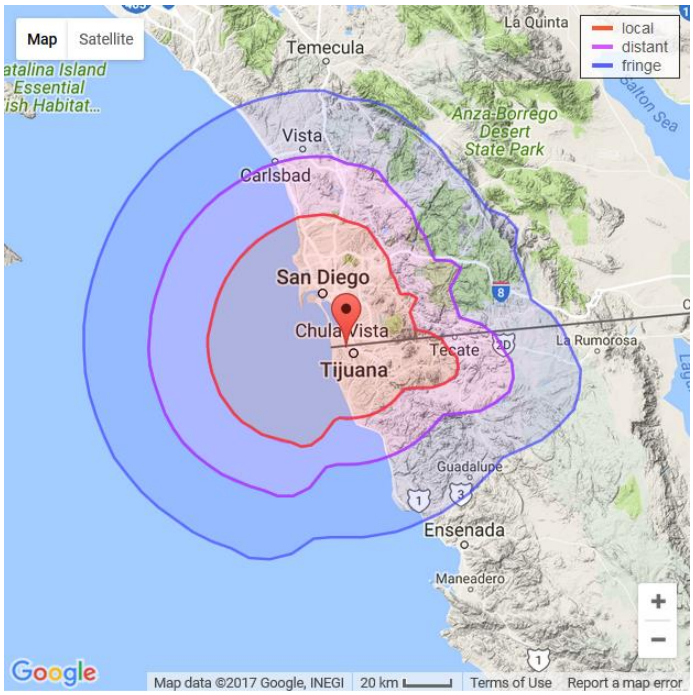

Figure B-6: Signal Coverage for FM Radio 98.9 MHz

Figure B-7: Signal Coverage for FM Radio 99.7 MHz

LIST OF REFERENCES

[1] N. Willis and H. Griffiths, *Advances in Bistatic Radar*. 2007.

[2] M. Cherniakov, *Bistatic Radar Principles and Practice*. John Wiley & Sons ltd, 2007.

[3] M. Skolnik, *Radar Handbook*, 3rd ed. McGraw Hill, 2008.

[4] H. D. Griffiths, "From a different perspective: principles, practice and potential of bistatic radar," *2003 Proc. Int. Conf. Radar (IEEE Cat. No.03EX695)*, vol. 2, pp. 1–7, 2003.

[5] B. Mojarrabi, J. Homer, and K. Kubik, "Power budget study for passive target detection and imaging systems," *System*, vol. 0, no. c, pp. 2–4, 2002.

[6] D. Kai, P. Tan, M. Lesturgie, H. Sun, and Y. Lu, "TARGET DETECTION PERFORMANCE ANALYSIS SUPELEC ONERA NUS DSTA Research Alliance (SONDRA), SUPELEC , Gif-sur-Yvette , France Temasek Laboratories @ Nanyang Technology University (TL @ NTU), NTU , Singapore," *Technology*, no. 1, pp. 3553–3556, 2010.

[7] H. Kuschel and D. O'Hagan, "Passive radar from history to future," *11-th Int. Radar Symp.*, pp. 1–4, 2010.

[8] H. Kuschel, "Approaching 80 years of passive radar," *2013 Int. Conf. Radar - Beyond Orthodox. New Paradig. Radar, RADAR 2013*, pp. 213–217, 2013.

[9] H. Griffiths and N. Willis, "Klein Heidelberg-—The First Modern Bistatic Radar System," *IEEE Trans. Aerosp. Electron. Syst.*, vol. 46, no. 4, pp. 1571–1588, 2010.

[10] H. Griffiths, “Klein Heidelberg: New Information and Insight,” *2015 IEEE Radar Conf. - Proc.*, pp. 527–532, 2015.

[11] H. Griffiths and N. Willis, “Klein Heidelberg – A WW2 Bistatic Radar System that was Decades Ahead of its Time.” [Online]. Available: http://www.bunkerpictures.nl/Klein Heidelberg-Hugh Griffiths.pdf. [Accessed: 01-Dec-2016].

[12] H. D. Griffiths and C. J. Baker, “Passive coherent location radar systems. Part 1: Performance prediction,” *IEE Proc.*, 2005.

[13] H. D. Griffiths, C. J. Baker, and I. Papoutsis, “Passive coherent location radar systems. Part 2: Waveform properties,” *IEE Proc.*, 2005.

[14] P. E. Howland, D. Maksimiuk, and G. Reitsma, “FM radio based bistatic radar,” *IEE Proceedings - Radar, Sonar and Navigation*. 2005.

[15] W. L. Melvin and J. A. Scheer, *Principles of Modern Radar Advanced Techniques*, 1st ed. Edison, NJ: Scitech Publishing, 2013.

[16] M. Cherniakov and M. Chernaikov, *Bistatic Radar Emerging Technology*, 1st ed. West Sussex England: John Wiley and Sons, 2008.

[17] “Radio Locator.” [Online]. Available: http://radio-locator.com/cgi-bin/locate?select=city&city=92109&state=&x=0&y=0. [Accessed: 01-Dec-2016].

[18] “HDTV Primer.” [Online]. Available: http://www.hdtvprimer.com/antennas/TVfrequencies.html. [Accessed: 01-Dec-2016].

[19] “Coastal Observing Research and Development Center.” [Online]. Available: Coastal

Observing Research and Development Center. [Accessed: 01-Dec-2016].

[20] A. Aldowesh, M. Shoaib, K. Jamil, S. Alhumaidi, and M. Alam, “A passive bistatic radar experiment for very low radar cross-section target detection,” *2015 IEEE Radar Conf. - Proc.*, no. 2, pp. 406–410, 2016.

[21] P. Abiven, T. J. Lim, and J. Pisane, “FM Passive Bistatic Radar Imaging of Airplanes in a Real Configuration,” vol. d, no. 1, pp. 1–6, 2014.

[22] N. J. Willis, *Bistatic Radar*, 2nd ed. Silver Springs, MD: Technology Services Corporation, 1995.

[23] H. Griffiths, C. Baker, H. Ghaleb, R. Ramakrishnan, and E. Willman, “Measurement and analysis of ambiguity functions of off-air signals for passive coherent location,” *Electron. …*, vol. 39, no. 13, pp. 1005–1007, 2003.

[24] P. Krysik, P. Samczynski, M. Malanowski, L. Maslikowski, and K. Kulpa, “Detection of fast maneuvering air targets using {GSM} based passive radar,” *Radar Symp. (IRS), 2012 13th Int.*, no. 1, pp. 69–72, 2012.

[25] D. K. P. Tan, “Sea and air moving target measurements using a GSM based passive radar,” *IEEE Int. Radar Conf. 2005.*, vol. 0, no. C, pp. 783–786, 2005.

[26] W. Junl, H. Shtiiiji, and C. Fengyun, “Application of GPS to Exospheric Target Detection Using Missile-Borne Passive Radar,” 2003.

[27] M. Ringer, G. Frazer, and Anderso, “Waveform Analysis of Transmitters of Opportunity for Passive Radar.” [Online]. Available:

http://dspace.dsto.defence.gov.au/dspace/bitstream/1947/4388/1/DSTO-TR-0809.pdf. [Accessed: 10-Aug-2015].

[28] D. Petri *et al.*, "A software defined UMTS passive radar demonstrator," *Radar Symp. (IRS), 2010 11th Int.*, pp. 1–4, 2010.

[29] Y. Li, W. Moran, S. P. Sira, A. Papandreou-Suppappola, and D. Morrell, "Adaptive waveform design in rapidly-varying radar scenes," *2009 Int. Waveform Divers. Des. Conf. Proceedings, WDD 2009*, pp. 263–267, 2009.

[30] G. Zhiwen, T. Ran, M. Yongfeng, and S. Tao, "DVB-T signal cross-ambiguity functions improvement for passive radar," *CIE Int. Conf. Radar Proc.*, no. 60232010, pp. 4–7, 2007.

[31] D. W. O'Hagan *et al.*, "Passive Bistatic Radar (PBR) for harbour protection applications," *IEEE Natl. Radar Conf. - Proc.*, pp. 0446–0450, 2012.

[32] M. M. Chitgarha, M. Radmard, M. N. Majd, and M. M. Nayebi, "Adaptive Filtering Techniques in Passive Radar," *2013 14th Int. Radar Symp.*, vol. 2, no. 1, pp. 1067–1072, 2013.

[33] J. L. Garry, G. E. Smith, and C. J. Baker, "Direct signal suppression schemes for passive radar," *2015 Signal Process. Symp. SPSympo 2015*, 2015.

[34] N. Johnson, M. Chergui, O. Sternberg, J. D. Rockway, and W. L. Jones, "Ambiguity Function Analysis for Passive Radar System Performance," in *MILCOM 2016 - 2016 IEEE Military Communications Conference*, 2016, pp. 872–876.

[35] H. D. Griffiths and C. J. Baker, "Measurement and analysis of ambiguity functions of

passive radar transmissions," *IEEE Int. Radar Conf. 2005.*, vol. 0, no. C, pp. 321–325, 2005.

[36] T. Tsao, M. Slamani, P. Varshney, D. Weiner, H. Schwarzlander, and S. Borek, "Ambiguity function for a bistatic radar," *1992 Proc. IEEESP Int. Symp. TimeFrequency TimeScale Anal.*, vol. 33, no. 3, pp. 497–500, 1992.

[37] a. Lauri, F. Colone, R. Cardinali, C. Bongioanni, and P. Lombardo, "Analysis and emulation of FM radio signals for passive radar," *IEEE Aerosp. Conf. Proc.*, pp. 1–10, 2007.

[38] S. Università, F. Ingegneria, and C. C. Bongioanni, "Multichannel Passive Radar : signal processing and experimental prototype development."

[39] B. Szlachetko and A. Lewandowski, "A Multichannel Receiver of the Experimental FM Based Passive Radar Using Software Defined Radio Technology," *Int. J. Electron. Telecommun.*, vol. 58, no. 4, pp. 301–306, 2012.

[40] a. Di Lallo, a. Farina, R. Fulcoli, P. Genovesi, R. Lalli, and R. Mancinelli, "Design, development and test on real data of an FM based prototypical passive radar," *2008 IEEE Radar Conf.*, 2008.

[41] P. Lombardo, F. Colone, C. Bongioanni, a. Lauri, and T. Bucciarelli, "PBR activity at INFOCOM: Adaptive processing techniques and experimental results," *2008 IEEE Radar Conf. RADAR 2008*, 2008.

[42] "Cavell Mertz Associates FCC Info." [Online]. Available: http://www.fccinfo.com/cmdpro.php?sz=L&wd=1536.

[43] M. C. C. Jackson, "The geometry of bistatic radar systems," *Commun. Radar Signal*

Process. IEE Proc. F, vol. 133, no. 7, p. 604, 1986.

[44] P. Varshney, D. Weiner, H. Schwarzlander, M. Slamani, and T. Tsao, "Ambiguity Function Analysis for Bistatic Radar," Rome, NY, 1995.

[45] T. Tsao, "Ambiguity Function for a Bistatic Radar," *IEEE*, 1994.

[46] Z. W. Chen, H.W., Li, X., Yang, J., Zhou, W., Zhuang, "EFFECTS OF GEOMETRY CONFIGURATIONS ON AM- BIGUITY PROPERTIES FOR BISTATIC MIMO RADAR," *Prog. Electromagn. Res. B, Vol. 30, 117–133, 2011*, vol. 30, no. May, pp. 117–133, 2011.

[47] a. S. Tasdelen and H. Koymen, "Range resolution improvement in passive coherent location radar systems using multiple FM radio channels," *IET Forum Waveform Divers. Des. Commun. Radar Sonar*, vol. 2006, pp. 23–31, 2006.

[48] P. F. Howland, "Target tracking using television-based bistatic radar," *IEE Proc. - Radar, Sonar Navig.*, vol. 146, no. 3, p. 166, 1999.

[49] M. A. Richards, *Fundamentals of Radar Signal Processing*. McGraw Hill, 2014.

[50] D. A. Shnidman, "Binary integration for swerling target fluctuations," *IEEE Trans. Aerosp. Electron. Syst.*, vol. 34, no. 3, pp. 1043–1053, 1998.